ADJACENT PRECAST PRESTRESSED CONCRETE BOX GIRDER BRIDGES TRANSVERSELY POST-TENSIONED AT TOP FLANGES ONLY

By

Shady Nasry Badie Labib

A Thesis Submitted to the Faculty of Graduate Studies of

The University of Manitoba

in partial fulfillment of the requirements of the degree of

MASTER OF SCIENCE

Department of Civil Engineering

University of Manitoba

Winnipeg, MB, Canada

April 2021

ABSTRACT

Adjacent precast, prestressed concrete box girders are widely used in short and medium span bridges in North America. Adjacent box girders are connected at their interface using partial- or full-depth grouted shear keys. Typically, transverse post-tensioning (TPT) is applied through diaphragms at discrete locations along the bridge span to improve the transverse load distribution and control differential deflections. Nevertheless, diaphragms only reduce the differential deflection between girders and do not eliminate it. In addition, the provision of transverse diaphragms is associated with an increased cost and time. The main objective of this research program is to investigate the feasibility of eliminating the transverse diaphragms by applying TPT in the top flange of the girders. The effect of applying TPT in the top flange of the girders, instead of being accommodated in discrete rigid diaphragms, on the transverse load distribution is studied.

The research program comprised two phases: experimental and numerical. The experimental phase consisted of four different tests on a one-third scale bridge model, (1) Strain distribution test – uncracked shear key, (2) Load distribution test – uncracked shear key, (3) Load distribution test – cracked shear key, and (4) Ultimate load test. On the other hand, the numerical phase included the construction of a finite element model (FEM) to validate the experimental results of the tested bridge. The validated FEM was then used to study the influence of varying several parameters including the presence of concrete topping, wheel load location and the width of the bridge on the transverse load distribution behavior of box girder bridges.

Results demonstrated the efficiency of distributing the TPT force at a shorter spacing along the length of the bridge in producing the minimum required concrete prestress. In addition, the influence of TPT force and spacing on the transverse load distribution behavior was found insignificant during the simulated service condition (fully-intact or partially-cracked shear keys). However, at failure, the

presence of TPT added redundancy to the bridge model and mitigated any sudden failure when shear keys were fully cracked. Furthermore, the presence of concrete topping reduced mid-span deflection up to 25%.

ACKNOWLEDGEMENTS

My first and sincere appreciation goes to my supervisor Dr. Ehab El-Salakawy, PEng, FCSCE, Professor of Structural Engineering and former Canada Research Chair in Durability and Modernization of Civil Infrastructures (2006-2016) in the Department of Civil Engineering at the University of Manitoba, for his dedicated support and guidance. His insight and knowledge carefully steered me through this research. I am greatly thankful for his patience, enthusiasm, and consistent encouragement throughout my study.

I would like to express my deep gratitude to my colleagues and friends for their valuable encouragement and help. Special thanks to Dr. Mohammed El-Gendy for his valuable contribution and consistent suggestions all along the work.

The completion of this project would not have been possible without the help and assistance of the W. R. McQuade structures laboratory technical staff, Dr. Chad Klowak, Samuel Abraha, and Syed Mohit.

The financial support received from the Canadian Precast/Prestressed Institute (CPCI) and the Natural Sciences and Engineering Research Council of Canada (NSERC) is gratefully acknowledged. The in-kind contributions received from Lafarge Canada Inc., Haywood Concrete Product Ltd., and Tetra Tech Canada Inc. are greatly appreciated.

Last but not the least, my wholehearted thanks to my parents, Nasry and Mervat Labib, for believing in me. Without them, I could not be able to make it.

To my beloved parents, sister, and brother.

Thanks for your endless support, and care.

TABLE OF CONTENTS

LIST OF FIGURES

LIST OF TABLES

LIST OF ABBREVIATIONS

AASHTO	=	American Association of State Highway and Transportation Officials;
CFRP	=	Carbon Fiber-Reinforced Polymer;
CHBDC	=	Canadian Highway Bridge Design Code;
FEA	=	Finite-Element Analysis;
FEM	=	Finite-Element Model;
FHWA	=	Federal Highway Administration;
IDOT	=	Illinois Department of Transportation;
LLMDFs	=	Live Load-Moment Distribution Factors;
LRFD	=	Load and Resistance Factor Design;
LVDTs	=	Linear Variable Displacement Transformers;
MAP	=	Magnesium Ammonium Phosphate;
MTO	=	Ministry of Transportation of Ontario;
NYDOT	=	New York Department of Transportation;
PCI	=	Precast/Prestressed Concrete Institute;
TPT	=	Transverse Post-Tensioning;
UHPC	=	Ultrahigh-Performance Concrete.

LIST OF NOTATIONS

A_{cr} = area of concrete section resisting shear along the crack interface (in.^{2});

B = area of vertical section through all the concrete keys(in.^{2});

b = width of a beam (in.);

D = depth of box girder (ft.);

d_e = the distance from the centerline of the exterior web of exterior girder to the interior edge of curb or traffic barrier (ft.);

e = correction factor for live load moment distribution;

f_c = compressive strength of grout;

I = moment of inertia (in.^{4});

J = St. Venant's torsional inertia for thin-walled closed sections (in.^{4});

K_s = correction factor for skew angle more than 0 degrees;

K = factor used in calculation of distribution factor for adjacent girders bridges

L = span of girder (ft.),

N_b = number of girders

P = the required transverse post-tensioning force (kip/ft.)

v_n = nominal shear strength of connection (ib)

w = the width of bridge (ft.),

θ = the skew angle (deg.).

ε_i = the longitudinal concrete tensile strain captured at the bottom of the ith girder.

1. INTRODUCTION

1.1. Background

Precast prestressed adjacent box girder bridges are load carrying crossing structures that typically consist of adjoined longitudinal flexure members. These members are typically composed of precast prestressed box girders that are transversely connected to allow for load distribution. The transverse connection could be achieved by placing grouting material in longitudinal shear keys. Partial or full-depth shear keys incorporating different grouting material are typically used. Transverse diaphragms including threaded rods or transverse post-tensioning (TPT) steel strands are used to assure the bridge integral behavior. Figure 1.1 shows a general transverse connection detail between two adjacent girders. Creating an interconnection between the girders with TPT and shear keys adjusts the bridge to act as a single plate instead of several individual girders (Kahl 2005). When load is applied, the girders deflect simultaneously due to transfer of vertical shear forces through the shear keys. In some cases, no topping is applied to the structure, while in other cases non-composite topping or a composite structural slab is provided (Russell 2011). According to Hanna et al. (2011), such bridges are widely used in North America for short spans (30 to 60 ft.) and medium spans (60 to 120 ft.) because of the following advantages:

- Easy and quick to construct because of concrete forming and placement elimination.
- Cost-effective compared to other cross sections such as I-girders and T-girders.
- Shallow superstructures necessary to provide needed vertical clearance.
- Hollow portions in the girders reduce overall weight of the structure and allow the passage of ducts, pipes, and other utilities.
- Aesthetical appealing appearance because of the flat soffits and slender superstructure.
- Higher torsional stiffness, which is suitable for curved bridges.

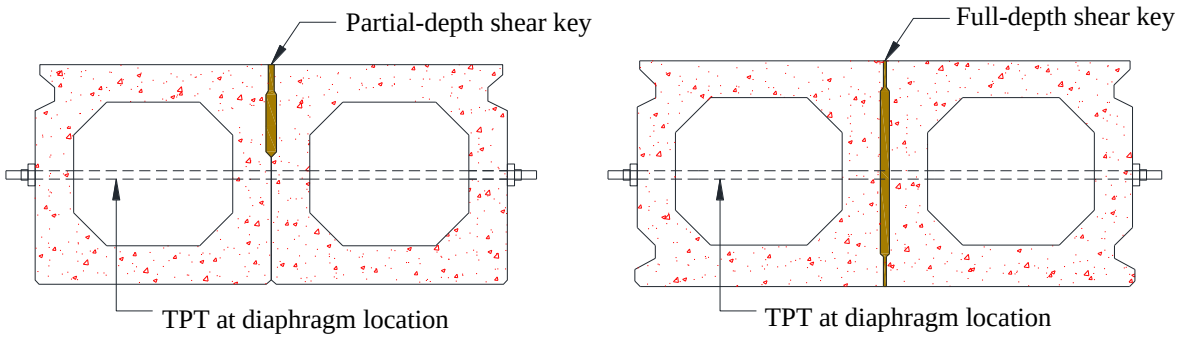

(a) Partial-depth grouted shear key (b) Full-depth grouted shear key

Figure 1.1 – General transverse connection between adjacent box girders

1.2. Problem Definition

Precast prestressed adjacent box girder bridges have been in service for years and have been recognized for their satisfactory performance. However, a recurring problem is cracking in the longitudinal shear keys that reflects to the deck surface as shown in Figure 1.2. Mostly, these longitudinal cracks lead to leakage between adjacent girders allowing salt laden water to penetrate to bottoms and sides of girders. This ultimately causes corrosion of the longitudinal steel strands, non-prestressed reinforcement. In severe cases, the shear key cracking could compromise the lateral load sharing mechanism among girders resulting in individual girders carrying loads more than original design loads (Huckelbridge et al. 1995; Miller et al. 1999). One example of bridges that experienced such kind of distress is the 2005 partial collapse of Lakeview Drive Bridge, Washington, PA., a fascia girder failed near mid-span and fell to the below highway. Inspections showed severe spalling and strands corrosion of the collapsed precast prestressed box girder bridge (Hanna et al. 2009).

(a) Asphalt overlay longitudinal cracking (b) Concrete topping longitudinal cracking

Figure 1.2 – Shear keys longitudinal cracking (Russell 2011)

Besides the inadequate design criteria, the majority of failures of box girders is primarily attributed to the poor drainage, and the difficulties associated with inspecting the distressed members.

In addition to grouted shear keys, TPT is commonly used for the assembly of these boxes to improve the distribution of live loads and control differential deflection. The current practice is to apply the TPT through discrete transverse diaphragms, which causes several problems including:

1. Interruption of utility lines and drainage ducts inside the hollow portion,
2. Differential deflection between adjacent girders still exist, which causes longitudinal cracks in the bridge deck (leakage) and reduces load-carrying share among girders,
3. Additional cost due to the increased weight of the girders and complex forms,
4. Additional cost in the case of skewed bridges that may have to be staggered or built in stages,
5. Inevitable leaking during grouting of transverse post-tension ducts.

Transverse diaphragms, incorporating TPT provided along the bridge span, constitute a geometric barrier that blocks the access to the TPT. Drainage ducts are widely separated between diaphragms,

leading to water accumulation, corrosion of the TPT and ultimately to bridge failure. Even if the problem is detected before collapse, inspection of the corroded TPT is problematic even with nondestructive testing. In addition, post-tensioned diaphragms provide transverse continuity at discrete points, which makes the bridge more susceptible to cracking and leakage (Hanna et al. 2011). This can be explained as the clamping stresses induced by TPT are mainly concentrated at stiffer diaphragms, while shear keys located in between diaphragms are under tension or zero stresses and would fail to constitute watertight surface without adequate TPT (Aktan et al. 2009). Another problem associated with diaphragms is related to their constructability, in skewed bridges they have to be staggered or built in stages. This leads to an increased construction cost and schedule due to varied diaphragm location, large number of TPT stressing operations, and excessive traffic interruption required in replacement projects (Hansen et al. 2012). Furthermore, grout leakage from bonded TPT conduits prefabricated in diaphragms causes environmental problems and increases the construction cost.

1.3. Motivation and Proposed Solution

The aforementioned problems may be resolved by developing new connection or assembly details that eliminate the need of transverse diaphragms while maintaining similar performance characteristics with better economy than currently used ones. Generally, the benefits of transverse diaphragms are debatable. Many studies have shown that transverse diaphragms have an insignificant effect on live load distribution while increasing bridge susceptibility to damage induced by lateral and impact loads since they act as stiffeners that transfer load to adjacent girders (Sithichaikasem et al. 1972; Sengupta et al. 1973; Cheung et al. 1986). In precast prestressed adjacent box girder bridges, diaphragms encapsulate the TPT strands and their elimination requires an alternative location for the TPT to be applied at. Hanna et al. (2011) first proposed two non-

post-tensioned connections that eliminate the need of diaphragms, TPT, and concrete topping. These two connections depend on non-post-tensioned bars placed in both top and bottom flanges of the girders to form a monolithic continuous connection. Hansen et al. (2012) performed follow-up work and modified these connections by introducing sleeves below the top flange and above the bottom flange to allow post-tensioning high strength rods. This transverse post-tensioned diaphragm-free connection was ultimately modified by moving the TPT ducts to be housed in the top and bottom flanges (Sun et al. 2018). However, placing TPT ducts in the congested bottom flange is challenging due to the presence of the longitudinal prestressing strands. Such congestion may require increasing the bottom flange thickness to accommodate both longitudinal and transverse strands, while maintaining the minimum concrete cover requirements.

In this investigation, a further modified transverse connection is proposed, that is, applying TPT at the top flanges of the girders only, eliminating the need of transverse diaphragms and costly TPT operation on both top and bottom flanges. The proposed method allows TPT to be distributed at shorter spacing providing a uniform stress distribution, without congesting the bottom flange, rather than being concentrated at discrete diaphragm locations. The main concern here is what adequate arrangement and level of TPT required to achieve transverse continuity without diaphragms. The TPT design charts developed by El-Remaily et al. (1996) and Hanna et al. (2009), which were adopted by the Precast/Prestressed Concrete Institute (PCI), assume that post-tensioned diaphragms are the primary load transfer mechanisms between adjacent girders and are valid only for bridges constructed by diaphragms (Hussein et al. 2017). Another concern that should be accounted for is related to joints opening and closing under applied eccentric TPT and external loads, and whether these movements will hinder the functionality of the bridge or will be counteracted by self-weight components of adjacent girders.

1.4. Study Objectives

The main objective of this research is to investigate the feasibility of applying TPT in the top flange of adjacent precast prestressed concrete box girders. The effect of applying TPT in the top flange of the girders, instead of being accommodated in discrete rigid diaphragms, on transverse load distribution and developed transverse strains is studied. Furthermore, the serviceability of that innovative transverse connection in terms of maximum relative displacement between adjacent girders, and joints opening and closing under applied load is monitored.

1.5. Scope of Study

A detailed experimental investigation has been designed to address the study objectives. A one-third scale, 6,400 mm span by 1,600 mm wide, bridge model, consisting of four adjacent precast prestressed concrete box girders, was erected and tested. The girders were transversely connected by partial depth grouted shear keys. Nine transverse circular ducts equally spaced at 750 mm were provided at the mid-depth of the top flange of the girders. The bridge model was subjected to strain distribution, load distribution, and ultimate load tests. Different levels of TPT forces were applied using No.13 (12.7-mm diameter) un-bonded seven-wire strands with different spacing for the transverse strain distribution test. For the load distribution test, a vertical point load was applied at the mid-span of each box-girder with similar TPT levels and arrangement to those used for strain distribution test. The bridge model was cracked at the shear key joints between the adjacent box girders in order to study the effect of the longitudinal cracks on the load distribution. The ultimate response of the TPT system was further evaluated during the ultimate load test of the bridge model.

1.6. Methodology

The research program consisted of two phases: experimental and numerical. The research started with the experimental phase, which involved the testing of precast prestressed concrete box girder

bridge model that consisted of four adjacent box girders assembly. Each girder measured 400-mm wide, 270-mm high, and 6,400-mm long. This assembly represented a one-third scale of a full-size bridge spanning 18,000 mm and of a total depth of 800 mm. Each box girder was reinforced with three size 13 prestressing steel strands (12.7 mm) and five size 10M non-prestressing steel bars (three at the bottom and two at the top). The experimental program was designed to capture the deterioration effects experienced by the bridge during its service. This was achieved by testing the bridge when shear keys were intact, and partially-cracked. The bridge model was tested using a concentrated vertical load applied to an interior and exterior girder, one at a time, to evaluate the efficiency of the proposed connection in transversely distributing live loads.

The numerical phase comprised two stages. In the first stage, a finite element model (FEM) was constructed to simulate the tested bridge assembly using a commercial software package, ATENA-Studio (Červenka et al. 2020). The FEM was validated against the experimental results obtained from the experimental phase. In the second stage, the validated FEM was used to conduct a parametric study investigating the influence of key parameters known to affect the transverse load distribution behavior of box girder bridges including the presence of concrete topping, wheel load location and the bridge width.

1.7. Thesis Outline

This thesis consists of five chapters as follows:

Chapter 1 introduces the problem definition, motivation and proposed solution, study objectives, and the scope maintained to achieve such objectives.

Chapter 2 synthesizes various research studies investigating the factors affecting the transverse load distribution behavior in adjacent box girder bridges. Of these factors, the effect of TPT and

incorporating different shear key materials, locations, and configurations is presented. Additionally, the current codes and guidelines are discussed. Furthermore, an insight into a set of innovative transverse connection details eliminating the need of intermediate transverse diaphragms is presented.

The following two chapters (Chapters 3 and 4) are presented in journal article format where they were published or currently under review.

Chapter 3 (Article 1, published) presents the experimental program including the bridge reinforcement details, material properties, testing procedures, and the instrumentation. The experimental program was carried out in four different tests to simulate the service and ultimate loading conditions experienced during the life cycle of actual bridge structures. The analysis of test results was also presented.

Labib, S., El-Gendy, M., and El-Salakawy, E. (2021). “Adjacent Concrete Box Girders Transversely Post-Tensioned at Top Flanges Only: Experimental Investigation." ASCE, Journal of Bridge Engineering, 26(4): 04021017. DOI: 10.1061/(ASCE)BE.1943-5592.0001699.

Chapter 4 (Article 2, submitted) discusses the numerical analysis using the finite element analysis software (ATENA). The validation process as well as the results of the parametric study were presented in this chapter.

Labib, S. and El-Salakawy, E.F. (2021). "FEA of Adjacent Concrete Box Girders Transversely Post-Tensioned at Top Flange Only." Computers and Concrete, Techno Press, Submitted in April 2021.

Chapter 5 presents the summary and the major findings and conclusions of the study and suggestions for future work.

Both flexural and shear design of the bridge assembly using the Canadian Highway Bridge Design Code - CHBDC (CSA 2019a) are demonstrated in Appendix A.

2. LITERATURE REVIEW

2.1. Overview

In this chapter, a summary of the construction guidelines and details in the current North American design codes, and provincial jurisdictions is presented. Additionally, a synthesis of the available research related to adjacent precast prestressed concrete box girder bridges is provided, with focus on the factors that affect the transverse behavior of such bridges including shear keys, transverse diaphragms and TPT. Furthermore, successful examples of innovative transverse connections that eliminate the need of intermediate diaphragms are discussed.

2.2. Load Transfer Mechanism

Adjacent precast prestressed concrete box girder bridges include different practices in designing and detailing transverse connection. The first practice includes the application of non-composite, non-structural overlay directly to the top flange of the adjacent girders. This configuration depends only on the grouted shear keys to transfer shear forces from one girder to another. The second practice includes casting thick cast-in-place concrete topping to develop composite action with the adjacent girders through protruded steel shear connectors from the top flanges of the girders. The third practice includes the application of transverse clamping forces using TPT steel strands or tie rods, which can be used in combination with composite or non-composite overlays to enhance the transverse connection behavior (Hanna et al. 2009). Figure 2.1 shows the aforementioned transverse connection practices.

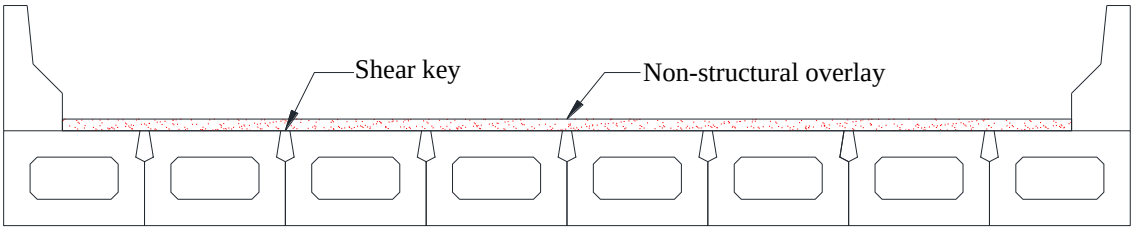

(a) Non-structural overlay with shear keys

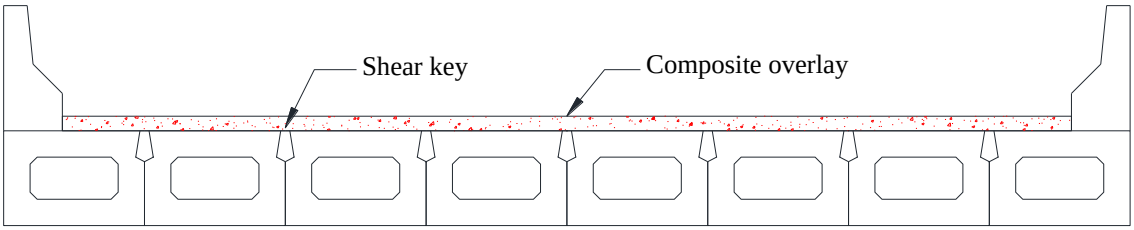

(b) Structural composite overlay with shear keys

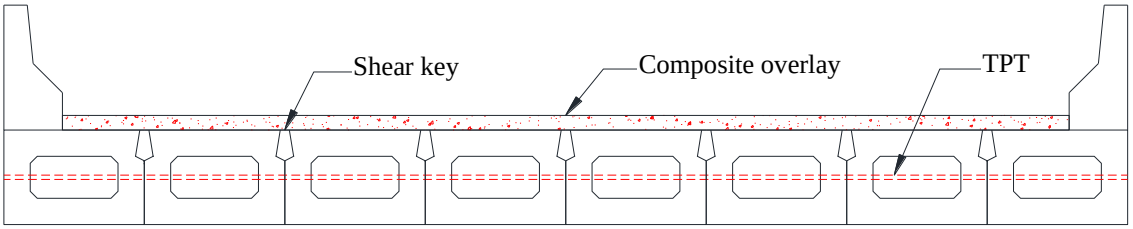

(c) Structural composite overlay with shear keys and TPT

Figure 2.1 – Adjacent precast prestressed box girder bridges possible transverse connection details (Hanna et al. 2009)

2.3. Current Practice

2.3.1. Canadian Highway Bridge Design Code

The Canadian Highway Bridge Design Code - CHBDC (CSA 2019a), Clause 8.21 states that: "multi-beam decks consisting of precast side-by-side placed members should have shear forces transfer mechanism that could be achieved by a combination of 150-mm thick concrete slab, and grouted shear keys with lateral post-tensioning providing a prestress of not less than 1.7 MPa, after all losses, over a compressed depth of joint not less than 175 mm; or an approved means capable

of live load and shear transfer between adjacent members". In the commentary of this clause, bolted connections have been suggested as an alternative connection capable of shear force transfer (CSA 2019a). The CHBDC provides a simplified method to analyze the longitudinal dead and traffic load effects for such bridges. To utilize this simplified method, the analyzed adjacent girders should meet some conditions. For adjacent girders without flexural rigidity at both top and bottom flanges, intermediate diaphragms are needed unless the thickness of the top and bottom flange is 10% or more of the girder width, the web thickness is at least 10% of the girder depth, the width of each girder is not more than 1,200 mm, and the width-to-height ratio is not greater than 1.50. If a minimum of two intermediate diaphragms maximally spaced at 18 m in addition to end diaphragms are not provided, special consideration to distortional warping shall be considered.

2.3.2. AASHTO LRFD Bridge Design Specifications

The design guidelines of adjacent precast prestressed box girder bridges are found in Section 5.12.2.3 "Precast Deck Bridges" of AASHTO LRFD-9 (AASHTO 2020). Article 5.12.2.3.2 requires a minimum shear key depth of 177.8 mm (7 in.) for joints intended to transfer shear forces only. Joints shall be filled with non-shrink grout of minimum compressive strength of 35 MPa (5 ksi) at 24 hours. Article 5.12.2.3.3 defines another kind of joints designed to transfer both shear and flexure by means of TPT, structural overlay, cast-in-place closure joints or a combination of these. In this case, TPT shall be uniformly distributed along the longitudinal direction and should be of 1.72 MPa (0.25 ksi) over a compression depth of 177.8 mm (7 in.).

2.3.3. Manitoba Infrastructure

According to Manitoba Infrastructure structures manual, the design of highway structures shall be performed according to AASHTO LRFD bridge design specifications and provisions. As shown in Figure 2.2, box girders are transversely connected with 75-mm partial depth shear keys and

laterally post-tensioned with mid-depth TPT steel strands of minimum diameter of 12.7 mm and jacking force per strand of 93.45 kN. A minimum of two strands shall be used per duct with minimum ultimate strength of 1,860 MPa. Ducts are encapsulated in rigid diaphragms provided at mid-span for bridges spanning from 10,000 mm to 15,000 mm, while a minimum of two intermediate diaphragms should be provided for spans larger than 17,500 mm. In all cases, end diaphragms should be provided. Non-shrink grout of minimum compressive strength of 35 MPa is used to fill shear key joints after the lateral stressing operations except for the shear key located at the roadway centerline, which is cast before TPT application. Typically, the girders are topped by a waterproofing membrane with a protection board followed by 85-90 mm asphalt wearing surface. In some cases, a structural overlay is used as in the Provincial Trunk Highways (PTH) 59 and 101 in Winnipeg, Manitoba.

2.3.4. Ministry of Transportation of Ontario (MTO)

According to the structural manual of Ministry of Transportation of Ontario, precast concrete box girders with an integral concrete structural slab do not require shear keys between adjacent girders nor TPT. Anchored embedded steel bearing plates are used to connect adjacent girders as shown in Figure 2.3. These bolted connections are located at third-point location for spans shorter than 24,000 mm, and at quarter-point locations for longer spans.

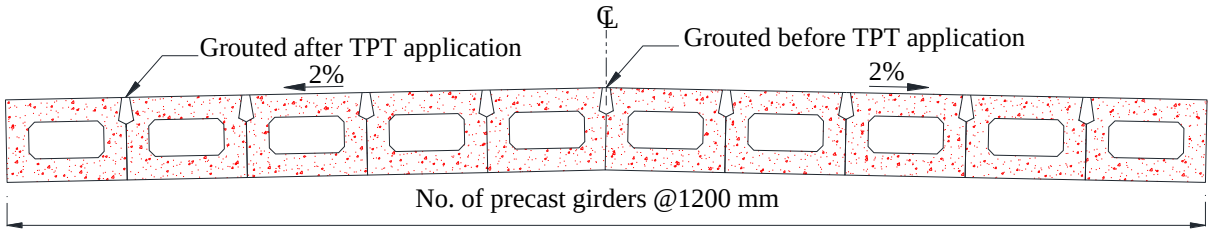

(a) Cross-section at midspan

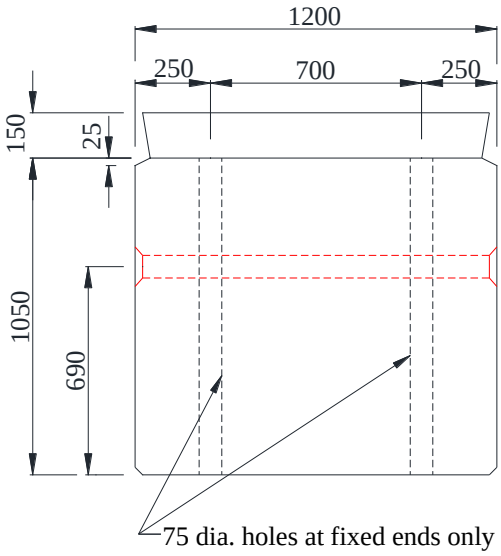

(b) Typical dimensions for exterior girder

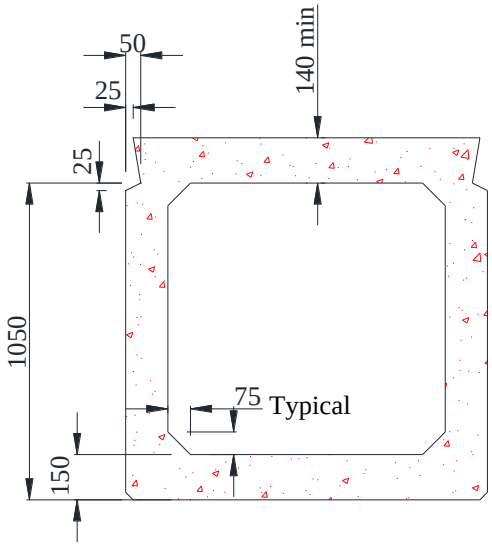

(c) Typical dimensions for interior girder

Figure 2.2 – Typical cross section detail according to Manitoba Infrastructure (dimensions in mm).

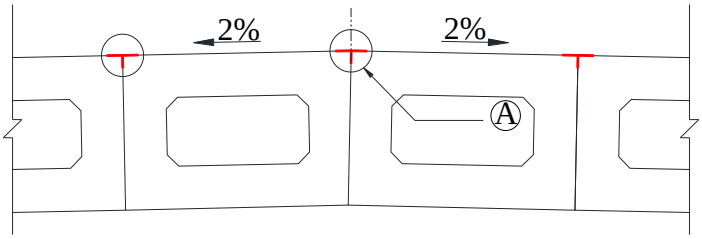

(a) Cross section at mid-span

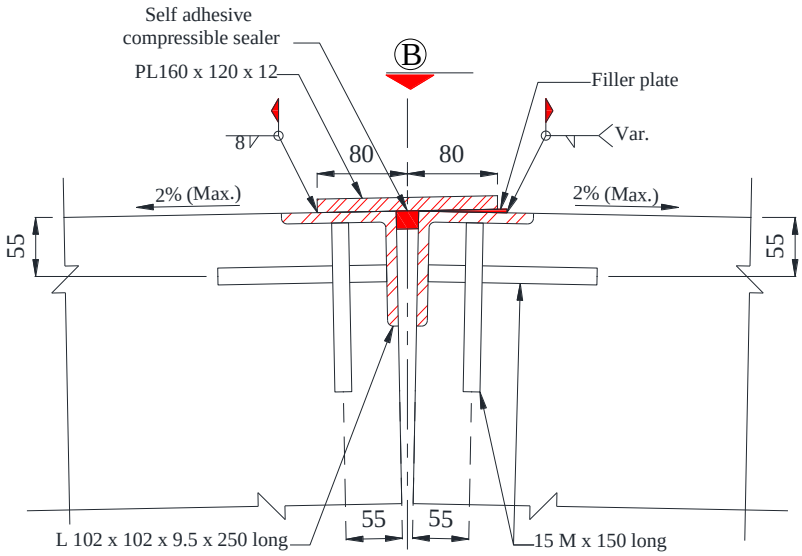

(b) Detail (A)

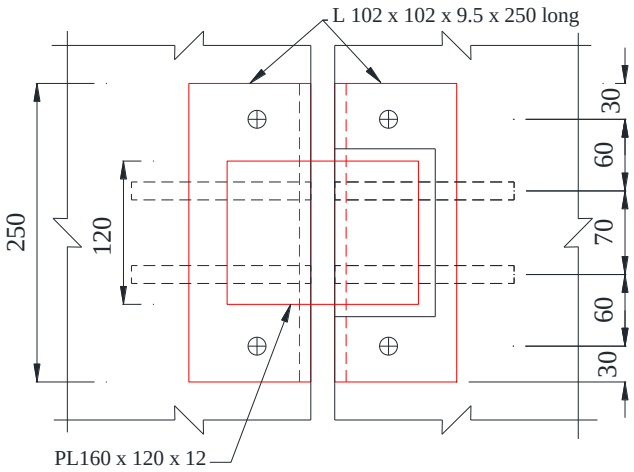

(c) Top view (B)

Figure 2.3 – Typical cross section detail according to Ontario ministry of transportation

2.4. Shear keys

Shear keys are typically created by placement of grouting material between two adjacent precast members that have facing recesses to enclose the grout. After curing, the grout develops shear keys which act as mechanical hinges (Hussein et al. 2017). The main function of shear keys is to provide vertical shear load transfer between adjacent members. The shear resistance of such joints depends on the strength of the shear key geometry and the presence of TPT (Annamalai et al. 1990). Failure of shear keys result in uneven live load distribution, and an excessive increase in the relative displacements between adjacent girders which consequently create partial depth or full depth shear keys cracks allowing for deicing materials to penetrate through, and severely damage the concrete. Throughout the literature review, the performance of shear keys is studied in terms of the effect of grouting material, shear key location and shear key configuration. This section includes a summary of these studies.

2.4.1. Shear Key Materials

Gulyas et al. (1995) compared the performance of non-shrink grouts and magnesium ammonium phosphate (MAP) as grouting materials for shear keys. As shown in Figure 2.4, three types of tests were conducted including direct vertical shear test to simulate unequally distributed axle loads between adjacent girders, direct transverse tension test to simulate creep and shrinkage shortening of precast elements, and longitudinal shear strength test to simulate the unequal shortening between grouting material and connecting concrete member due to creep of concrete. Sixteen sub assemblages were cast and tested; two specimens were cast for each mortar type. Eight for non-shrink grout and eight for MAP mortar. The vertical shear test setup was conducted twice, for 203 mm (8 in.) and 305 mm (12 in.) deep shear keys, respectively. The longitudinal shear setup was conducted with the 305 mm-depth shear keys while the direct tension test was performed with the

203 deep shear key. The specimens with MAP mortars showed higher direct tensile bond strength, vertical shear, and longitudinal shear strength than those of the non-shrink grout specimens. In addition, MAP mortars showed significantly lower chloride absorption ability, which is beneficial for stopping chlorides' percolation to the underside of precast element through failed joints or grout itself.

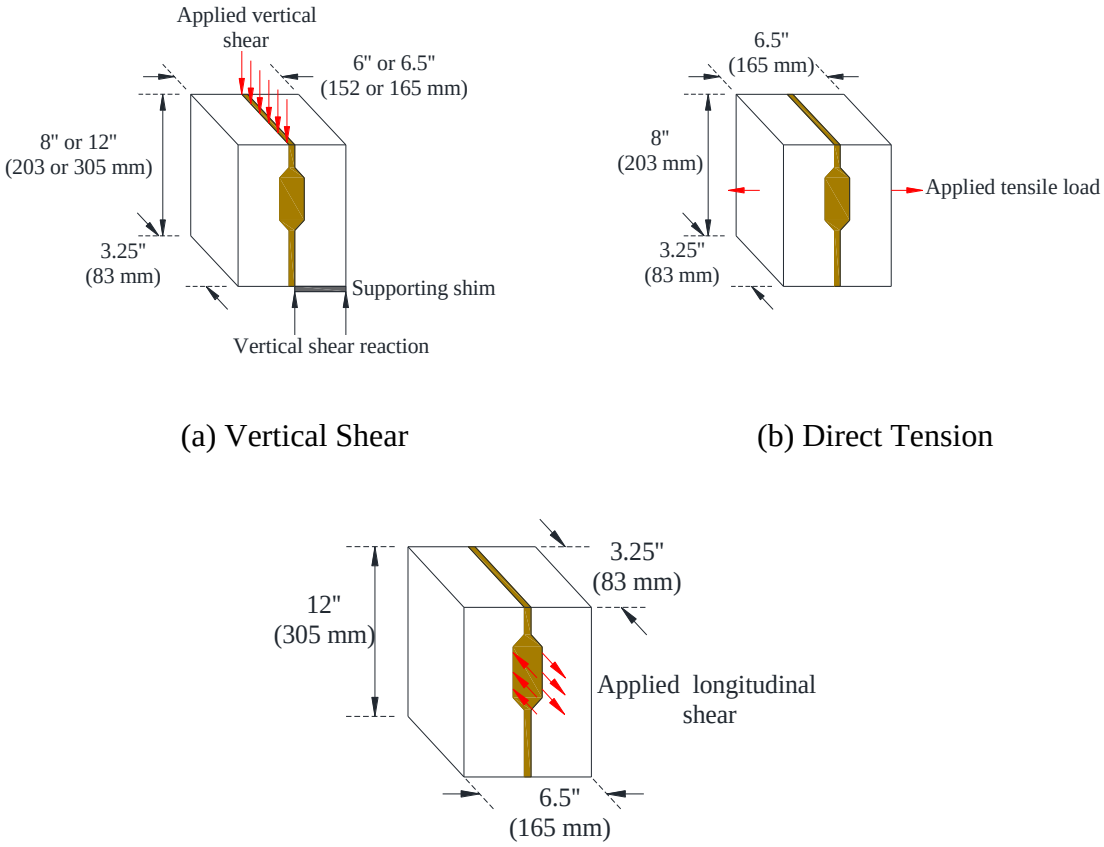

(a) Vertical Shear

(b) Direct Tension

(c) Longitudinal Shear

Figure 2.4 – Schematic of tested specimens (Reproduced from Gulyas et al. 1995)

Huckelbridge et al. (1997) studied the problem of shear key failure in adjacent precast prestressed box girder bridges and suggested a new shear key design detail based on both three-dimensional finite element model and experimental testing. In the three-dimensional finite element model, sub

assemblage of 12,192 mm (40 ft.) length by 3,658 mm (12 ft.) wide comprising three adjacent girders was analyzed. A concentrated wheel load of 44.5 kN (10 kips) was applied at the mid-span of the middle girder. Analytical results revealed that transverse tensile stresses due to that single concentrated load, considering the frequency and severity of the actual applied load, could lead to longitudinal cracking and shear keys failure. They concluded that shear key failure could be attributed to either failure of grouting material itself in case of low tensile stresses or bond failure between grouting material and connecting concrete member if high transverse tensile stresses were reached. To overcome this problem, the authors proposed using different grouting materials, shifting the shear key towards the girders' neutral axis, or changing the transverse post-tensioning design. Because of the experimental difficulties of having a full-scale model spanning 12,192 mm (40 ft.), a two-dimensional subassembly incorporating three adjacent girders of 305 mm (1 ft.) length in the longitudinal direction was tested. The subassembly was tested with a proposed new location for the shear key located near the neutral axis of the girders. The testing program also used different grouting materials with the proposed new shear key configuration.

The results showed that with the new shear configuration, the ultimate static load capacity was tripled from the traditional shear key design using the same grouting material. They recommended not using stronger grouting material other than non-shrink grout for the proposed configuration. Considering different grouting materials, the disadvantage of carbonated concrete surface sensitivity of MAP mortar outweighed its rapid setting advantage. The epoxy grout was very strong grouting material; however, its long-term behavior under thermal gradient cycles was mentioned to require more research since it had different coefficient of thermal expansion than girders' concrete. Finally, the authors proposed a watertight shear key design with a mid-depth shear key topped by a foam sealant, waterproofing membrane and asphalt overlay as shown in Figure 2.5.

Testing results also showed that this shear key design eliminated water leakage after fatigue testing; however, further studies were recommended.

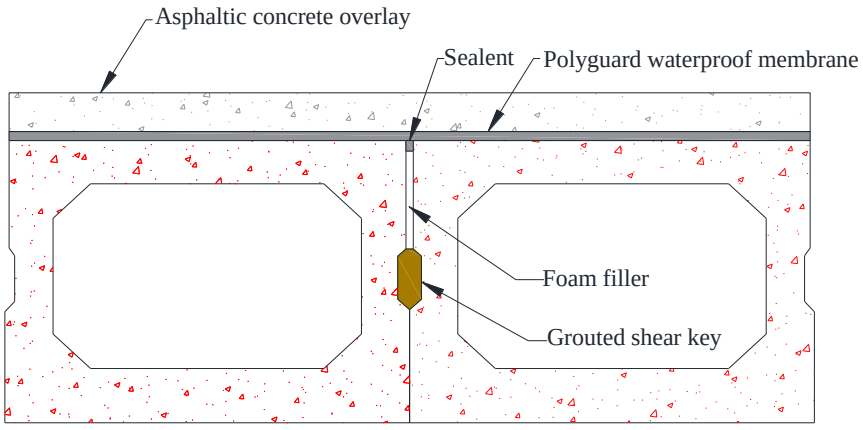

Figure 2.5 – Proposed water tight shear key design. (Reproduced from Huckelbridge et al. 1997)

Issa et al. (2003) evaluated the performance of different fillings for grouting shear key joints. Thirty-six specimens were tested in vertical shear, direct tension and flexural capacity to simulate real conditions experienced in the shear key. The materials used in the testing were set grout, set 45 for normal temperature, set 45 for hot weather, and polymer concrete. Polymer concrete showed the highest shear, tensile, and flexural strengths, lowest shrinkage, and rapidest setting among all types of the tested materials. In addition, chloride permeability tests were conducted by passing electric current through standard specimens and polymer concrete was found to be the least permeable. The authors recommended using polymer concrete in case rapid erection of bridge decks was required, this way, transverse post-tensioning could be applied one hour only after filling shear key joints. However, polymer concrete was very expensive and special surface preparation was required. Therefore, the authors recommended the use of polymer concrete in highly stressed joint locations and set grout for other joints.

2.4.2. Shear Key Location

Lall et al. (1998) compared the performance of full depth shear key configuration adopted in New York since 1992 to the conventional partial depth shear key design. Before 1992, precast adjacent girders were connected by 305mm (12 in.) partial depth shear key. Transverse post-tensioning was applied across the bridge width using one tendon of 133.4 kN (30 kips) located at girders mid depth for bridges spanning between 15,240 mm (50 ft.) to 22,860 mm (75 ft.) and five tendons distributed along the bridge quarter points for spans longer than 22,860 mm (75 ft.). Inspection results of 187 bridges, built between 1985 and 1990, showed that more than half of the studied bridges experienced longitudinal cracking. Consequently, in May 1992, the New York Department of Transportation (NYDOT) adopted a full depth shear key configuration with increased number of transverse post-tensioning; three for spans less than 15,240 mm (50 ft.) and five for longer spans. After adopting the new design detail, 21 out of 91 surveyed bridges showed reflective cracking. Of the 21 bridges, two showed longitudinal cracking of widths 0.8 mm to 1.6 mm and five had marks of leakage, while only two experienced cracking along more than half of its length.

Based on the inspection results, the authors concluded that the newly adopted full depth shear key configuration was capable of reducing reflective cracking. Additionally, the authors recommended using full width bearing pads, higher reinforcement ratio in the concrete deck and higher transverse post-tensioning amount distributed through two tendons at both the top and bottom of girders' depth. Figure 2.6 shows the shear key configuration adopted by NYDOT before and after 1992.

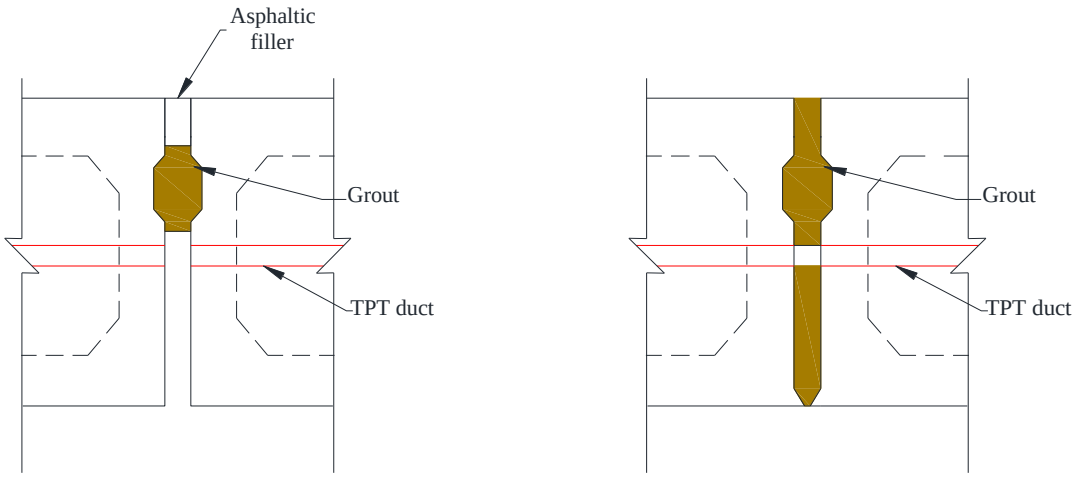

(a) Before 1992 (b) After 1992

Figure 2.6 – NYDOT transverse connection details (reproduced from Lall et al. 1998)

Miller et al. (1999) compared the performance of partial depth shear keys grouted with different filling material including non-shrink grout and epoxy, to a proposed mid-depth shear key configuration. Full scale testing was conducted on four girders assembly spanning 22,860 mm (75 ft). Five tie rods were used to transversely connect the girders before filling the shear key joints with the grouting material. The bridge model was loaded at mid-span by four actuators, each actuator applied a load of 10 kips, thus, a total load of 20 kips was applied at each transverse strip simulating the HS20-44 wheel load including an impact factor of 25%. For the bridge with shear key located at top depth, shear key cracking is observed before starting the test. This was attributed to the tensile strains developed due to thermal gradients and girders' misalignment. A 300 με was recorded at top surface of shear key joints, which was mentioned to be sufficient to initiate cracking. Under applied loads, the cracks continued growing without a definite reason, whether the crack propagation was attributed to applied loads or continuous exposure to environmental conditions. For the proposed mid-depth shear key, shorter cracks were observed before starting loading. However, only one crack propagated upon loading. Testing was re-conducted on typical

top depth shear key but with epoxy instead of non-shrink grout. No cracks were observed throughout testing. However, the coefficient of thermal expansion of epoxy was mentioned to be three times that of the concrete in the girders making the shear key more susceptible to cracks induced by thermal gradients. Based on the experimental program, it was concluded that thermal gradients were capable of inducing cracking in the top depth grouted shear keys with reduced effect on the mid-depth one. Epoxy-filled joints showed superior performance in cracks limiting but the coefficient of thermal expansion variation compared to concrete members could induce thermal stresses in the shear key. Another important observation was, regardless the presence of cracking, shear keys were capable of transferring load between adjacent girders.

2.4.3. Shear Key Configuration

El-Remaily et al. (1996) reviewed the Japanese practices in detailing adjacent box girder bridges. Longitudinal cracking was rarely reported in those bridges. The Japanese system followed the same design criteria and had similar cross-sectional shapes to those in the United States, except the fact that it had wider, and deeper longitudinal joints filled with cast in place concrete as shown in Figure 2.7. Higher amount of TPT was applied at four to seven equally distributed diaphragms along the bridge span. The amount and location of TPT were determined from flexure design. Finally, 50 to 80 mm cast-in-place concrete or asphalt wearing surface was used to cover those bridges.

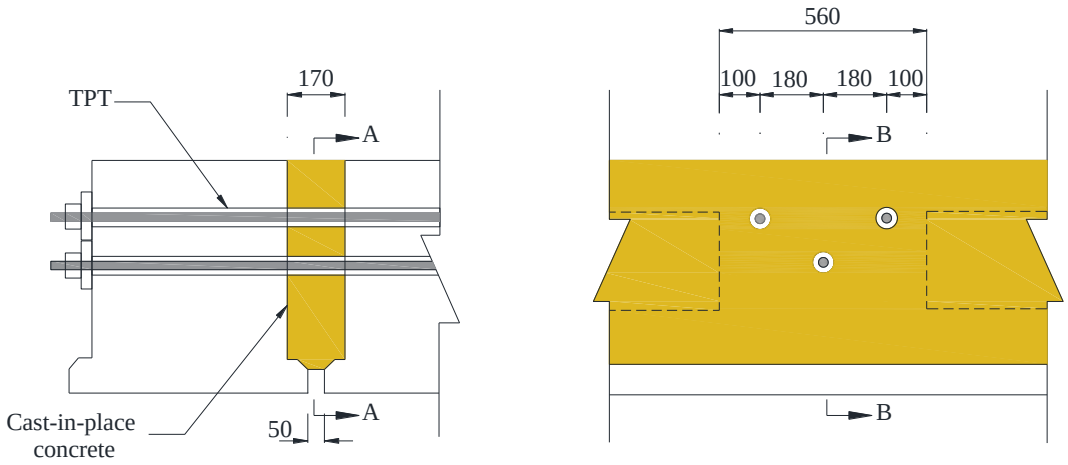

(a) Section A-A (b) Section B-B

Figure 2.7 – TPT detail for Japanese box girder bridges (reproduced from EL-Remaily et al. 1996)

2.4.4. In-Situ Performance of Grouted Shear Keys

Huckelbridge et al. (1995) conducted a series of six field tests to prestressed box girder bridges aimed at investigating the grouted shear keys performance located at the longitudinal joints of adjacent girders. Five different box girder bridges were tested. The authors discussed the results of three tests in that report. A 20° skewed single span bridge carrying two traffic lanes was tested prior and after deteriorated joints' repair caused by deicing salts penetration through the deck surface. The other bridge carried four lanes over four continuous spans with 17.5° skew alignment. A dump truck of leading axle load of 53.3 kN (12 kip) and 84.7 kN (19 kip) for each of the tandem axles was used to perform the onsite multiple passage testing. The tested bridges were instrumented by relative displacement transducers and foil strain gauges attached to the bottom surface of girders at mid-pan to measure the inter-girder displacements and live load bending moments strains respectively. Based on finite-element analysis and field observations the authors recommended a maximum threshold for relative displacement between intact adjacent girders of 0.0254 mm, exceeding this value was assumed by authors to have at least partially cracked shear

key along its length. For the tested bridges, fractured shear keys were obviously located in the vicinity of the loaded truck wheel position and exhibited relative displacement between 0.08 mm and 0.5 mm. Inter-girder displacement was not limited to the distressed joints exhibiting water leakage and reflective cracking in the deck above, but also joints located nearest to wheel tracks.

2.5. Transverse Post-Tensioning and Diaphragms

Transverse post-tensioning when used can help to reduce differential deflections between adjacent girders by applying clamping stresses. The LRFD-9 (AASHTO 2020) and CHBDC (CSA 2019a) requirements of minimum prestress of 1.7 MPa is ambiguous. It is not clear through which area the TPT should be applied (El-Remaily et al. 1996; Lall et al. 1998; Hanna et al. 2009; Grace et al. 2010; Hanna et al. 2011; Russell 2011; Hansen et al. 2012; Yuan et al. 2016; Semendary et al. 2017). In double tee girders, it is obvious that the flange area is that to be considered (El-Remaily et al. 1996). Therefore, many studies have been conducted to determine the required transverse stresses that will make the bridge behave monolithically in the transverse direction.

Annamalai et al. (1990) conducted push-off tests on transversely post-tensioned grouted shear key small assemblies. Twenty-eight specimens were tested up to the maximum shear load. The studied parameters were the number of shear keys, joints thickness, level and distribution of the transverse post-tensioning. One, two and three shear keys configurations were tested, joint thickness varied from 25 to 75 mm, level of transverse post-tensioning varied from 0 (No TPT) up to 6.90 MPa (1000 psi), and the TPT was linearly varied along specimens' height. The authors concluded that transverse post-tensioning significantly enhanced the shear strength and the monolithic action of grouted shear key connections. Specimens of three shear keys showed higher rigidity than those of two. For the same prestress level, 25-mm thick joints showed higher shear strength than those of 50-mm thickness. In addition, a prestress of 800 psi was found adequate to exhibit monolithic

action without the need of shear keys. Furthermore, shear strength was found not affected by prestress variation along the specimens' height. Based on those experimental tests, they finally introduced an equation (Equation 2.1) to estimate the shear strength of transversely post-tensioned grouted shear keys connection.

$$\frac{v_n}{f_c} = 0.16\frac{B}{A_{cr}} + 0.66\frac{N_p}{A_{cr} f_c} \qquad \text{(Equation 2. 1)}$$

where;

v_n = Nominal shear strength of connection

f_c = Compressive strength of grout

B = Area of vertical section through all the concrete keys

A_{cr} = Area of concrete section resisting shear along the crack interface

N_p = Prestressing force across the connection

El-Remaily et al. (1996) proposed a new precast prestressed box girder bridge design requiring the deck to act as a rigid assembly of longitudinal and transverse members. The study advocated the significant role of diaphragms in limiting differential deflection among adjacent girders and distributing live loads in the transverse direction. Without diaphragms, each box girder would be designed to carry full wheel load without any contribution of adjacent girders and consequently larger differential deflections followed by reflective cracking in the above overlay, if exists, occurs. However, if integrity among adjacent girders is guaranteed, load is transversely distributed across the full bridge width and smooth deflection curve is obtained. For spans up to 30,500 mm (100 ft.), the use of five diaphragms uniformly distributed at quarter-span points outweighed the three diaphragms located at both ends and mid-span in limiting differential deflection to less than

0.02 in. (0.5 mm). Despite using three diaphragms required less transverse post-tensioning, it might result in unacceptable differential deflection. An insignificant change was proposed to allow grouting at diaphragms locations; a recess of 25 mm was provided at each side of each girder as shown in Figure 2.8. A grillage analysis was adopted by modeling adjacent girders as a series of longitudinal beam elements transversely connected by cross beams resembling the diaphragms. The authors provided charts for TPT determination for standard girder depths and common widths as shown in Figure 2.9. Charts were developed for both quarter and mid-span diaphragms. However, 250 psi prestress was recommended for end diaphragms' cross-sectional area to ensure adequate stiffness at the bridge ends. The authors also recommended applying transverse post-tensioning, equally distributed between both top and bottom of the diaphragm, after grouting shear keys. In addition, full-depth vertical shear keys at each diaphragm location was suggested. Post-tensioning seemed to be constant along the bridge span and significantly variable with the bridge width. The developed charts were then adopted by PCI Bridge Design Manual (PCI 2003).

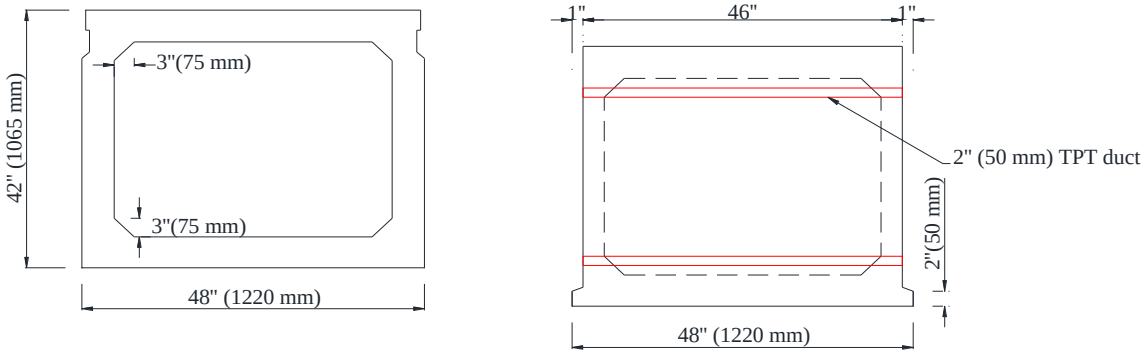

(a) Original precast girder (b) Modified precast section at diaphragms

Figure 2.8 – Modifications to precast concrete sections (Reproduced from El-Remaily et al. 1996)

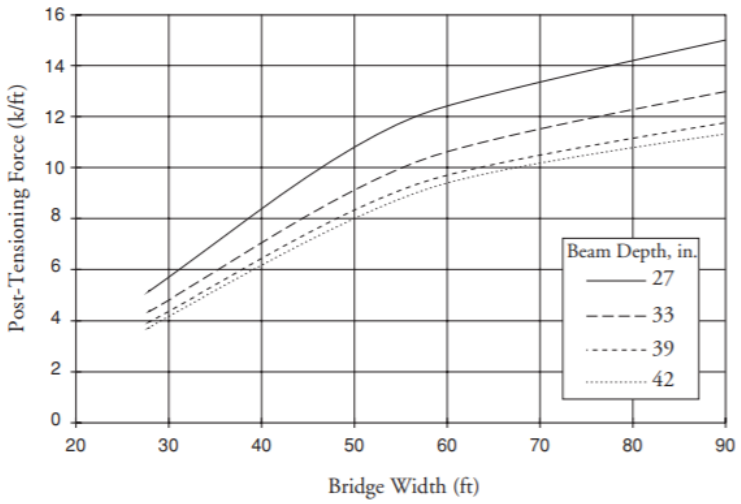

Figure 2.9 – TPT forces for quarter and mid span diaphragms (PCI Bridge Design Manual 2003)

The developed design charts by El-Remaily et al. (1996) were limited to bridges with mild skew angles (less than 15 deg.), medium span lengths, and AASHTO HS-25 truck loading. Hanna et al. (2009) updated the aforementioned design charts to consider highly skewed bridges with different span lengths and the AASHTO LRFD-3 (AASHTO 2004) specifications for truck and lane live loads (HL-93) including dynamic load allowance of 33% for truck load only. Grid analysis was used to calculate TPT forces considering these variables. The updated charts exhibited an increase up to 40% in the required TPT for adjacent box girder bridges. Results showed that required TPT is primarily affected by the bridge width and girder depth, that is, for a given girder depth, a higher amount of TPT was required as the bridge width increased. Additionally, for the same bridge width, shallower girders required higher TPT than deeper ones as shown in Figure 2.10. Skew angles had insignificant effect on the required TPT per unit length for deeper girder used in longer spans; however, highly skewed shallower girders required more TPT forces. The authors proposed a simplified design equation (Equation 2.2) to calculate the required TPT forces per unit length of

the bridge accounting for its width, span to depth ratio, and skew angles. The proposed equation showed an average deviation of 7.7% from the grid analysis.

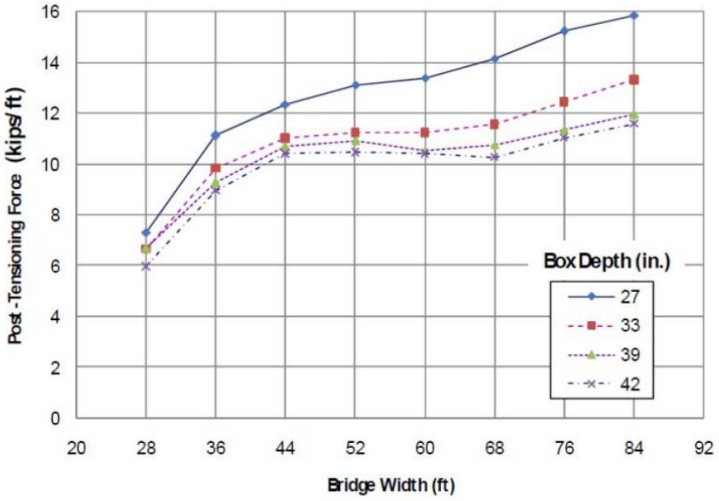

Figure 2.10 – TPT forces for quarter and mid span diaphragms (PCI Bridge Design Manual 2014)

$$P = \left(\frac{0.9w}{D} - 1\right)(K_l K_s) \le \left(\frac{0.2w}{D} + 8\right)(K_l K_s) \qquad \text{(Equation 2. 2)}$$

where,

P is the required transverse post-tensioning force (kip/ft.),

w is the bridge width (ft.),

D is box girder depth (ft.),

K_l is a correction factor for span-to-depth ratio $K_l = 1 + 0.003\left(\frac{L}{D} - 30\right)$,

K_s is a correction factor for skew angle more than 0 degrees = 1.0 + 0.002 θ,

L is the bridge span (ft.), and

θ is the skew angle (deg.).

Aktan et al. (2009) performed finite element modeling (FEM) to evaluate the effect of TPT value and location, number of diaphragms, the bridge width and the material properties on the behavior of side-by-side adjacent precast prestressed box girder bridges. The model comprised three 15,240 mm (50 ft.) long box girders connected with full depth shear keys. For the same grouting material, decreasing the number of transverse diaphragms from five to three had an insignificant effect on transverse strain distribution measured along the shear key at the girders' mid-depth as shown in Figure 2.11. The five diaphragms configuration reduced girders' differential displacements by 0.12 mm (0.005 in.) compared to similar model with three diaphragms. The authors concluded that transverse clamping stress primarily transferred through stiffer diaphragms, shear keys in between, were non-stressed or under tension and unable to prevent water leakage without adequate compressive force. Transverse post-tensioning had insignificant effect on limiting mid-span deflections as long as shear keys were kept intact. However, transverse post-tensioning was required to increase the system's redundancy and to guarantee load transfer among adjacent girders. AASHTO LRFD-3 (AASHTO 2004) recommendations of minimum clamping prestress of 250 psi was concluded to be unachievable even at points of stress concentration within diaphragms locations.

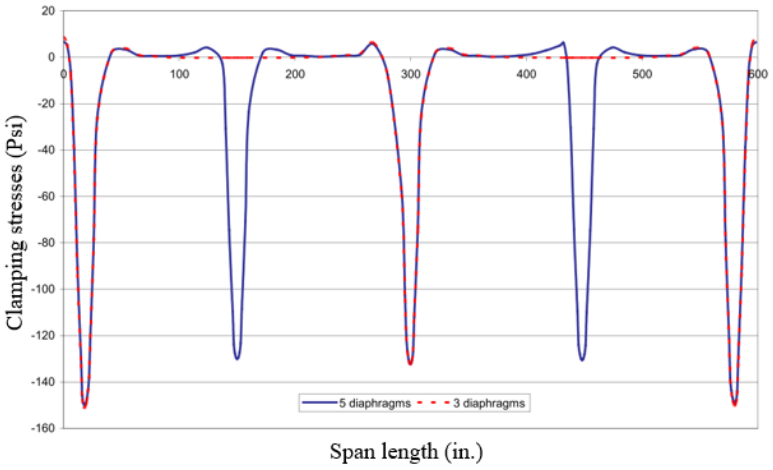

Figure 2.11 – Number of diaphragms effect on transverse strain (Aktan et al. 2009)

The use of carbon fiber-reinforced polymer (CFRP) prestressing tendons for TPT was studied by Grace et al. (2010). A 30° skewed half-scale precast prestressed adjacent box girder bridge model was tested. The model consisted of four precast prestressed girders placed side-by-side, forming a full depth female-to-female shear keys, and topped by 75-mm reinforced deck. Each girder was 457 mm (18 in.) wide, 355 mm (14 in.) deep and a total span of 9,450 mm (31 ft.). Five transverse diaphragms were provided at an equal spacing of 2,286 mm (7.5 ft.) to accommodate transverse post-tensioning tendons. To simulate differential camber usually observed in field, different amounts of prestressing forces were applied to the individual girders. The testing program aimed at studying the effect of transverse post-tensioning forces and the number of diaphragms on transverse strain and load distribution of those bridges. The testing program was conducted in three phases simulating what a real highway box girder bridge might face during its service lifetime, namely; uncracked deck slab, cracked deck slab, and damaged beam replacement phase. Three different tests were conducted on the bridge model including strain distribution test, load distribution test and ultimate load test. The strain distribution test was conducted by varying the level of transverse post-tensioning forces at different diaphragms arrangements and monitoring the

transverse strains captured by strain gauges mounted on the deck slab over shear key locations. The load distribution test was conveyed by applying a single point load of 67 kN (15 kip) on each girder for different arrangement of transverse post-tensioning forces and different number of transverse diaphragms as well. Deflection of girders was monitored using linear displacement transducers attached to the bottom of all girders at mid-span. In the ultimate load test, the bridge model was loaded at one interior girder using two-point loading frame up to failure to evaluate the behavior of CFRP strands and to determine the bridge model ultimate load capacity. A non-uniform distribution of transverse post-tensioning forces along the bridge model was observed. Under increasing the levels of transverse post-tensioning forces, points located along the post-tensioned diaphragms experienced higher transverse strains compared to those located between points of TPT application. Tests results also showed that increasing the number of diaphragms did not affect the differential deflection among adjacent girders and had insignificant effect on the transverse strain developed between diaphragm areas, as long as adjacent girders were kept intact. However, notable improvement in deferential deflection and load distribution among adjacent girders was observed in cracked deck slab testing phase. It was also observed that none of transverse post-tensioning arrangement produced uniform compression of 1.7 MPa along the entire bridge length as per AASHTO LRFD recommendations.

Fu et al. (2011) introduced a new approach for transverse post-tensioning design for adjacent precast solid multi-beam bridges without diaphragms based on shear friction concept. Finite element modeling was used to validate actual strains measured from field-testing. Solid beams, shear keys, topping and curbs were modeled with solid elements while link elements were used to model transverse post-tensioning. Three boundary conditions were considered in the analysis, which were, pinned connection at both ends, pinned at one end whereas the other end was sliding,

and pinned at one end with spring at the other end which successfully presented the onsite tested bridge behavior. The onsite tested bridge composed of eleven 10,970 mm (36 ft.) long adjacent solid girders topped by 150 mm-thick concrete deck. The girders were connected with 178 mm-high shear keys and transversely post-tensioned with 25.4 mm in diameter tie rods distributed at one-third points of the bridge span. Tests results showed that structural integrity was not significantly affected by transverse post-tensioning forces as long as shear keys were kept intact. However, once shear keys and above overlay cracked, transverse post-tensioning contributed to bridge's monolithic behavior and prevented further deterioration. The authors recommended transverse post-tensioning of 311 kN (70 kip) for spans shorter than 12,190 mm (40 ft.) and 489 kN (110 kip) for longer spans to replace the previously 133 kN (30 kip) used by the state department of transportation. The coefficient of friction between precast beam-shear key interfaces played an important role to determine the required TPT. A lower TPT force was required to ensure monolithic integral behavior as the coefficient of friction increased. The authors recommended tensioning the transverse rods to one-sixth of the design level before casting the shear keys, then the rest of TPT to be applied after filling the shear keys. In addition, full depth shear keys among girders were suggested to mitigate shear keys and overlay cracking.

The behavior of adjacent precast prestressed bridges under combined effect of thermal gradients and traffic loads was studied by Grace et al. (2012). Field observation, experimental testing and numerical modeling were conducted to evaluate the minimum TPT arrangement required to eliminate longitudinal deck cracking. Field observation was conducted on two bridges, the first bridge consisted of six 690-mm deep adjacent girders spanning 15,200 mm topped by a 230-mm thick deck slab. The bridge was provided with three diaphragms located at both ends and mid-span. Daily temperature changes resulted in positive and negative temperature gradients were

monitored over one-year period. The second bridge consisted of 22 side by side precast girders, each girder had a width of 1200 mm and a depth of 1220 mm and topped by a 150-mm thick deck slab. Experimental testing was conducted on half-scale bridge model to determine the load deflection response due to traffic load under different TPT levels. The bridge model comprised four box girders connected by transversely post-tensioned diaphragms and full depth shear keys. Finite element model was used to verify the experimental half scale model under traffic loads then extended to simulate the combined effect of traffic load and temperature gradient. The results revealed non-uniform stress distribution of TPT forces with local concentration of transverse strains at diaphragms locations. The minimum number of diaphragms required to eliminate longitudinal cracking increased with increasing the bridge span. However, increasing the bridge width required higher amount of TPT forces per diaphragms to mitigate such cracks. The required TPT slightly decreased when using higher strength concrete in deck slab and was independent of the widths of individual girders. Finite element models showed that positive temperature gradient was the main contributor for longitudinal deck cracks in side by side box girder bridges. Under positive temperature gradients, adjacent girders tended to separate from one another generating high tensile stresses at the bottom of deck slab, which in turn, resulted in longitudinal cracks.

Hussein et al. (2017) investigated the contribution of tie bars and high strength bars to the load distribution in precast prestressed adjacent box girder bridges under static and dynamic loading using field observations and finite element modeling (FEM). The inspected bridge was 15,500 mm long, single span that consisted of precast prestressed adjacent box girders. The bridge consisted of six adjacent girders, each was 1220 mm in width and 690 mm in height. The adjacent girders were connected by 178 mm partial depth shear keys along with transverse post-tensioning tie bars housed in diaphragms provided at the span's third points and topped by 50 mm pavement layer. The bridge

was instrumented by longitudinal strain gauges, thermocouples, and linear variable differential transformer sensors to measure strains and deflection throughout the onsite controlled testing program. Based on the FEM and field observations, it was concluded that tie bars effectively contributed to the load transfer mechanism under both static and dynamic loads, oppositely to earlier research assumptions of limited bars' contribution up to shear key cracks initiation. Dynamic load allowance recommended by AASHTO LRFD bridge design specification was concluded to be insufficient. The maximum observed relative displacement was 0.04 mm below the range of 0.08 mm-0.5 mm suggested by Huckelbridge et al. (1995) to have intact shear keys. Joints movements of -0.17, and 0.03 mm were observed under multiple loading conditions, i.e., different truck locations, where the negative sign indicates joint closing. The authors concluded that the initial transverse post-tensioning force applied to the tie bars played an important role in limiting relative displacements and enhancing the load distribution between girders. High strength bars outperformed conventional grade 60 tie bars in terms of load distribution and girders' relative displacements. Based on the strains measured in tie bars before loading over 10 months-period, thermal gradients and environmental loads caused load distribution among adjacent girders. However, the authors recommended further research to investigate TPT bars behavior under environmental loads.

2.6. Innovative Transverse Connections

2.6.1. Diaphragm-Free Box Girder Bridges

Generally, the efficiency of intermediate transverse diaphragms provision in bridges has been questionable. The use of intermediate diaphragms in precast prestressed concrete box girder bridges (not adjacent girders) has been surveyed in all U.S state departments of transportation and seven Canadian provinces. Abendroth et al. (1995) presented the results of that survey, 85% of the responding design agencies required the use of intermediate diaphragms. Of these, 50% required diaphragms at mid-span, 30% required diaphragms to be located at one-third-points of the span, and 10% of the agencies positioned diaphragms at the quarter-points of the span. While many researchers concluded that intermediate diaphragms provision increase girders' susceptibility to damage induced by lateral and impact loads. (Sithichaikasem et al. 1972; Sengupta et al. 1973; Cheung et al. 1986), others advocated the presence of intermediate diaphragms in terms of improving live load distribution and reducing girders design moments and deflections (Kim et al. 1997; Eom et al. 2001).

Hanna et al. (2011) proposed two new transverse connections for precast prestressed adjacent box girder bridge based on the elimination of intermediate diaphragms, concrete topping, and the use non-post-tensioned interfaces to transfer shear, torsion, and flexure among adjacent girders. These two connections were entitled the wide joint system and the narrow joint system. For the wide joint connection, full depth, full length shear keys filled with concrete were used to accommodate top and bottom transverse reinforcement to form monolithic continuous joint capable of transferring both shear and moment between adjacent girders. To house the proposed reinforcement, modifications to the standard 850 mm deep and 1200 mm wide AASHTO PCI box section were introduced. The modifications included 65 mm (2.5 in.) recesses at the bottom flange

to form the 130 mm (5 in.) full depth shear keys, and block outs in both top and bottom flanges spaced at 1220 mm (48 in.) as shown in Figure 2.12. Reinforcing bars protruded through these block outs from the top and bottom flanges and spliced by a 6 mm (1/4 in.) thick coiled wire to ensure adequate development length. Self-consolidation concrete was recommended to substitute costly and lengthy grouting process.

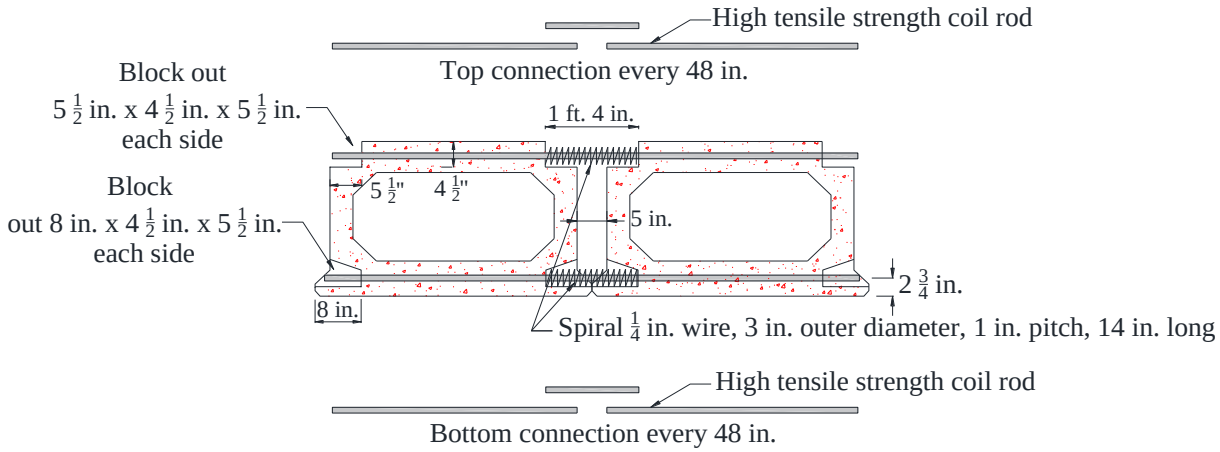

Figure 2.12 – Wide joint transverse connection detail (Reproduced from Hanna et al. 2011)

For the narrow joint connection detail, the standard box section was modified to house plastic ducts in both top and bottom flanges. The bottom duct was placed between the longitudinal prestressing layers, while the top duct was provided 75 mm from the top fiber to maintain adequate concrete cover as shown in Figure 2.13. The plastic ducts contained 520 MPa threaded rods provided at 2.4 m (8 ft.) interval to have continuous connection at the top and bottom flange that was able to efficiently transfer shear and moment between adjacent girders.

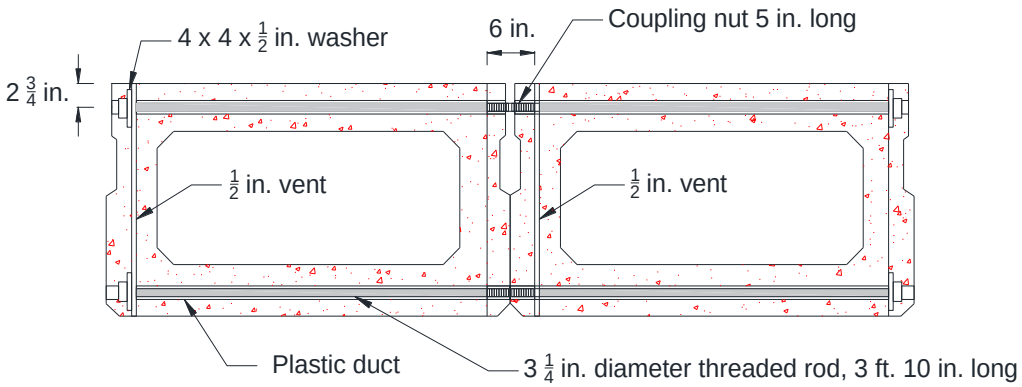

Figure 2.13 – Narrow joint transverse connection detail (Reproduced from Hanna et al. 2011)

Finite element models were prepared to study the effect of span length, bridge width and girders depth on the proposed connections. The AASHTO LRFD-4 (AASHTO 2007) live load combined with dynamic allowance factors were applied to calculate the required reinforcement. Design charts were provided for each connection incorporating different width (ranging from 8,500 to 2,600 mm); span-to-depth ratio of 25, 30 and 35; and standard depth of 690, 840, 990, and 1,070 mm. Based on the results, the authors observed an increase in connection reinforcement corresponding to the increase in bridge width and span-to-depth ratio. However, the required reinforcement decreased as the bridge depth increased. Experimental testing under static and repeated cyclic loading for the proposed two connections, along with a currently used detail by Illinois Department of Transportation (IDOT), was conducted. Each specimen composed of two 2,400-mm long girders rested on 300-mm wide steel beams. Each girder had a 1200-mm width and a 690-mm depth. The load was applied at a distance of 130 mm from the centerline of the assembled girders through a360-mm square loading plate. The current IDOT detail was loaded by 81.8 kN cyclic load simulating the fatigue wheel load for 10,000 cycles after which the joint failed and leakage occurred. Another cyclic load test with an amplitude of 81.8 kN was conducted after casting a 130 mm non-composite deck. The specimen sustained 2 million cycles maintaining its

stiffness and failed ultimately at 616.9 kN (138.7 kip). The wide connection was tested with the same load amplitude under static and cyclic loads and no stiffness deterioration nor leakage occurred and ultimately failed at 721 kN (162 kip). Similarly, the narrow joint connection was tested with no signs of leakage and stiffness loss until failure at an ultimate load of 694 kN (156 kip). Accordingly, based on experimental test results, it was concluded that the new proposed connections could have similar performance to the post-tensioned connection, but more economical and easier in application.

Hansen et al. (2012) proposed a modified connection detail based on the narrow joint connection introduced by Hanna et al. (2011) to allow for post-tensioning of high strength rods as shown in Figure 2.14. The system eliminated the need of intermediate diaphragms and concrete topping as means of transverse load distribution mechanism by providing a connection capable of transferring shear and moment in the transverse direction.

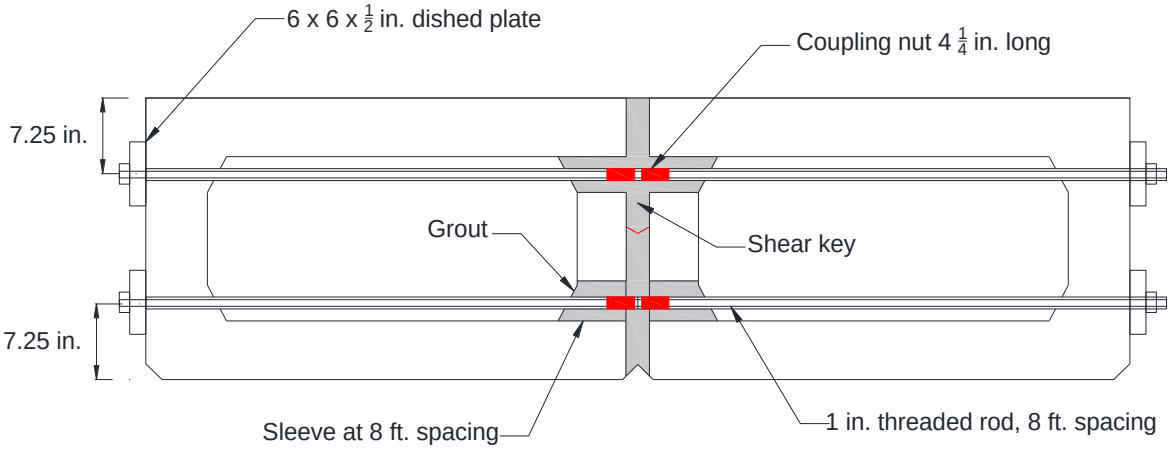

Figure 2.14 – Modified narrow joint detail (Reproduced from Hansen et al. 2012)

Sleeves were introduced above the girders' bottom flanges and below the top flanges to house ducts, high strength steel rods, and couplers. The required post-tensioning forces were calculated

based on the design chart developed by Hanna et al. (2009). Experimental testing included the applying of 82 kN (18.4 kip) for 5 million cycles at an exterior joint of four girders assembly supported at center and opposite end, was conducted. This way, maximum tensile stresses were induced in top flange. No cracking or strain change at loaded joint was recorded during testing. The supports were then moved to both ends to have mid span maximum loading configuration. Similarly, no cracking or strain change at loaded joints was recorded when a load of 77.4 kN (17.4 kip) was applied for 5 million cycles. The authors recommended using this system to have a comparable performance to traditional connections using transverse post-tensioned intermediate diaphragms.

Sun et al. (2018) reviewed the St. Clair Bridge, Michigan. A diaphragm-free, simple-span, adjacent box girder bridge was implemented with a span of 26,000 mm (85 ft.) and a width of 7,670 mm (25 ft. 2 in.). The bridge consisted of six adjacent precast girders connected by full depth shear keys and transversely post-tensioned by two pairs of tendons placed in the top and bottom flanges of the girders and equally distributed at 4,940 mm (16.2 ft.) intervals. Each tendon contained three 15-mm diameter, Grade 1,860 MPa mono-strands. The amount of post-tensioning was calculated based on PCI bridge design manual charts developed by Hanna et al. (2009) and verified by FEM. The transverse post-tensioning strands were housed in polyethylene sheathing which in turn housed in PVC tube. This system eliminated the intermediate diaphragms and resulted in lighter concrete sections. This innovative system allowed for future widening due to the use of un-bonded tendons and achieved higher durability by preventing water leakage and eliminating reflective longitudinal cracks. Figure 2.15 shows the used transverse connection detail.

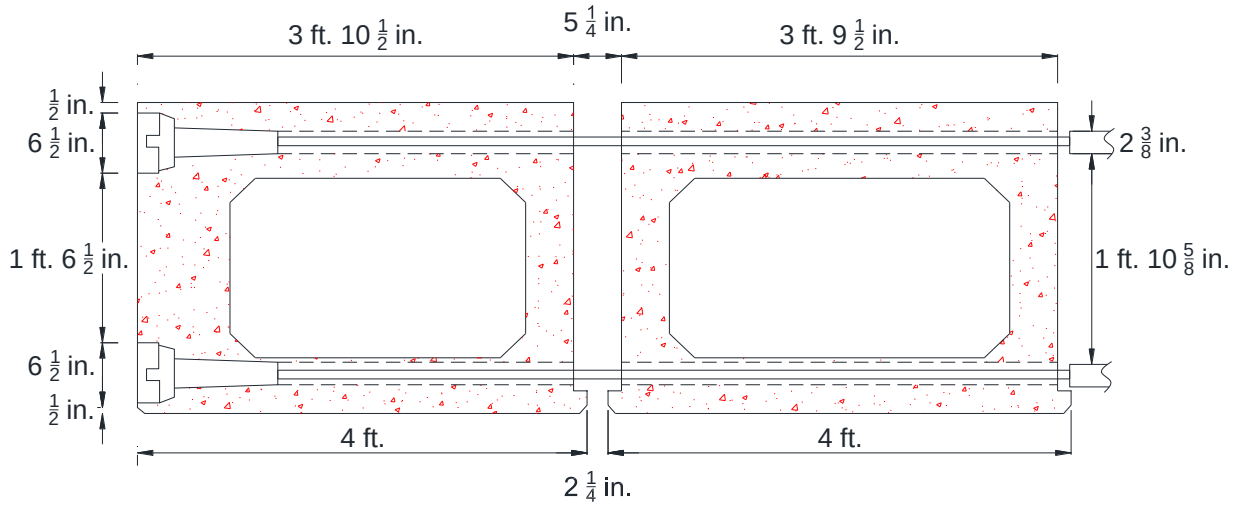

Figure 2.15 – Transverse connection detail of The St. Clair bridge, Michigan (Sun et al. 2018)

2.6.2. Ultrahigh-Performance Concrete (UHPC) Connections

In the past few years, the Federal Highway Administration (FHWA) has authorized the use of ultrahigh-performance concrete (UHPC) as a connecting material in the precast applications. The UHPC is characterized by superior compressive and tensile strengths, as well as durability performance. Such concrete can exhibit a compressive strength between 120-200 MPa and an increased impermeability compared to conventional connecting materials (Graybeal 2006 & 2014; Hussein et al. 2018). In Northwestern Ontario, Rahman et al. (2016) reported the construction of 42 adjacent box girder bridges with UHPC shear keys.

Yuan et al. (2016) conducted full scale testing to compare the performance of transverse connections considering traditional non-shrink grout in combination with transverse post-tensioning to those developed using ultra high-performance concrete (UHPC). Four types of shear keys were tested, two per each connection as shown in Figure 2.16. The UHPC connection detail included non-contact lap splice extended from each side of the precast girders with no TPT nor diaphragms.

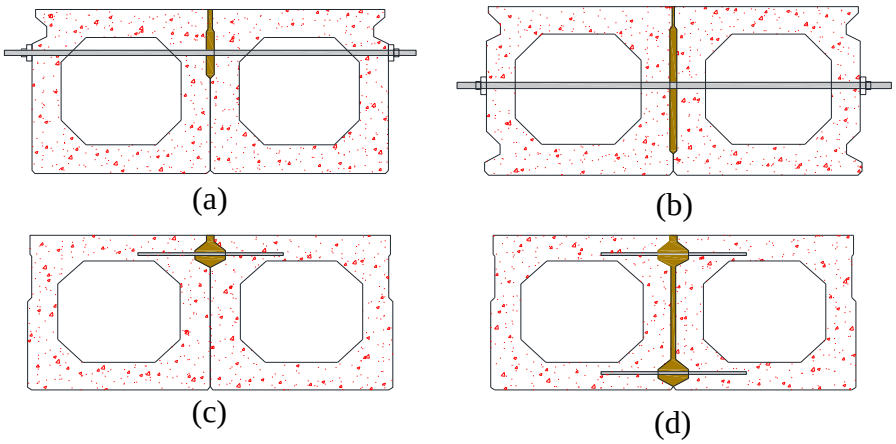

Figure 2.16 – Shear key connections: (a) partial-depth conventional grout; (b) full-depth conventional grout; (c) partial-depth UHPC; (d) full-depth UHPC (Yuan et al. 2016)

The four shear key configuration were tested under thermal and cyclic loading with different TPT values for the conventional connection. A four-point loading configuration was adopted by applying point loads 152 mm away from the girders' centerline to have more severe torsional moments. The applied loads were out of phase by 180°; i.e., one girder was maximally loaded while the load was kept minimum for the other girder. Thermal loading was obtained by pumping steam in the top flanges and a temperature gradient of 28° C along the girders' depth was created. All connections were perfectly intact before cyclic loading except for the full depth conventional grout connection which exhibited cracking resulted from TPT removal after grouting process. During cyclic loading test, all connections were intact under millions of cycles including the partial depth conventional shear key connection along with the two UHPC connections. The cyclic loading test was re-conducted after cracking the shear keys. Moment distribution and differential deflections were measured by strain gauges and linear variable differential transformers (LVDTs) attached to girders' bottom flanges at mid span. The partial-depth conventional shear key connection was loaded under different levels of TPT levels of 45, 222, and 445 kN. Based on the experimental observations The authors concluded that TPT had insignificant effect on the

transverse behavior of partial depth conventional shear key connections when shear keys were perfectly intact, intact connections effectively distribute the load among adjacent girders with limited differential deflection of 0.127 mm (0.005 in.), this observation was reached by obtaining similar strains and deferential deflections for both intact and cracked shear key connections. However, under no TPT, differential deflections tended to increase under increasing the applied load. UHPC performed very similar to conventional grouted connections in terms of differential deflections and moment distribution among adjacent girders with the advantage of limiting crack width by the means of the extended steel reinforcement distributed along the connection's length. The authors recommended the partial depth UHPC connection to have comparable performance requirements to the conventional post-tensioned connection.

Semendary et al. (2017) studied live load-moment distribution factors (LLMDFs) for a precast prestressed adjacent box girder bridge with a new ultra-high-performance shear key connection and non-contact lap splice bars. The bridge did not incorporate transverse post-tensioning, intermediate diaphragms, or composite topping. Since this connection was recently developed and it was not clear under which category of AASHTO LRFD bridge design specification it should lie, LLMDFs were evaluated using static truck onsite testing and validated by finite element modeling. The investigated bridge was an 18,600 mm single span bridge of an overall width of 8,500 mm. the bridge's super structure consisted of seven adjacent precast girders transversely connected by partial depth UHPC-grouted shear keys and No.4 dowel bar forming non-contact lap splice of 121 mm length as shown in Figure 2.17. Diaphragms were only provided at both ends of each girder.

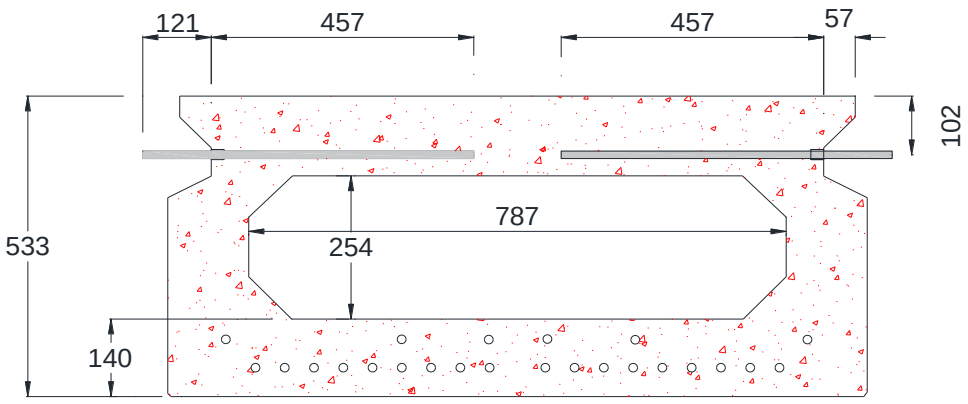

Figure 2.17 – Transverse connection detail (Semendary et al. 2017)

Based on experimental investigations, LLMDFs provided by AASHTO LRFD bridge design specification were conservative for exterior and interior girders by 4.3% and 12.7% respectively, assuming an integral one-unit bridge behavior. When this connection was assumed to vertically transfer shear at the interface (hinges), the AASHTO LRFD bridge design specifications were conservative for exterior and interior girders by 41.3% and 46.4% respectively. The joints were concluded to act in a continuous monolithic behavior transferring shear forces and bending moments. However, the authors recommended further studies to assure this observation.

In another study, Semendary et al. (2018) investigated the long-term behavior of adjacent precast prestressed concrete box girder bridges with a new UHPC shear key connection and non-contact lap splice bars. The investigated bridge did not incorporate TPT, intermediate diaphragms, or composite topping. The bridge was of a single span and consisted of seven adjacent girders. The bridge had a total length of 18,600 mm and an overall width of 8,500 mm. Similarly, the movement of the joints in the transverse direction were monitored at the bottom of the girders using horizontal LVDTs. Relatively small movements were observed with the change in temperature, where joints closed

when temperature decreased and vice versa. The maximum recorded joint movement ranged between -0.077 mm and 0.045 mm, where the negative sign indicates joint closing.

3. ADJACENT CONCRETE BOX GIRDERS TRANSVERSELY POST-TENSIONED AT TOP FLANGES ONLY: EXPERIMENTAL INVESTIGATION

Authors and Affiliation:

- Shady N. Labib, M.Sc. Student, Department of Civil Engineering, University of Manitoba.
- Mohammed G. El-Gendy, Structural Engineer, Tetra Tech Canada Inc., Winnipeg, MB, Canada.
- Ehab F. El-Salakawy, Professor, Department of Civil Engineering, University of Manitoba.

Journal and Status: American Society of Civil Engineers, ASCE, Journal of Bridge Engineering, published on February 4, 2021.

Reference:

Labib, S., El-Gendy, M., and El-Salakawy, E. (2021). "Adjacent Concrete Box Girders Transversely Post-Tensioned at Top Flanges Only: Experimental Investigation." ASCE, Journal of Bridge Engineering, 26(4): 04021017. DOI: 10.1061/(ASCE)BE.1943-5592.0001699.

Note:

The manuscript had been slightly edited from the original paper by renumbering the tables and figures to include the chapter number. In addition, the reference list and list of notations have been moved to the appropriate sections in the thesis as indicated in the table of contents.

Abstract:

In this study, a new transverse post-tensioning (TPT) technique for box girder bridges is investigated, where TPT is applied at the top flange of the girder resulting in eliminating the intermediate transverse diaphragms. A one-third-scale bridge model consisting of four adjacent box girders with partial-depth shear keys was erected and tested. The bridge model was investigated for the optimal TPT force and spacing to ensure a uniform distribution of the clamping prestress. The efficiency of the proposed technique in transversely distributing live loads during simulated service and ultimate conditions was also investigated. Test results demonstrated that distributing the TPT force at a shorter spacing along the length of the bridge is more efficient than increasing the TPT force at discrete distant locations in producing the minimum required concrete prestress. It was observed that the effect of TPT force and spacing was insignificant during the simulated service condition, where shear keys remained intact or partially cracked. However, at failure, the presence of TPT added redundancy to the bridge model and mitigated any sudden failure when shear keys were fully cracked.

Author Keywords: Adjacent box girders; Transverse post-tension; Diaphragm; Shear key; Prestress.

3.1. Introduction

Adjacent precast, prestressed concrete box girder bridges are widely used in short- and medium-span bridges, due to their ease and speed of construction, shallow superstructure necessary for clearance requirements, and cost-effectiveness compared to other types of bridges (Miller et al. 1999; Hanna et al. 2011). To share carrying the vertical loads among the adjacent girders, partial- or full-depth grouted shear keys are typically used to connect such girders at their interface. However, a recurring problem in this structural system is the longitudinal cracking in the shear

keys and, consequently, in the concrete overlay, if any. The development of these longitudinal cracks over the shear keys compromises the durability of such bridges. Commonly, water saturated with deicing salts seeps through these longitudinal cracks initiating reinforcement corrosion and concrete deterioration. In severe cases, transverse load distribution among adjacent girders is jeopardized, resulting in overstressing individual girders with loads exceeding the design loads (Miller et al. 1999; Russell 2011).

During the last few decades, transverse post-tensioning (TPT) of adjacent box girders has been introduced to ensure the monolithic behavior of the bridge and to control longitudinal cracking and differential deflections (Lall et al. 1998; Hanna et al. 2009). The current practice is to apply TPT through transverse concrete diaphragms cast monolithically with the girders at discrete locations (typically, at three to five locations depending on the span of the bridge). A combination of grouted shear keys and TPT is suggested by current standards in North America as a means of transverse load distribution. The Canadian Highway Bridge Design Code (CHBDC), CSA S6-19 (CSA 2019a), and the AASHTO specification LRFD-8 (AASHTO 2017) require adjacent box girder bridges to have a transverse load distribution mechanism. This mechanism can be achieved by a concrete structural overlay, a combination of grouted shear keys and TPT providing a prestress of at least 1.7 MPa, or any other approved means capable of distributing transverse load among adjacent girders.

Nevertheless, there are very limited design specifications on the amount, spacing, and vertical alignment of such prestressing force in the TPT strands. For instance, the area over which the recommended prestress (1.7 MPa) applies is not clearly defined (El-Remaily et al. 1996; Lall et al. 1998; Hanna et al. 2009; Fu et al. 2011; Hansen et al. 2012; Hussein et al. 2017). If the contact area of the shear key is assumed to be the area over which this pre- stress applies, shallower shear

keys would require fewer TPT forces (Semendary et al. 2017). Considering the entire contact area (interface) between adjacent girders, on the other hand, may result in extremely exaggerated TPT forces that cannot be practically achieved (Hanna et al. 2009). The Precast/Prestressed Concrete Institute (PCI) bridge design manual (PCI 2014) provides a design procedure to estimate the TPT force, which is adapted from previous research (El-Remaily et al. 1996; Hanna et al. 2009). This design procedure assumes that the TPT diaphragms are the primary mechanism for the distribution of wheel loads across a bridge. Design charts are provided to estimate TPT values for common girder depth and width. These charts were developed based on limiting the diaphragm concrete stress under the combination of external loads and prestressing forces to the allowable limits (i.e., allowable compressive stress of 60% of the concrete compressive strength and allowable tensile stress of zero). The latter limit was set to completely prohibit tensile stresses in the diaphragms to mitigate any possible cracking at the interface between the girders and the grouted shear keys.

Due to the need for transverse diaphragms to house the TPT strands, the current TPT practice has several disadvantages. Because TPT can only be applied at locations of discrete diaphragms, differential deflections and longitudinal cracking of shear keys are only controlled in the vicinity of transverse diaphragms; the relatively long portions of the bridge between discrete diaphragms are still susceptible to such deformations (Aktan et al. 2009). In addition, the presence of diaphragms increases construction cost due to the increased weight of the girders, the complexity of the associated formwork, and the interruption of utility lines and drainage ducts inside the hollow portions of the girders. This cost increase is further magnified in skew bridges, where diaphragms may need to be staggered or constructed in stages involving a large number of TPT stressing operations and excessive traffic interruption during replacement projects (Hansen et al. 2012). Therefore, several studies have investigated the feasibility of eliminating transverse

diaphragms from the transverse load distribution mechanism. Hanna et al. (2011) proposed two non-post-tensioned connections that eliminate the need for diaphragms. These two connections depend on non-post-tensioned bars placed in both top and bottom flanges of the girders to form a monolithic continuous connection. Hansen et al. (2012) introduced sleeves below the top flange and above the bottom flange to allow post-tensioning unbonded high-strength rods and creating a diaphragm-free TPT connection. Recently, Sun et al. (2018) reported a field implementation of a new TPT system, where TPT ducts were housed in the top and bottom flanges of the girders. However, placing TPT ducts in the congested bottom flange is challenging due to the presence of the longitudinal prestressing strands. Such congestion may require increasing the bottom flange thickness to accommodate both longitudinal and transverse strands while maintaining the minimum concrete cover requirements. Another concern associated with the current TPT practice is the replacement of damaged or deteriorated exterior girders. In concrete highway bridges, a high-impact load on the edge box girders is potentially induced by the collision of over-height vehicles (Grace et al. 2002). Damage resulting from a collision of an over-height vehicle may require replacement of the entire superstructure when individual girders cannot be practically replaced. In adjacent box girder bridges, replacing a damaged exterior girder is challenging when bonded TPT strands are used. The use of unbonded TPT strands has been successfully implemented in the field (Grace et al. 2002). In this study, a new TPT mechanism is investigated, where unbonded TPT is applied at the top flanges of the girders only. Therefore, transverse diaphragms can be eliminated, while maintaining a uniform prestress distribution across the entire length of the bridge without congesting the bottom flange. The proposed TPT mechanism has several other advantages, including the ease of installation and the reduced cost due to the reduction in the post-tensioning operations. Placing the TPT strands in the top flanges closer to the

riding surface may raise durability concerns. Nonetheless, the TPT ducts could be grouted, injected with corrosion-inhibiting grease, or encased in polyethylene sheathing according to ASTM A416 (ASTM 2018) to protect the strands from harmful environmental conditions. In addition, a slab is likely to be placed on the top of the girders, which further protects the strands and reduce exposure to the harsh environment. Similarly, different precautions could be applied to protect the anchorage such as embedding the anchorage in the flanges and encapsulating them with high-strength non-shrink grout (Sun et al. 2018).

3.2. Experimental Program

A one-third-scale bridge model consisting of four adjacent box girders was erected and tested. The model was subjected to four different tests to investigate the feasibility of applying TPT at the top flange of the girder only, the optimal TPT force and spacing to ensure a uniform distribution of a minimum prestress of 1.7 MPa, and the efficiency of the proposed technique in transversely distributing live loads among adjacent girders under service and ultimate conditions. The four different tests were as follows: Test A: strain distribution test—uncracked shear key; Test B: load distribution test —uncracked shear key; Test C: load distribution test—cracked shear key; and Test D: ultimate load test.

3.2.1. Details of Bridge Girders

Each girder measured was 400-mm wide, 270-mm high, and 6,400-mm long, as shown in Figure 3.1. The thickness of all flanges and webs was 75 mm. To allow for the shear key, a reduction of 13 mm of the width of the top flange was made on the contact side such that the width of the top flange measured 374 and 387 mm for interior and exterior girders, respectively (Figure 3.1). Nine, 25-mm diameter PVC ducts were housed in the top flanges at an equal spacing of 750 mm to accommodate the TPT. To provide full bearing contact at the location of the ducts, no shear key

was made for a distance of 75 mm centered with the ducts (Figure 3.1). Away from the TPT location, the width of the vertical shear key was 26 mm at the top surface of the girder and was widened to 50 mm at a depth of 75 mm, as shown in Figure 3.1. Two, 400-mm long end blocks near the supports were provided to resist the localized stresses due to the release of the longitudinal pre- tensioning forces applied to the box girders. As shown in Figure 3.2, the longitudinal reinforcement of each box girder comprised three size 13 prestressing steel strands (12.7 mm) and two 10-M non-prestressing steel bars as bottom reinforcement equally spaced at 60 mm. In addition, three 10-M non-prestressing steel bars equally spaced at 120 mm were provided as top reinforcement. The concrete cover to the top and bottom reinforcement layers was 20 and 38 mm, respectively. The top reinforcement was retained in its position by using 10-M vertical stirrups spaced at 70 mm near supports and at 140 mm in the mid-span region.

3.2.2. Assembled Bridge Model

The bridge model was simply supported on two rigid steel I-beams. A 150-mm wide elastomeric pad (25-mm thick) was placed between the box girders and the steel support. The maximum differential camber among the adjacent girders was approximately 11 mm. This was accommodated through the wider diameter of the TPT ducts (25 mm) compared to the diameter of the used strands (12.7 mm). After placing the girders on the supports, a relatively low TPT force of 20 kN was applied at three locations, i.e., both ends and mid-span, to secure the girders in place during the grouting process. This force represents approximately one-sixth of the maximum possible TPT force (110 kN). Non-shrink cementitious grout was placed in the shear keys. The exposed surfaces of the shear keys were sand-blasted prior to casting the grout. This surface roughening was performed by the manufacturer according to the current standard specifications.

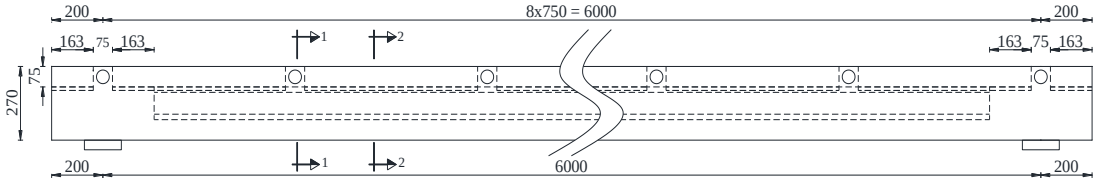

(a) Elevation view

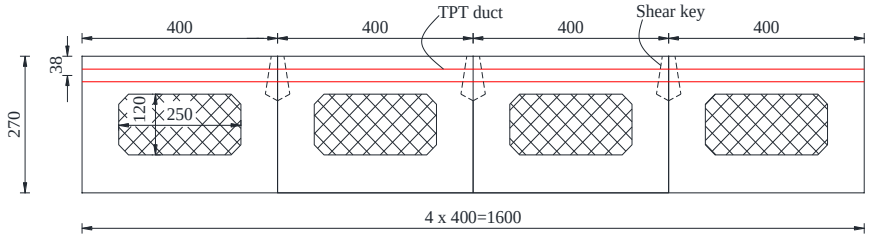

(b) Section 1-1

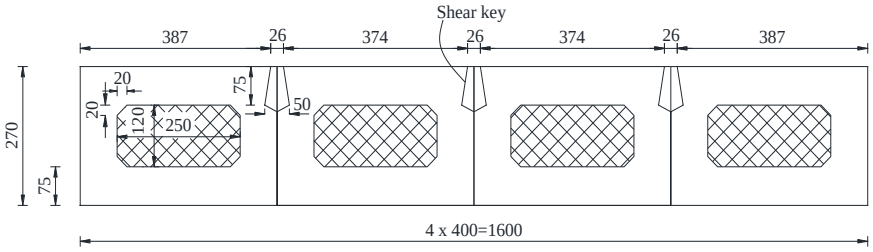

(c) Section 2-2

Figure 3.1 - Geometry of bridge model (dimensions in mm).

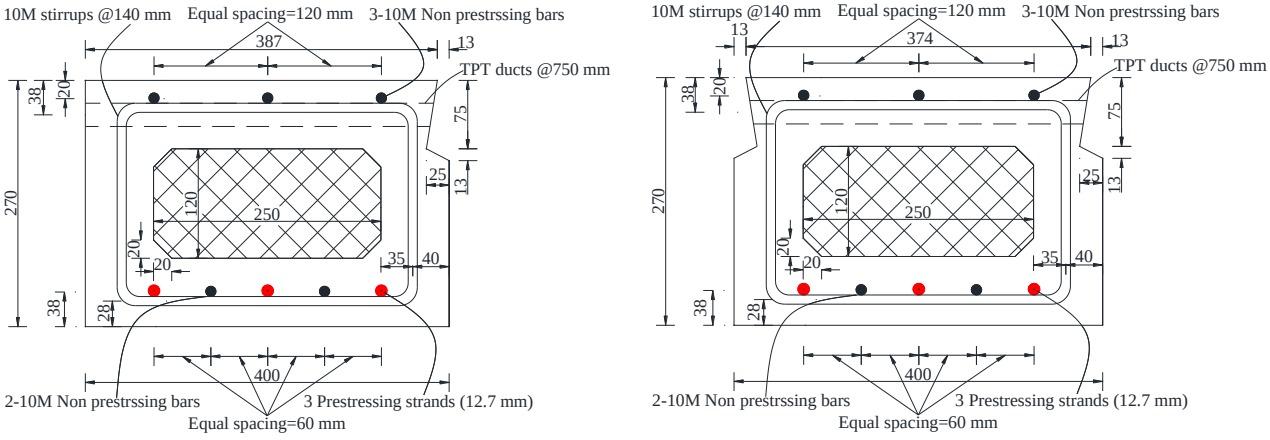

(a) Exterior girder (b) Interior girder

Figure 3.2 - Typical reinforcement configuration (dimensions in mm).

3.2.3. Material Properties

The box girders were fabricated at a precast plant using concrete with a target 28-day compressive strength of 50 MPa. The actual concrete compressive strength was determined by testing standard cylinders (100 × 200 mm) at 28 days and on the day of testing according to CSA A23.1-19 (CSA 2019b). The properties of the used concrete are listed in Table 3.1. Size 10 M deformed, non-prestressed G400 steel bars and stirrups were used as non-prestressed flexural and shear reinforcement, respectively. On the other hand, size 13 (12.7-mm diameter) high-strength, low-relaxation, seven-wire strands were used as flexural prestressing reinforcement and for applying the TPT. The mechanical properties of the used reinforcement, as provided by the manufacturers, are listed in Table 3.2. High-performance, non-shrink, bleed-resistant, sand-free, cementitious grout was used to fill the shear keys. The actual grout compressive strength was determined by testing standard 50-mm cubes after 28 days and on the day of testing according to ASTM C-942 (ASTM 2015), as listed in Table 3.1.

Table 3.1 - Concrete and grout properties

Girder	Air (%)	Slump (mm)	Compressive Strength (MPa)				
			at 28 days	Test A	Test B	Test C	Test D
Exterior Girder (G1)	7.1	170	54.5	55.5	55.7	55.8	55.9
Interior Girder (G2)	8.2	180	55.7	56.4	56.5	56.7	56.9
Interior Girder (G3)	6.6	180	55.0	55.9	55.9	56.1	56.1
Exterior Girder (G4)	7.1	170	54.5	55.5	55.7	55.8	55.9
Non-shrink grout			85.0	85.2	85.4	85.5	85.7

Table 3.2 - Mechanical properties of used reinforcement

Bar type	Bar Size	Diameter (mm)	Area (mm^2)	Tensile Strength (MPa)	Elastic Modulus (GPa)
Non-prestressing bars	10M	11.3	100	400[a]	200
Prestressing strands	13	12.7	98.7	1,860	202

[a] Yield strength.

3.2.4. Test A: Strain Distribution Test — Uncracked Shear Key

As mentioned previously, the area over which the prestress of 1.7 MPa applies was assumed by different researchers to be the compressed diaphragm area, the area of the shear key only, or the entire contact area between two adjacent girders. Grace et al. (2010, 2011a, b) converted this minimum required stress to an equivalent concrete strain using the elastic theory to facilitate the assessment of TPT efficiency. For concrete with a compressive strength of 55 MPa, a minimum compressive strain value of 55 με must be achieved at the top surface of the bridge model to satisfy the requirements of the CHBDC and the LRFD-8. In the strain distribution test, different values of TPT forces were applied at different spacing, while the concrete compressive strain was monitored to determine the adequate level of TPT force to achieve the minimum required compressive strain. Three different arrangements of TPT have been investigated, as follows:

- Case I: TPT is applied at three ducts spaced at 3,000 mm (at two ends and mid-span).
- Case II: TPT is applied at five ducts spaced at 1,500 mm (at two ends, mid-span, and two quarters).
- Case III: TPT is applied at nine ducts spaced at 750 mm (at two ends and seven eighths).

In the three cases, the effective TPT force was applied at four different levels of 50, 70, 90, and 110 kN. The jacking TPT force, however, was slightly higher than these values to account for the prestress losses. The anchorage seating losses accounted for most of the prestress losses, owing to the short length of the tendons. The anchorage seating losses were estimated by calibrating the anchorage system before the start of the test. On the other hand, time-dependent losses, i.e., relaxation, creep, and shrinkage, were insignificant as the tests were performed immediately after applying the transverse prestressing. For the anchorage system, standard steel chucks were used at both ends of the strands. Three U-shaped detachable steel plates were used as bearing plates to facilitate varying the TPT force. For every TPT force, such plates can be pulled off to secure a room for the chuck to be loosened to achieve the required TPT force.

3.2.5. Test B: Load Distribution Test — Uncracked Shear Key

To investigate the efficiency of the proposed transverse connection (partial-depth shear key and TPT at the top flanges only) in distributing live loads in the transverse direction, a load distribution test was conducted by applying a vertical concentrated load at the mid-span of a single girder. Due to symmetry about longitudinal axis, the test was conducted only twice, once on an exterior girder and once on an interior one. Figure 3.3 shows the test setup for the exterior girder. The same setup was used to test the interior girder. The applied load was monotonically increased until it reached 80 kN, which is 56% of the theoretical cracking load (142 kN) of the assembled bridge model (4 girders). The vertical load was applied by a 1,000-kN capacity hydraulic actuator, which was bolted to a rigid, heavy steel cross beam spanning 3,500 mm between two rigid steel space frames anchored to the laboratory's strong floor. Based on the results of Test A, as discussed in the following, only two arrangements (Cases II and III), as aforementioned, and three levels (50, 70, and 90 kN) of TPT were considered for the load distribution test. To simulate the footprint of the

CHBDC design truck (CL-625) (CSA 2019a), the load was transferred to the girders through a one-third-scale (250 × 180 mm) rectangular steel plate. These dimensions were selected to produce a contact pressure under the plate similar to that generated under the heaviest wheel of a standard CL-625 truck (CSA 2019a).

3.2.6. Test C: Load Distribution Test—Cracked Shear Key

During service, reflective longitudinal cracking at the shear key location of box girder bridges is inevitable due to the application of structural forces and thermal gradients (Miller et al. 1999; Grace et al. 2010; Ulku et al. 2010; Attanayake and Aktan 2015). Therefore, the load distribution test was repeated after cracking the shear key joints. Shear keys cracking was developed by inducing longitudinal cuts along 90% of the length and up to 90% of the depth of the shear key, using a concrete saw with a blade thickness of 3 mm. To simulate a real crack that eliminates friction while maintaining transverse bearing between the two sides of the cracked shear key, plastic sheets were then inserted in the cuts, and the remaining space was refilled with concrete paste.

3.2.7. Test D: Ultimate Load Test

In this test, the efficiency of the proposed TPT system under ultimate loading conditions was evaluated. The bridge model was subjected to a TPT force of70 kN applied at all nine locations (Case III arrangement). This TPT arrangement was found to be adequate to achieve the minimum prestress of 1.7 MPa, as discussed in the following. A two-point load was applied to the exterior girder. The load was transferred to the girders through rectangular steel plates of dimensions similar to that of the plate used in the load distribution tests (Tests B and C). The distance between the centerlines of the two loading plates was set to 750 mm, which corresponds to the distance between TPT ducts. This way, the concentrated loads were applied at mid-distance between TPT

ducts, i.e., the location with the lowest transverse strains along the span. The exterior girder was selected to be loaded in light of the results of Tests B and C (load distribution tests), as discussed in the following. The load was applied through several loading and unloading cycles. A similar approach was adopted in the literature (Grace 2000; Grace et al. 2011a). The maximum load of the first cycle was 40 kN, which corresponds to a one-third-scale wheel load of the CHBDC design truck (CL-625) (CSA 2019a), including a 40% dynamic load allowance. The maximum load of each following step was increased in increments of 40 kN until failure.

Figure 3.3 - Load distribution test setup (vertical load applied at an exterior girder).

3.2.8. Instrumentation

The bridge model was instrumented on the top surface with both PI-gauges (a displacement transducer that consists of an arch-shaped spring plate with strain gauges mounted on it) and concrete strain gauges at several locations to measure concrete strains in the transverse direction at the top of the bridge model. On the bottom surface of the bridge model, several linear variable displacement transducers (LVDTs) were used to measure deflection and joint movement. One LVDT was placed vertically underneath the mid-width of each girder to measure mid-span deflection (a total of four LVDTs). In addition, three horizontal LVDTs were attached to the bottom surface of the girders, i.e., one beneath each shear key location, to capture the joint movement, if any. On the other hand, four longitudinal strain gauges were attached to the mid-width of the bottom flange of the girders at mid-span to record the flexural tensile strains of each individual girder. When the load distribution test was repeated after cracking the shear keys (Test C), four additional LVDTs were placed vertically underneath the girders to measure quarter-span deflections (one LVDT at the mid-width of each girder). Furthermore, four vertical LVDTs were installed at the mid-span to measure the relative vertical displacements among girders. Figure 3.4 shows the instrumentation distribution on both top and bottom surfaces of the bridge model. The location of each instrumentation at the joints is identified by a letter and number; the letter indicates the shear key over which the instrumentation was placed (A, B, or C), and the number indicates the axis spaced at 375 mm and labeled longitudinally along with the considered shear key (from 1 to 17).

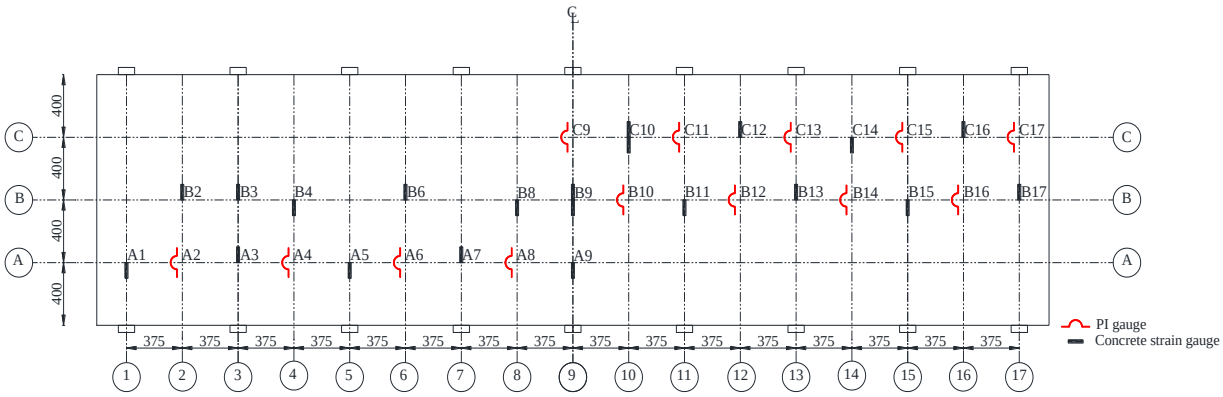

(a) Instrumentation distribution on the top surface of the bridge model.

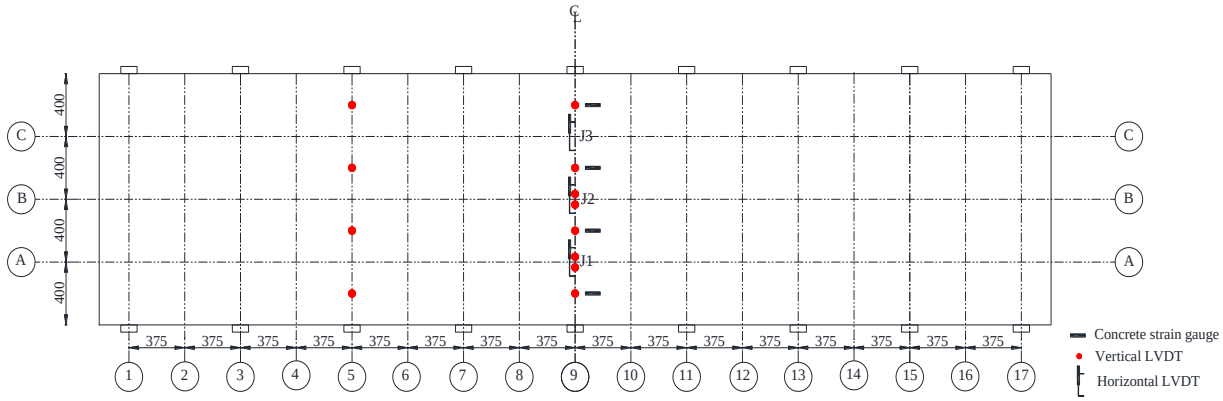

(b) Instrumentation distribution on the bottom surface of the bridge model.

Figure 3.4 - Instrumentation distribution of the bridge model.

3.3. Results and Discussion

3.3.1. Test A: Strain Distribution Test — Uncracked Shear Key

3.3.1.1. Joint Movement (Opening) Due to TPT Application

One of the main concerns regarding applying TPT at the top flanges only is the possibility of girder's rotation about their longitudinal axes due to the eccentricity of the TPT force. This would result in a gap between the girders at the bottom of the bridge. As mentioned previously, three LVDTs were attached at the bottom of the bridge model to monitor joint movement, if any. For all loading cases, no movements were observed throughout the test. This is attributed to the high torsional stiffness of the box girders and the restraints provided by the supports in addition to the

tensile capacity of the grout. This observation can be extended to include full-scale applications because a full-scale bridge structure would have a higher torsional rigidity due to the larger cross-section dimensions. Therefore, despite the increase in the span length, the torsional stiffness is likely to be enhanced. As a result, the joints are expected to perform comparably, if not better, in the case of full-scale bridges.

3.3.1.2. Transverse Concrete Strains

The transverse concrete strain distribution at an exterior shear key for Case I (TPT applied at three ducts) is shown in Figure 3.5. It is to be noted that, in all figures, bold vertical lines indicate the locations of TPT application, while the horizontal axis represents the axis number along the shear key, as previously presented in Figure 3.4. In general, the bridge surface experienced the highest transverse strains at locations coinciding with locations of applied TPT forces with a drastic drop in the strains at points located between the applied TPT forces. As shown in Figure 3.5, when TPT was applied at three ducts only, the compressive concrete strains along the shear key at A-1, were approximately 44, 57, 84, and 96 με when the TPT force was 50, 70, 90, and 110 kN, respectively. However, compressive concrete strains at A-3 (750 mm away from the applied TPT force) were only 8, 14, 25, and 32 με, respectively, for the same TPT levels, which represents approximately 67% decrease in the compressive concrete strain at a TPT force of 90 kN. Compressive strains were further reduced to no more than 5 με at A-5. This indicates that the minimum required prestress of 1.7 MPa (corresponds to a compressive strain of 55 μs) can only be achieved near the TPT locations even when TPT is applied at the top flanges of the girders (closer to the concrete surface). Similar behavior was observed when the TPT force was applied at five ducts (Case II), as shown in Figure 3.6. On the other hand, as expected, when TPT was applied at all nine ducts, a significantly better compressive concrete strain distribution was achieved. As shown in Figure 3.7,

at a relatively low TPT force of 70 kN, all monitored locations along shear key A experienced compressive strains higher than 55με. With further increasing TPT forces to 110 kN, compressive strains between 98 and 115 με were recorded. This indicates that distributing the TPT force at a shorter spacing along the length of the bridge is more efficient in producing the minimum required concrete prestress along the entire length of shear keys than increasing the TPT force at discrete distant locations. Furthermore, this observation indicates that the TPT force of 110 kN is too high and overstressing the girders to values that significantly exceed code requirements. Consequently, this TPT load (110 kN) was eliminated from the remaining tests.

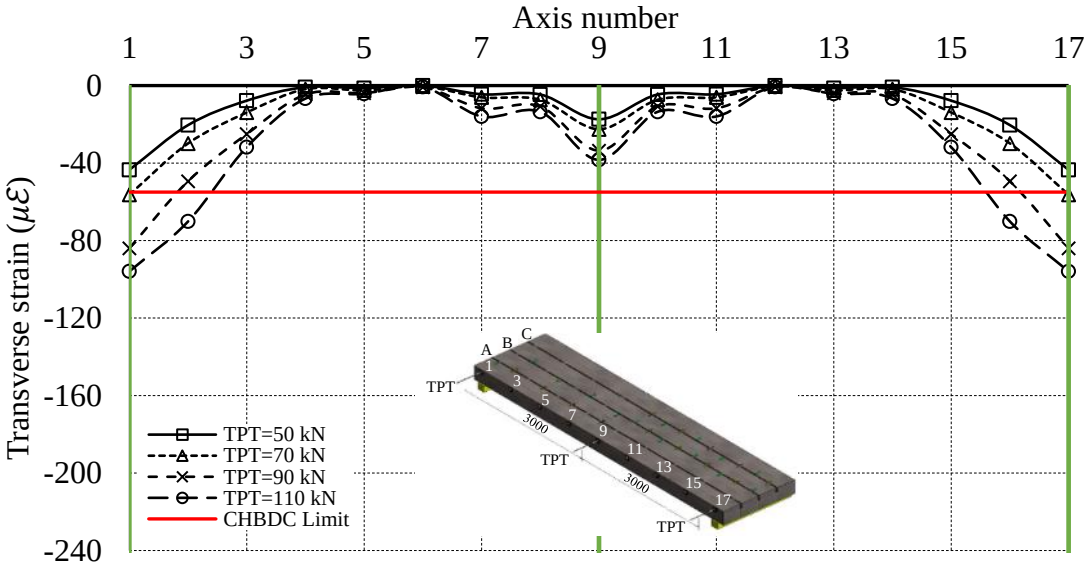

Figure 3.5 - Concrete strain distribution at shear key A – Case I: TPT at three ducts.

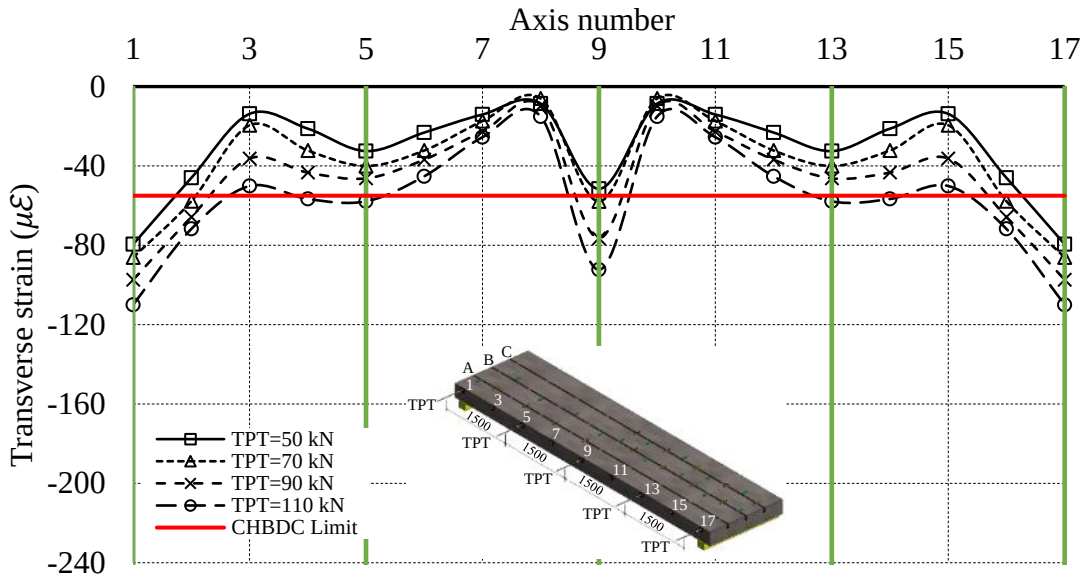

Figure 3.6 - Concrete strain distribution at shear key A – Case II: TPT at five ducts.

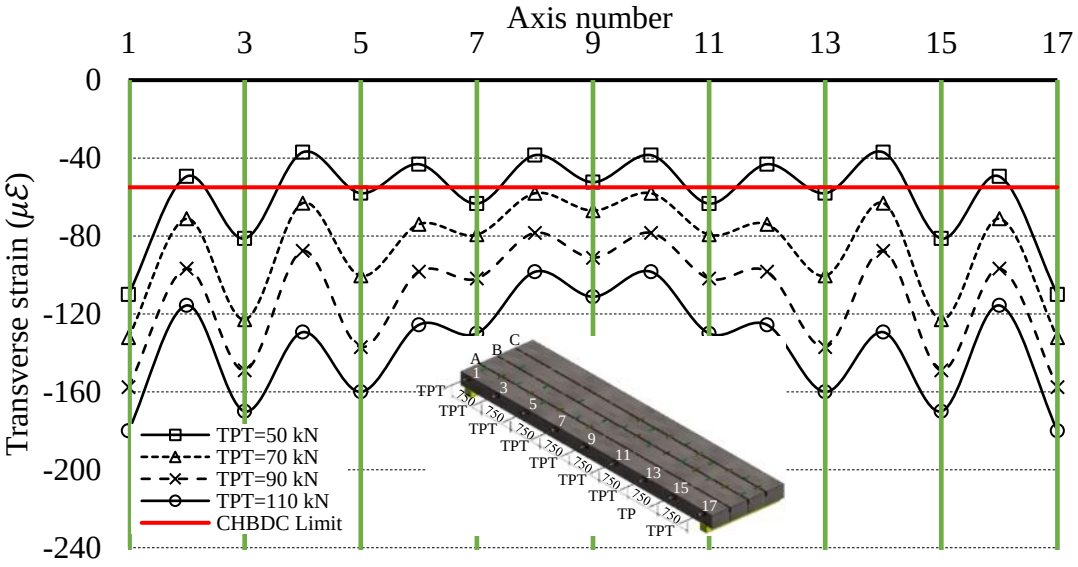

Figure 3.7 - Concrete strain distribution at shear key A – Case III: TPT at nine ducts.

3.3.2. Test B: Load Distribution Test — Uncracked Shear Key

3.3.2.1. Deflection Response

Increasing the TPT level resulted in enhancing the overall stiffness of the bridge model, which in turn, limited the deflection of the girders. This is attributed to the improved clamping effect introduced by the TPT. Figure 3.8 shows the mid-span deflection profiles of the bridge model when the exterior Girder G1 was loaded (i.e., subjected to a vertical load of 80 kN). It is to be noted that bold vertical lines indicate the centerline of each individual girder of the assembled bridge model and the horizontal axis represents the transverse distance measured from the outermost side surface of Girder G1. Under all TPT levels, the loaded Girder G1 experienced the highest mid-span deflection. For Case II arrangement under a TPT force of 50 kN, mid-span deflections of 6.42, 5.07, 4.30, and 1.90 mm were recorded at the mid-width of Girders G1, G2, G3, and G4, respectively. These deflections slightly dropped to 6.10, 4.80, 3.93, and 1.89 mm upon increasing the TPT level to 70 kN. However, further increasing the TPT level to 90 kN resulted in insignificant improvements, where the deflections were approximately the same as those experienced at the 70 kN TPT level. A similar trend was observed when the TPT forces were applied at all nine ducts (Case III arrangement). At a TPT force of 50 kN, mid-span deflections of 6.21, 4.89, 4.13, and 1.89 mm were recorded at the mid-width of Girders G1, G2, G3, and G4, respectively. Nonetheless, these values are slightly lower than their counterparts experienced in Case II arrangement. Increasing the TPT force to 70 kN decreased these deflections to 6.11, 4.74, 3.87, and 1.88 mm, respectively. These values were not significantly changed when the TPT force was further increased to 90 kN. When the interior Girder G2 was loaded, the exterior Girder G1 also experienced the maximum deflection. In addition, varying the TPT arrangement (Case II and

Case III) had an insignificant effect on the mid-span deflection profiles of the bridge model regardless of the TPT level.

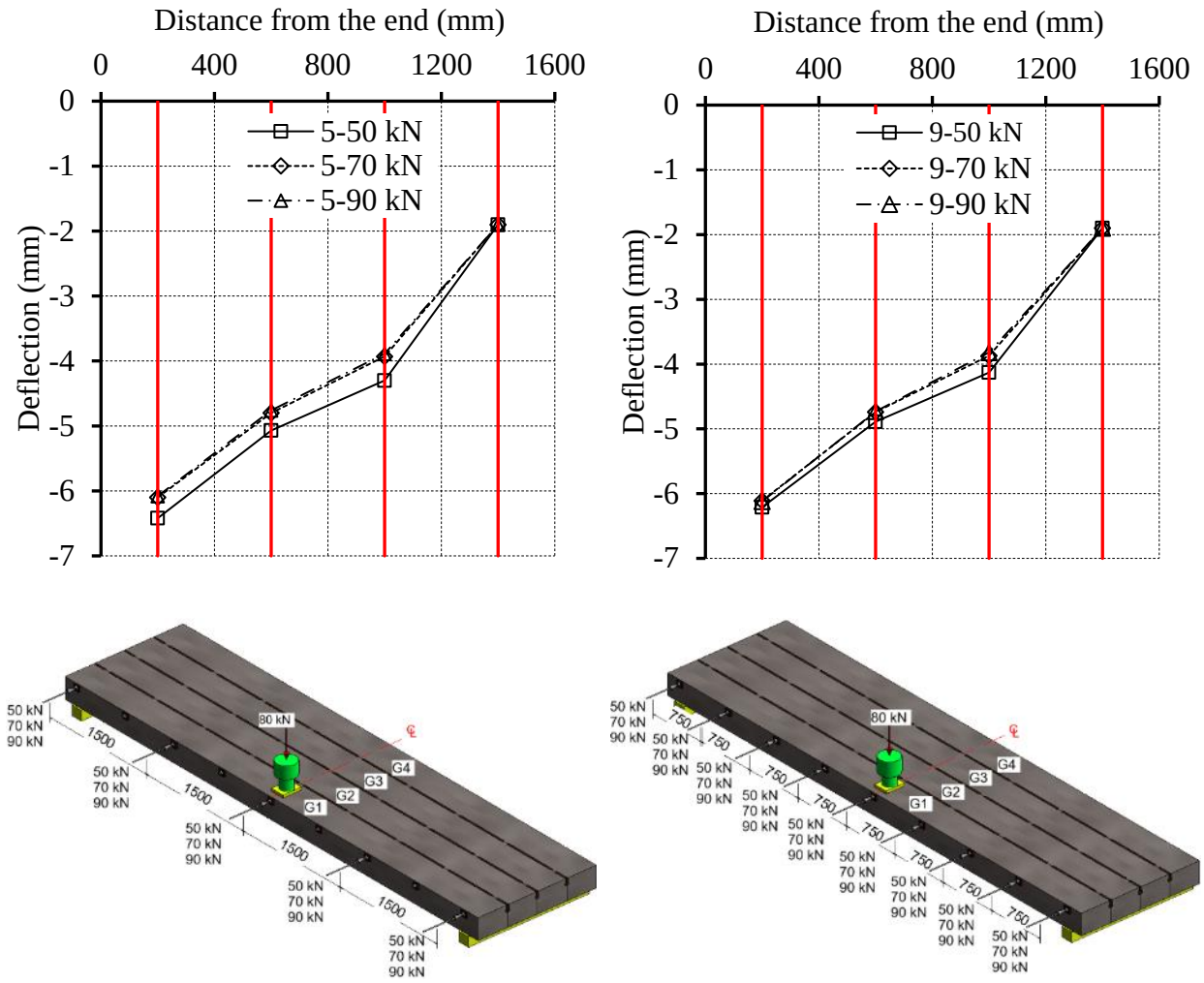

(a) Case II TPT arrangement (b) Case III TPT arrangement

Figure 3.8 - Mid-span deflection profile of the bridge model - girder G1 loaded.

3.3.2.2. Longitudinal Concrete Strains

Another aspect that is widely used in the literature to quantify the transverse load distribution among adjacent girders is the distribution of longitudinal concrete tensile strains on the bottom surface of the girder. Unlike the measured deflections at the mid-width of each girder, the loaded

girder always developed the highest longitudinal concrete tensile strains. For instance, when a TPT force of 50 kN was applied under Case II arrangement, the highest developed longitudinal strain of 248 με was recorded at the loaded Girder G1. This value is 69% higher than the lowest strain experienced by Girder G4 (147 με). When Girder G2 was loaded under the same arrangement, the maximum recorded strain was 206 με in Girder G2, which is only 30% higher than the lowest strain experienced by Girder G4 (159 με). Increasing the TPT force (from 50 to 70, then to 90 kN) had an insignificant effect on the longitudinal concrete strains. Yuan and Graybeal (2016) reported longitudinal concrete strains ranging approximately between 155 and 165 με when the TPT force was increased from 45 to 445 kN. Their tests were conducted on a box girder bridge model with uncracked, partial-depth shear keys, where the TPT forces were applied through transverse diaphragms. Ghosn et al. (1986) defined a live load moment distribution factor (LLMDF) for adjacent girders by dividing the longitudinal concrete tensile strain measured at the bottom of a girder at mid-span (ε_i) by the summation of all measured strains for all girders as expressed in Equation 3.1, where ε_i is the longitudinal concrete tensile strain captured at the bottom of the i^{th} girder. This analogy is explained by assuming the applicability of the beam theory assumptions, i.e., plane sections remain plane after bending. Consequently, the measured strains are proportional to the curvature of each girder, which are proportional to the bending moment (Hughs and Idriss 2006). This analogy has been used by many researchers to quantify the applied live load share at each girder (Kim and Nowak 1997; Eom and Nowak 2001; Deng et al. 2016; Semendary et al. 2017).

$$LLMDF = \frac{\varepsilon_l}{\sum_{i=1}^{i=n} \varepsilon_i} \qquad \text{Equation 3.1}$$

The LLMDFs were calculated for all tested TPT arrangements. Regardless of the position of the vertical load, the loaded girder always had the highest LLMDF. As shown in Figure 3.9, when Girder G1 was loaded, and a TPT force of 50 kN was applied under Case II arrangement, LLMDFs of 33.0, 25.5, 21.9 and 19.6% were obtained for Girders G1, G2, G3, and G4, respectively. These LLMDFs indicate good load distribution among adjacent girders, where the farthest girder, G4, was able to share up to 19.6% of the applied load. This value is 60% of the load share of the loaded Girder G1. On the other hand, a lower LLMDF was observed for Girder G2 when loaded (26.5%) compared to that of its counterpart Girder G1 when loaded (33.0%). In this case, the ratio between the LLMDF of the least loaded Girder G4 to that of the most loaded Girder G2 is 77%, which indicates that the load is more evenly allocated among adjacent girders. Similar to the developed longitudinal tensile strains at the bottom of girders, LLMDFs appeared to be insubstantially changing upon varying TPT level and arrangement. This indicates that TPT is not beneficial to the structural system as long as the shear keys remain intact. Similar results and LLMDFs factors were obtained by Yuan and Graybeal (2016), who conducted full-scale tests on box girder bridge models in which the TPT was applied through discrete diaphragms.

3.3.2.3. Joint Movement

One main concern regarding the eccentric application of the TPT at the top flanges only is the possibility of girders rotation about their longitudinal axes under the action of structural loads. Such rotations, if excessive, will force the bridge model to open at the bottom interface of the adjacent girders. The current North American codes and guidelines (PCI 2014; AASHTO 2017; CSA 2019a) lack restrictions on such movement. In addition, very limited research was conducted to monitor and quantify such movement (Hussein et al. 2017; Semendary et al. 2018). In this study, as shown in Figure 3.10, joint movement was observed by placing horizontal LVDTs at the bottom

of each joint to capture any opening and closing under the applied vertical load. When Girder G1 was loaded, no joint movement was observed at the closest Joint J1. However, the movement in Joints J2 and J3 were −0.07 and −0.06 mm, respectively, where the negative sign indicates joint closing. The recorded closing movement shows that the bridge model experienced slight rotation about the farthest unloaded Girder G4. When Girder G2 was loaded, on the other hand, movements of 0.10, 0.06, and −0.03 mm were observed for Joints J1, J2, and J3, respectively. Under the applied vertical load, Joints J1 and J2 were trying to open; however, Joint J3 was trying to close. It can be noted that the joints that were directly beneath the applied load exhibited an opening behavior. This effect diminishes as the distance of the joint from the load increases. This observation agrees with those reported by Hussein et al. (2017), who conducted a field investigation to study the load distribution of box girder bridges in which adjacent girders were connected by partial-depth shear keys and TPT was applied through discrete diaphragms.

3.3.3. Test C: Load Distribution Test—Cracked Shear Key

3.3.3.1. Deflection Response

When the load distribution test was repeated after partially cracking the shear keys, comparable behavior to that of the intact shear keys was observed. Similar to the observation in Figure 3.8, slight reductions in the mid-span deflection were noticed when the TPT force was increased from 50 to 70 kN under both Case II and Case III arrangements. Similar trend was observed for the quarter-span deflection profile. Further increasing the TPT level to 90 kN in both cases did not significantly alter the deflections. This was observed regardless of the position of the vertical load on exterior or interior girders. This trend was also observed for the longitudinal concrete tensile strains and joint movement. A previous study on a box girder bridge model constructed with partial-depth shear keys reported a similar trend, where partially cracked connections performed

similar to intact ones (Yuan and Graybeal 2016). The authors defined a partially cracked shear key as a shear key that was intentionally cracked approximately half the span of the bridge; however, similar to the approach followed in this study, the two sides of the crack were not completely separated.

3.3.3.2. Mid-span Differential Deflection

Another characteristic that can be used to assess the efficiency of a transverse connection is the differential deflection of adjacent girders (Yuan and Graybeal 2016). Excessive differential deflections lead to longitudinal cracking that, if severe, might reflect to the overlay, if any. As mentioned previously, water saturated with deicing salts would seep through these longitudinal cracks initiating reinforcement corrosion and concrete deterioration. The maximum recorded relative deflection at mid-span of 0.47 mm was recorded at Joint J1 when Girder G2 was loaded and the least TPT force of 50 kN was applied under Case II arrangement. This value is below the maximum allowed value of 0.51 and 0.50 mm specified by the PCI bridge design manual (PCI 2014) and Huckelbridge et al. (1995), respectively. In the current study, the applied load on a one-third-scale bridge model with cracked shear keys represents 90% of the CHBDC (CSA 2019a) wheel load of truck CL-625% and 110% of the AASHTO (AASHTO 2017) wheel load of truck HS-20. This indicates that the proposed connection detail will limit differential deflections to an acceptable limit under normal circumstances in full-scale applications. Differential deflections were slightly affected by the TPT level and arrangement. For instance, when Girder G2 was loaded under Case II arrangement, increasing the TPT level from 50 to 70 kN decreased the maximum differential deflection at Joint J1 by 17% (from 0.47 to 0.39 mm). However, further increasing the TPT force to 90 kN or changing the TPT to Case III arrangement had insignificant effect on the mid-span relative deflection, as shown in Figure 3.11.

3.3.4. Test D: Ultimate Load Test

3.3.4.1. Ultimate Capacity and Mode of Failure

Ultimate Capacity and Mode of Failure The bridge model failed in a brittle punching shear mode before developing its full flexural capacity. The steel loading plates penetrated the top surface (flange) of the loaded Girder G1. The punching failure plane was extended to enclose the two loading plates in an elliptical surface on the boundary of the loaded girder internal web, as shown in Figure 3.12. No signs of concrete crushing nor rupture of bottom reinforcement was observed confirming punching shear as the controlling mode of failure. The ultimate load was 229.8 kN, which is 22% higher than the calculated punching shear capacity of 188.2 kN according to CHBDC (CSA 2019a). The theoretical flexural load carrying capacity of the scaled bridge model was 375 kN, calculated according to CHBDC (CSA 2019a). This capacity was calculated assuming the bridge model acting as a single, wide beam, and thus, the flexural capacity of the bridge model was based on the summation of the capacities of each individual girder. Each girder was designed as under reinforced section accompanied with yielding of both top and bottom reinforcements. Nonetheless, the loading plates were directly placed on the top flange (in-between the webs); thus, stress concentration occurred under the bottom of those plates shifting the mode of failure from flexural to punching shear. However, bridges constructed with composite concrete overlays showed that the flexural failure mode was predominant (Grace et al. 2011a, b).

3.3.4.2. Deflection Response

The load–deflection relationship of each girder was characterized by two regions: pre-cracking and post-cracking regions. In the pre-cracked region, up to a load of 156.4 kN as shown in Figure 3.13, the load–deflection curve exhibited the first slope change indicating cracks initiation and reduction in the initial stiffness of the bridge model. This cracking load represents 96% of the

theoretical cracking load of the assembled bridge model. At this load, deflections of 13.98, 10.59, 8.86, and 5.70 mm were recorded for Girders G1, G2, G3, and G4, respectively. Upon exceeding the cracking load, the slope of the load–deflection curve kept decreasing indicating the higher intensity of cracks propagation. An ultimate load of 229.8 kN was reached and the corresponding recorded deflection were 37.70, 29.89, 25.55, and 20.75 mm for Girders G1, G2, G3, and G4, respectively. Once the ultimate load was reached, the mid-span portion of the transverse connection at Joint J1 provided by the shear key was lost. This resulted in a sudden drop in the load carrying capacity from 229.8 to 214.3 kN at a vertical deflection of 42.11 mm at Girder G1, as shown in Figure 3.13. At this point, the transverse load distribution between Girder G1 and the adjacent girders was only provided by the TPT strands, which adds redundancy to the bridge model. If TPT was not provided, the entire load of 229.8 kN would have been suddenly transferred to Girder G1 alone, which has a theoretical flexural capacity of only 80 kN, and a sudden failure would have occurred.

Nonetheless, the presence of the TPT strands prevented such failure and re-engaged the other three girders in resisting the vertical load. Therefore, the TPT strands managed to maintain the integrity of the bridge model following the failure of the shear key. Consequently, it significantly enhanced the deformability of the bridge model (Figure 3.13) and prevented a potential catastrophic mode of failure. As Girder G1 deflected, Girder G2 acted as a pivot line for the TPT strands, while undergoing relatively lower deflections. This resulted in Girders G3 and G4 experiencing an upward movement in a seesaw mechanism. Once Girder G1 deflected enough to engage the TPT strands in the seesaw movement, the load carrying capacity started to gradually increase again to a peak value of 220.4 kN at a deflection of 57.47 mm, this latter value is 35% higher than that

when Girder G1 was separated. At this point, the loading plates punched through the top flange of Girder G1 and the load carrying capacity was entirely lost.

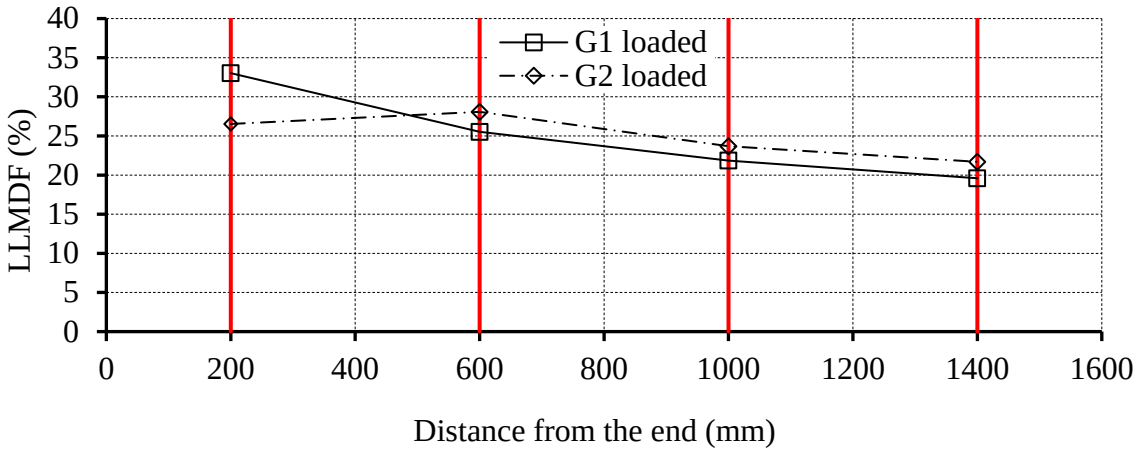

(a) LLMDFs for the two loading positions

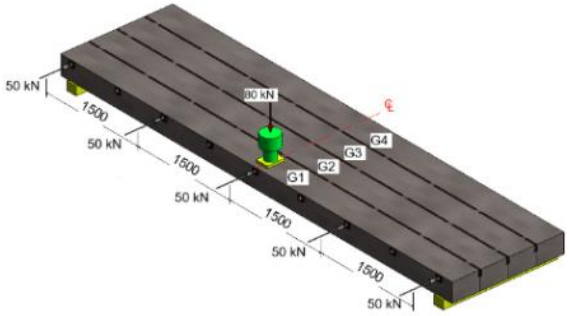

(b) Girder G1 being loaded

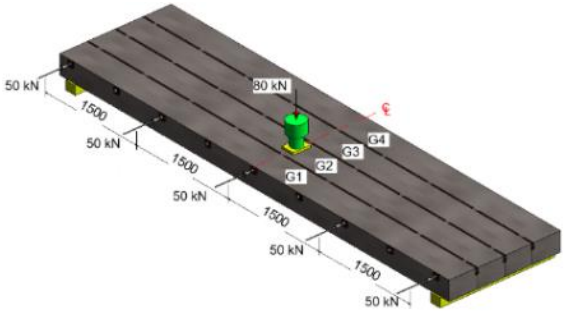

(c) Girder G2 being loaded

Figure 3.9 - Live load moment distribution factors (LLMDFs) - Case II, and TPT force = 50 kN.

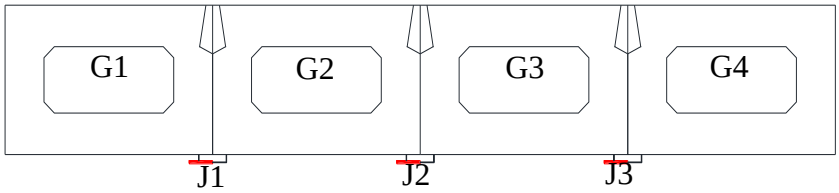

(a) Bridge model before loading

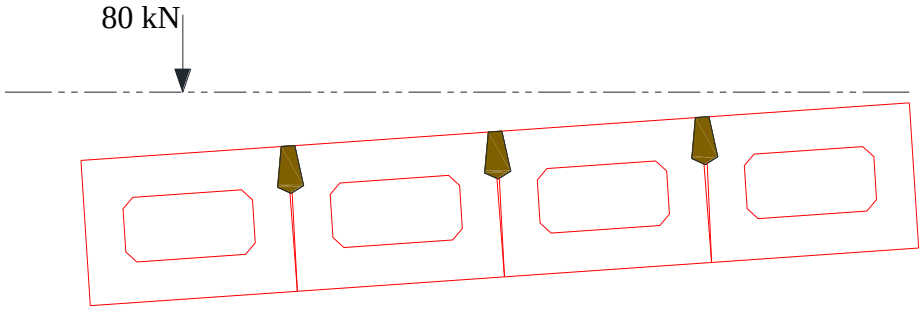

(b) Girder G1 loaded

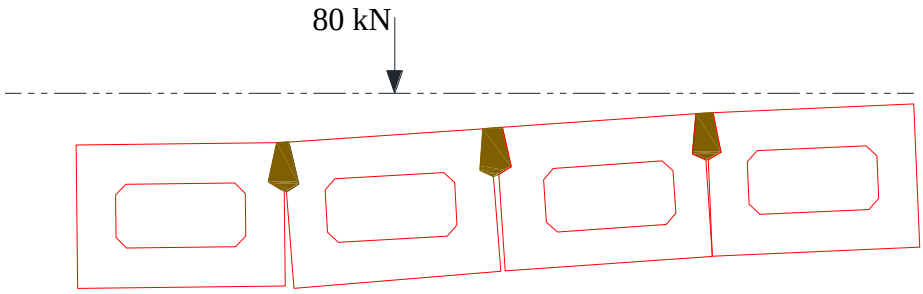

(c) Girder G2 loaded

Figure 3.10 - Schematic of joints movements (G1 and G2 loaded).

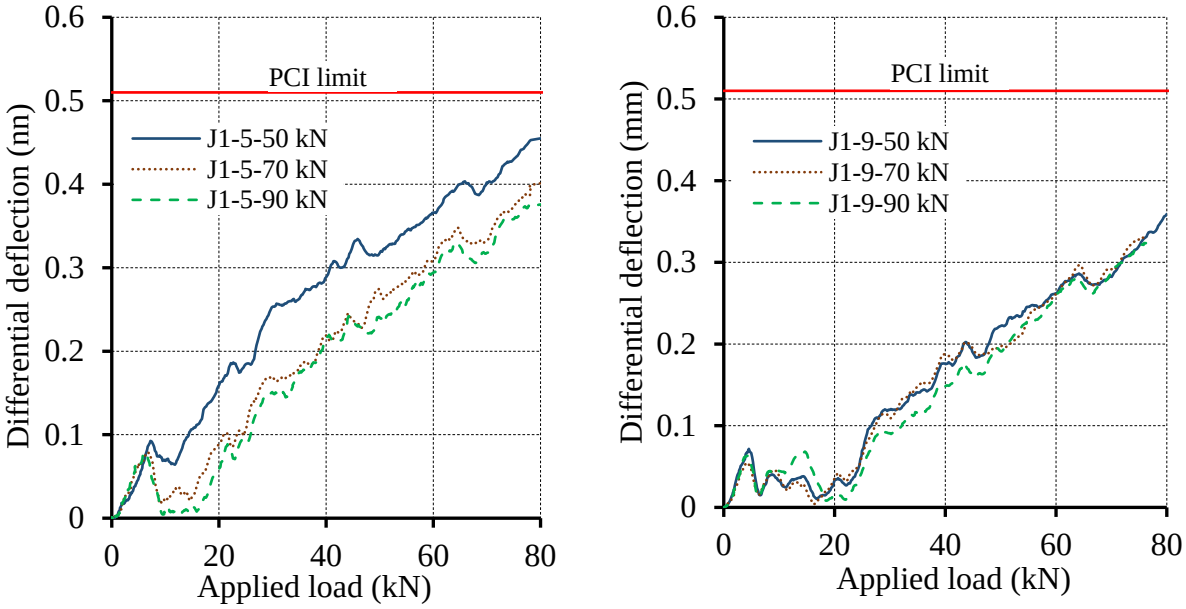

a) Case II arrangement

b) Case III arrangement

Figure 3.11 - Differential deflection between girders G1 and G2 when girder G2 is loaded.

Figure 3.12 - Punching shear failure mode

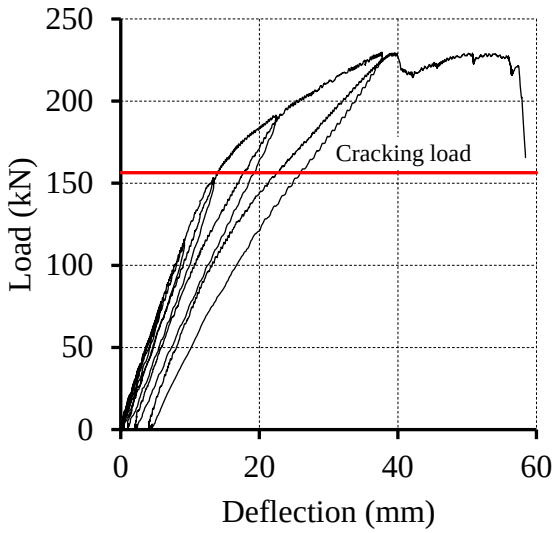

a) Load-deflection response of girder G1

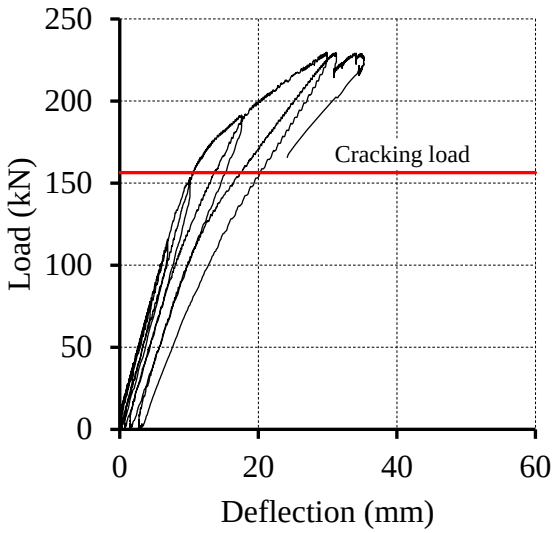

b) Load-deflection response of girder G2

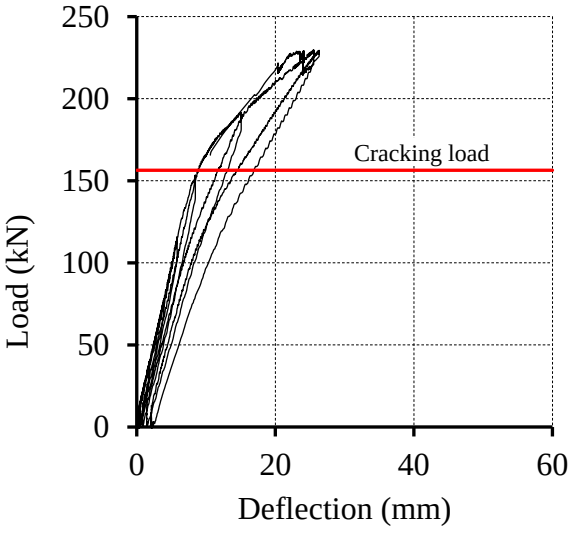

c) Load-deflection response of girder G3

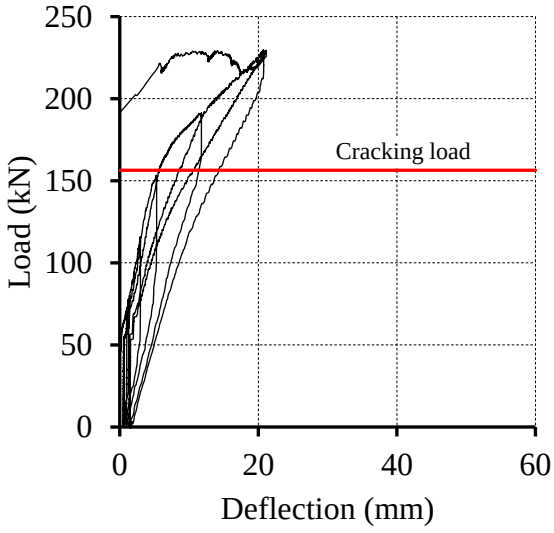

d) Load-deflection response of girder G4

Figure 3.13 - Load-deflection response of individual adjacent girders.

3.4. Conclusions

A one-third-scale bridge model with an innovative transverse connection, where TPT was applied at the top flanges only, was subjected to transverse strain distribution test and simulated service and ultimate load tests. Based on the discussed test results, the following conclusions are drawn:

- Regardless of the level of TPT force, the minimum required prestress of 1.7 MPa can only be achieved near the TPT locations even when TPT is applied at the top flanges of the girders, which is closer to the concrete surface.
- Distributing the TPT force at a shorter spacing along the length of the bridge is more efficient in producing the required concrete prestress along the entire length of shear keys than increasing the TPT force at discrete distant locations. At a relatively low TPT force of 70 kN spaced at one-eighth of the span, the measured compressive strains are higher than the minimum required value of 55 με.
- Under a monotonically increased vertical load of 80 kN, regardless of the position of the vertical load, the mid-span deflection was slightly reduced with increasing the TPT level from 50 to 70 kN, especially when TPT was applied at all nine ducts. However, further increasing TPT level to 90 kN did not affect the deflection of the girders.
- Regardless of the position of the vertical load, varying the TPT level and arrangement did not significantly affect the LLMDFs for all girders. At all TPT levels and arrangements, the loaded girder always had the highest LLMDF.
- Insignificant joint movement was observed when the bridge model was loaded. When the exterior girder was loaded (80 kN), the joints tended to close up with a maximum recorded joint closing of 0.07 mm. On the other hand, when the interior girder was loaded, the joints

closest to the applied load tended to open with a maximum recorded joint opening of 0.10 mm.

- Under the applied vertical load of 80 kN, partially cracked shear keys performed comparably to the intact shear keys condition in terms of mid-span deflection profile, longitudinal concrete tensile strains, and joint movements.
- Differential deflections were slightly affected by the TPT force and arrangement. When Girder G2 was loaded under Case II arrangement, increasing the TPT force from 50 to 70 kN decreased the maximum differential deflection at Joint J1 by 17%. However, further increasing the TPT force to 90 kN or changing the TPT arrangement to Case III did not significantly alter the mid-span differential deflections.
- The proposed TPT detail (TPT applied at the top flange only) managed to maintain the integrity of the bridge model following the failure of the shear key. Consequently, it significantly enhanced the deformability of the bridge model and prevented a potential catastrophic mode of failure.
- The proposed TPT system was proven to add redundancy to the assembled bridge model. When the shear key was fully fractured, no sudden failure nor rupture in the TPT strands was observed. Conversely, the separated girders (Girders G2, G3, and G4) continued to deform simultaneously with slight rotations about the loaded girder (exterior Girder G1).
- The mode of failure experienced by the bridge model was brittle punching shear. The ultimate load carrying capacity of 229.8 kN is 22% higher than the predicted punching shear capacity of 188.2 kN.

4. FINITE-ELEMENT ANALYSIS OF ADJACENT CONCRETE BOX GIRDERS TRANSVERSELY POST-TENSIONED AT TOP FLANGES ONLY

Authors and Affiliation:

- Shady N. Labib, M.Sc. Student, Department of Civil Engineering, University of Manitoba.
- Ehab F. El-Salakawy, Professor, Department of Civil Engineering, University of Manitoba.

Journal and Status: Journal of Computers and Concrete, Techno Press, under review.

Reference:

Labib, S., El-Salakawy, E.F. (2021). "FEA of Adjacent Concrete Box Girders Transversely Post-Tensioned at Top Flange Only." Computers and Concrete, Techno Press, Submitted in April 2021.

Note:

The manuscript had been slightly edited from the original paper by renumbering the tables and figures to include the chapter number. In addition, the reference list and list of notations have been moved to the appropriate sections in the thesis as indicated in the table of contents.

Abstract:

A three-dimensional non-linear finite-element model (FEM) was constructed using a commercial software (ATENA-Studio) to investigate the transverse load distribution behavior of adjacent precast prestressed concrete box girder bridges. An innovative connection between box girders was used, where transverse post-tensioning was applied at the top flanges only eliminating the need for intermediate transverse diaphragms. The FEM was validated in terms of deflections, strains, cracking and ultimate loads, against experimental results previously reported by the authors. The validated FEM was then used to perform a parametric study investigating the influence of adding concrete topping, load location, and bridge width on the transverse load distribution behavior of the newly developed connection. The results of the FEM demonstrated the efficiency of concrete topping in limiting mid-span deflections up to 25%. Additionally, the maximum live load moment distribution factors (LLMDFs) for different load locations and bridge widths were evaluated.

Keywords: Adjacent box girders; Finite-element analysis; transverse post-tension; diaphragm; shear key; load distribution.

4.1. Introduction

Adjacent precast, prestressed concrete box girders are of favorable choice for short- and medium-span bridges by virtue of their easy and fast construction (Miller et al. 1999; Hanna et al. 2011). This kind of bridges typically composed of longitudinal precast members connected at their interface using partial-or full-depth grouted shear keys. In the last few decades, transverse post-tensioning (TPT) has been introduced to promote the monolithic behavior of such bridges and control longitudinal cracking recurrently develops over shear keys (Lall et al. 1998; Hanna et al. 2009). Typically, TPT is applied at transverse solid diaphragms cast monolithically with the

girders. Nevertheless, the presence of such diaphragms is associated with an increased cost and time. Such increase is more pronounced in skew bridges, where diaphragms need to be staggered or cast in stages. Additionally, the provision of diaphragms imparts complex formworks, and interruption of utility lines provided through the hollow portions of the girders (Hansen et al. 2012). Therefore, several studies have considered the elimination of transverse diaphragms from such kind of bridges and proposed different alternatives to apply the TPT. Hansen et al. (2012) introduced a diaphragm-free TPT connection incorporating sleeves above, and below the bottom, and top flanges, respectively, to house the TPT. Recently, Sun et al. (2018) reported a novel transverse connection, implemented in the St. Clair road bridge, Michigan, where TPT was applied at both top and bottom flanges. Nonetheless, placing the TPT ducts in the bottom flange might interfere with the longitudinal prestressing, and eventually require increasing the bottom flange thickness. Labib et al. (2021) conducted a pioneer experimental study to investigate the feasibility of applying TPT at top flanges only, eliminating the need for transverse diaphragms. The study investigated the efficiency of the proposed TPT technique in effectively distributing the applied load under simulated service and ultimate conditions. The studied parameters included the location of the applied load, level and distribution of TPT along the longitudinal direction of the bridge. Nevertheless, the effect of several parameters still needs to be studied. Accordingly, it was decided to use the nonlinear finite-element analysis (FEA) to predict the behavior of the newly developed connection when several key parameters are altered.

Numerous studies have adopted FEA to investigate the behavior of adjacent box girder bridges. These studies have assumed different modeling techniques when simulating different bridge components such as the interface among adjacent girders and the boundary conditions. Aktan et al. (2009) evaluated the transverse stress among adjacent girders. The grout-to-girder interface was

modeled as tightly-bonded joints given that these joints were initially intended to ensure moisture seal and to be crack-free. Similar approach was adopted by Semendary et al. (2017), where a simpler model using a continuous deck instead of shear keys was able to capture the overall bridge behavior. In that study, a single span bridge consisting of seven adjacent girders, with a total length of 18,600 mm, and overall width of 8,500 mm, was subjected to truckloads of 249.5 and 237.5 kN. Grace et al. (2012) studied the stress distribution and cracks development due to the combined effect of traffic and thermal loads. In that study, the grout material was modeled as friction interface elements among the adjacent girders. Similar approach was assumed by Fu et al. (2011), where a contact friction material of a specified coefficient of friction was employed between adjacent girders. Other studies have adopted a surface-to-surface contact to model the grout-to-girder and girder-to-girder interface (Steinberg et al. 2013; Hussein et al. 2017; Semendary et al. 2017). In those studies, a friction coefficient and critical shear values were assumed to characterize the tangential behavior of the interface between the shear key and girder surfaces. On the other hand, several assumptions have been suggested to simulate the bridge boundary conditions. Badwan and Liang (2007) assumed restrained translational movements when modeling supports at interior piers and restrained translational movements, except the longitudinal direction, when modeling supports at end abutments. Semendary et al. (2017) demonstrated that using a pin-roller with longitudinal stiffness resulted in a very similar behavior to a field-tested bridge. In that study, translational movements were restrained at one end, and allowed only in the longitudinal direction with a longitudinal stiffness of 2.6 kN/mm at the other end.

In this study, a three-dimensional (3D) nonlinear finite-element model (FEM) is constructed using the ATENA-Studio software (Červenka et al. 2020). The interactive graphical user interface GiD program (Coll et al. 2018) was used to create the input data and to generate the mesh. The FEM

was validated against the experimental results of a bridge model previously tested by the authors (Labib et al. 2021). Consequently, the validated FEM was used to carry out an extensive parametric study investigating key parameters influencing the load distribution behavior of the bridge including the presence of concrete topping, load location, and bridge width.

4.2. Summary of the Experimental Program

4.2.1. Details of Tested Bridge

A one-third-scale, single span bridge was erected and tested. The bridge consisted of four adjacent precast box girders. Each girder was 400 mm in width, 270-mm high, and 6,400-mm long, as shown in Figure 4.1. The thickness of all flanges and webs was 75 mm. Partial-depth shear keys of 75-mm depth, filled with gout, were used to connect the adjacent girders. Nine, 25-mm diameter PVC ducts were placed in the top flanges equally-spaced at 750 mm to house the TPT. Two end blocks of 400-mm long were provided near the supports to withstand the localized stresses upon releasing the longitudinal pre-tensioning forces. As shown in Figure 4.2, each box girder was reinforced with three size 13 prestressing steel strands (12.7 mm). In addition, five size 10M non-prestressing steel bars, three at the bottom and two at the top, were used in the longitudinal direction. Shear reinforcement of each girder comprised size 10M vertical stirrups spaced at 70 mm at end blocks and 140 mm in the mid-span region.

4.2.2. Material Properties

All box girders were constructed at a precast plant using concrete with a target 28-day compressive strength of 50 MPa. The mechanical properties of the used reinforcement are listed in Table 4.1. High-performance, non-shrink, bleed-resistant, sand-free, cementitious grout with a target 28-day compressive strength of 75 MPa was used to fill the shear keys (Labib et al. 2021).

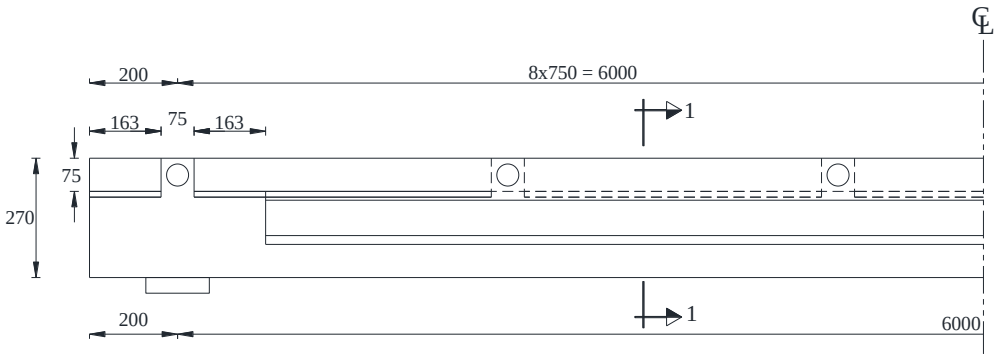

a) Elevation view

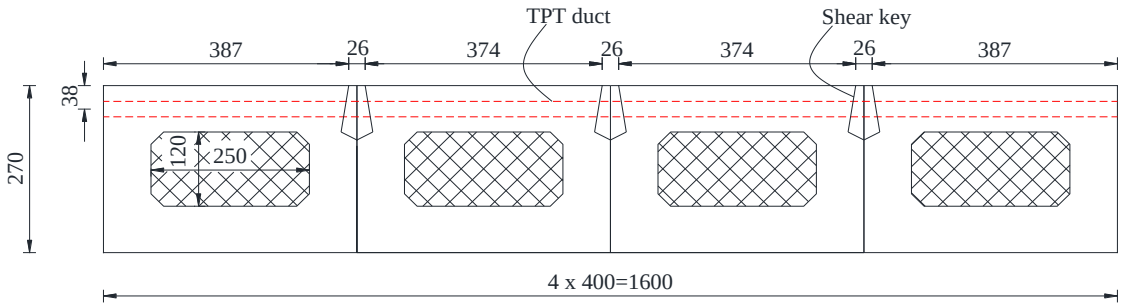

b) Section 1-1

Figure 4.1 - Geometry of bridge model (dimensions in mm).

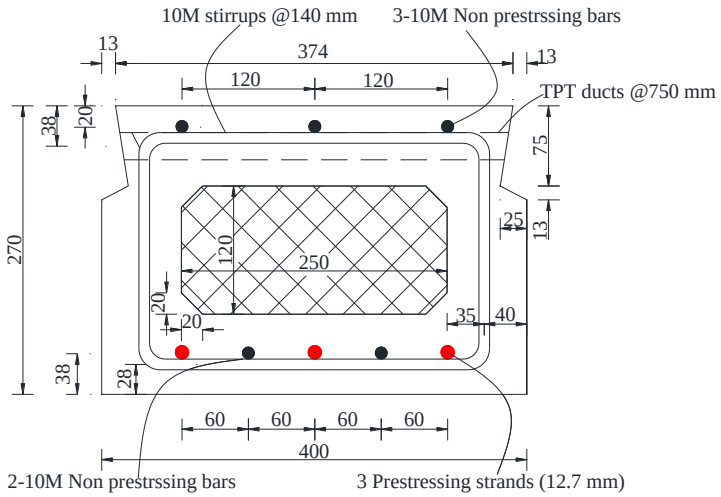

Figure 4.2 - Reinforcement details of an interior girder (dimensions in mm)

Table 4.1 - Mechanical properties of used reinforcement

Bar type	Bar Size	Diameter (mm)	Area (mm^2)	Tensile Strength (MPa)	Elastic Modulus (GPa)
Non-prestressing bars	10M	11.3	100	400*	200
Prestressing strands	13	12.7	98.7	1,860	202

* Yield strength.

4.2.3. Loading and Instrumentation

The bridge was subjected to four different tests, (1) Strain distribution test – uncracked shear key, (2) Load distribution test – uncracked shear key, (3) Load distribution test – cracked shear key, and (4) Ultimate load test. The strain distribution test was conducted to determine the adequate level of TPT force to achieve the minimum required prestress of 1.70 MPa suggested by the current CHBDC CSA/S6-19 (CSA 2019) and AASHTO specification LRFD-9 (AASHTO 2020). In this respect, different values of TPT forces (50, 70, 90 and 110 kN) were applied at different spacing utilizing either 3 ducts (spaced at 3,000 mm), 5 ducts (spaced at 1,500 mm) or 9 ducts (spaced at 750 mm). The load distribution tests (uncracked and cracked shear key conditions), and the ultimate load test were designed to investigate the efficiency of the proposed transverse connection in distributing live loads in the transverse direction under simulated service, and ultimate load conditions, respectively. The load distribution test was conducted by applying a single concentrated vertical load of 80 kN (below the cracking load of the assembled bridge) twice, once on exterior and once on interior girders, taking advantage of the symmetry about longitudinal axis. The load was applied using a rectangular steel plate (250 × 180 mm) that represents a one-third scale footprint of the standard wheel load. The load distribution test was repeated after partially cracking the shear key joints simulating longitudinal cracking recurring during the bridge service time. Three different TPT levels of 50, 70 and 90 kN were applied at two TPT arrangements (5

ducts spaced at 1,500, and 9 ducts spaced at 750 mm). For all TPT levels and arrangements, live load moment distribution factors (LLMDFs) were estimated by dividing the longitudinal concrete strain measured at the bottom of one girder to the summation of all measured strains for all girders (Ghosn et al.1986). In the ultimate load test, an exterior girder was loaded in several loading and unloading cycles up to failure when a TPT force of 70 kN was applied at each of the nine TPT locations equally spaced at 750 mm. Figure 4.3 shows the test setup used throughout the tests. Several PI-gauges and concrete strain gauges were distributed on the top surface of the bridge model to measure concrete strains in the transverse direction. In addition, several linear variable displacement transducers (LVDTs) were placed at the bottom surface of the bridge model to measure deflection and joint movement at mid-span. Furthermore, four longitudinal strain gauges were attached to the mid-width of the bottom flange of the girders at mid-span to measure the flexural tensile strains. More details about the instrumentation layout can be found in Labib et al. (2021).

4.2.4. Main Findings

The strain distribution test demonstrated no joint opening due to the eccentric application of TPT and the capability of the proposed TPT technique, when distributed on all nine ducts spaced at 750 mm, in achieving the required concrete prestress of 1.7 MPa along the entire length of shear keys. On the other hand, the load distribution tests demonstrated an insubstantial effect of TPT level and arrangement on the transverse load distribution behavior (mid-span deflection and LLMDFs) regardless of the position of the applied vertical load or the shear key condition. In the ultimate load test, the presence of TPT managed to maintain the integrity of the bridge model after partial debonding of the middle shear key preventing a potential catastrophic mode of failure. More details about results and discussions can be found in Labib et al. (2021).

Figure 4.3 - Load distribution test setup (vertical load applied at an interior girder).

4.3. Characteristics of Finite Element Model

To extend the investigation of the behavior of the developed TPT connection, a series of FEMs were prepared using the software package ATENA-Studio to study the effect of key parameters on the transverse load distribution behavior. The following sections describe the basic characteristics of the constructed FEMs. Further details can be found elsewhere (Červenka et al. 2020; Coll et al. 2018).

4.3.1. Geometry and Boundary Conditions

Figure 4.4 shows the FEM of the tested bridge. Taking advantage of the symmetry about the transverse axis, only half of the bridge model was constructed and analyzed. The concrete, grout, and steel elements were modeled using four-node tetrahedral elements. These elements can

accommodate the geometrical irregularities associated with the hollow portions and indented edges of each box girder. A semi-structured mesh was employed in the GiD interface, where the mesh is only structured in the topologically prismatic direction of the volume, i.e., the longitudinal direction of the bridge model. In a preliminary study, a mesh sensitivity analysis was conducted, and it was demonstrated that further reduction of the average element size to less than 50 mm compromised the computing effort with inappreciable difference in the analysis results. Accordingly, a total of 122,444 tetrahedral elements of an average size of 50 mm were used to model the geometry of the bridge model. The monolithic behavior between the end blocks and the hollow portions of each girder was simulated using fixed contact boundary condition at the block-to-girder interface. Thus, deformation compatibility between end blocks and the remaining hollow portion of each girder was enforced. Boundary conditions were selected to have a hinge support at one end and a roller support at the other end of the bridge model, i.e., pin-roller condition. This was achieved by restraining the displacement perpendicular to the plane of cut (plane of symmetry) and allowing only longitudinal displacement at the other end. As such, the system forces were balanced, and the bridge model was kept in static equilibrium.

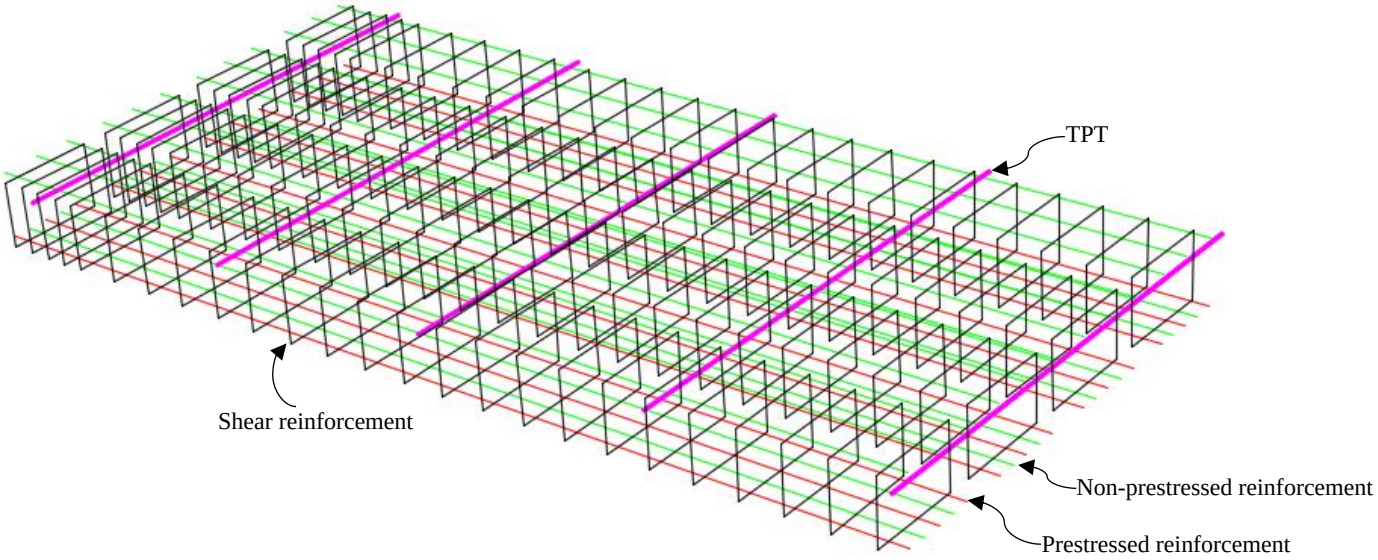

a) Descrete reinforcement.

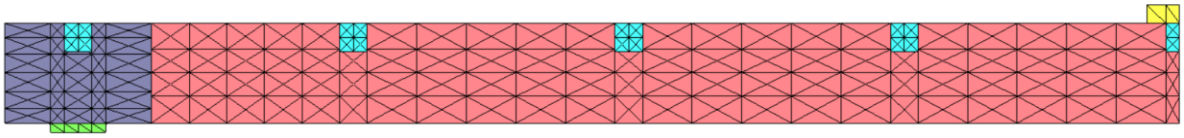

b) Mesh discretization in longitudinal direction.

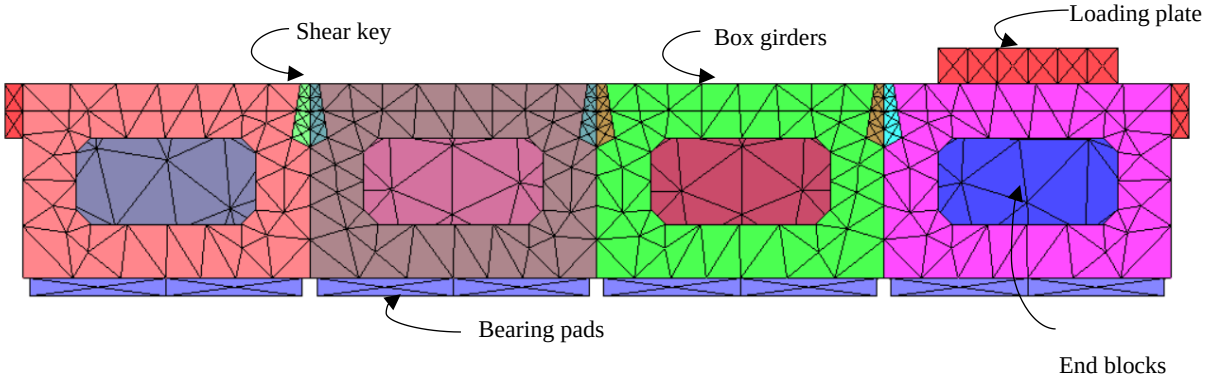

c) Mesh discretization in transverse direction.

Figure 4.4 - FEM and reinforcement configuration of the bridge model.

4.3.2. Concrete and Grout Material

In the ATENA-GiD interface, a fracture-plastic constitutive model was assigned to the geometrical entities. The fracture-plastic model combines two different constitutive models for tensile (fracture) and compressive (plastic) behavior (Cervenka et al. 2020). The ATENA software adopts special algorithm to allow both models, i.e., fracture and plastic models, to be developed and formulated separately. This way, the cases when failure surfaces of both models are active, can be captured. The fracture model adopts the classical orthotropic smeared crack formulation and crack band model employing Rankine failure criterion and exponential softening. The smeared crack model can be either rotated or fixed crack model. In both models, a crack is initiated when the principal stress exceeds the tensile strength of the material. In the fixed crack model, the crack direction is defined by the principal stress direction at crack initiation. During further loading steps, the principal stress direction is fixed, which represents the material orthotropic axis. In the rotated crack model, the direction of the principal stress coincides with the principal strain direction. Accordingly, no shear stresses are induced on the crack plane. In this study, the fixed crack model was adopted. The smeared crack model was adopted in several studies (Ventura-Gouveia et al. 2011; Markou and Papadrakakis 2013). The compressive (plastic) model, on the other hand, adopts softening/hardening plasticity model based on Menétrey-Willam failure surface. As shown in Figure 4.5, the softening/hardening law is based on the uniaxial compressive test. The nonlinear hardening branch is based on strains whereas the softening branch is based on displacements. The parameters of the constitutive model, i.e., modulus of elasticity, fracture energy and tensile strength are dependent on of the concrete compressive strength (Červenka et al. 2020). The values of the main parameters used for the concrete and grout materials are listed in Table 4.2.

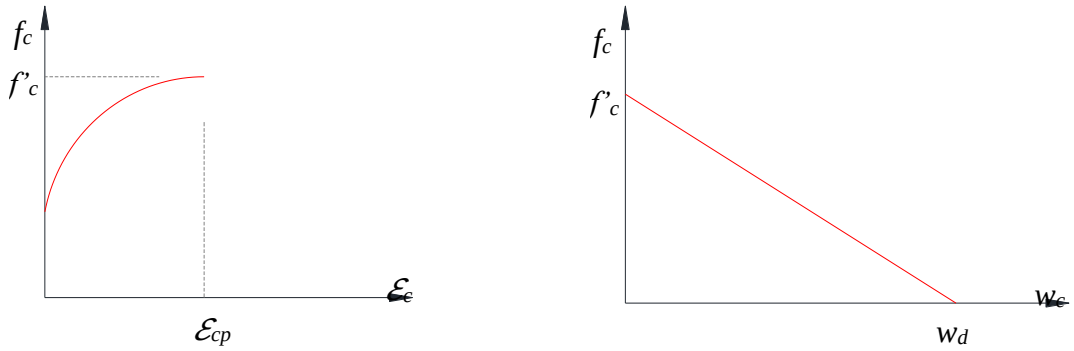

a) Hardening law b) Softening law

Figure 4.5 - The softening/hardening plasticity constitutive model (Červenka 2020).

Table 4.2 - Main parameters of concrete and grout constitutive models

Parameter	Concrete	Grout
Compressive strength, $f'c$ (MPa)	55	85
Modulus of elasticity, E_c (GPa)	40,129	44,410
Poisson's ratio, μ	0.2	0.2
Fracture energy, G_f (N/mm)	97.5	130
Tensile strength, f_t (MPa)	3.9	5.2
Critical compressive displacement, w_d (GPa)	0.5	0.5
Crack model	Fixed	Fixed
Reduction of compressive strength factor, rc^{lim}	0.8	0.8

4.3.3. Reinforcement Material

All reinforcement (prestressing strands and regular non-prestressed steel) were modeled as discrete reinforcement using truss elements embedded in the solid elements (tetrahedral elements). A bi-linear material model with strain hardening was assigned to the reinforcement entities. The ascending line has a slope equals to the elastic modulus of reinforcement material. The second line represents the plasticity of the reinforcement material associated with hardening, and its slope is

zero in case of perfect plasticity. Reinforcement properties listed in Table 4.1 were used for the FEM.

4.3.4. Loading and Bearing Plates

Elastic isotropic material was used to model the loading and bearing plates. This material was defined with a modulus of elasticity of 200 GPa and a Poisson ratio of 0.3.

4.3.5. Bond Model

ATENA introduces the bond-slip of reinforcing bars in two predefined models in addition to a user-defined model. The two models are the CEB-FIB model code from 1990, the bond-slip law by Bigaj (1999). These models take into account the concrete compressive strength, and reinforcement diameter and type (Cervenka et al. 2020). In this study, the bond-slip model proposed by Bigaj (1999) was used to model prestressed and non-prestressed reinforcement. Such model was reported to reduce the effect of mesh size associated with the full-bond model, where relatively large mesh size results in very limited slip values (Jendele and Červenka 2006). This bond model was successfully used to model the bond behavior of prestressed reinforcement (Mahmoud et al. 2018). On the other hand, internal cable model with coefficient of friction set to zero, was used so simulate the un-bonded TPT.

4.3.6. Interface and Bonding Materials

The interface between the adjacent girders was modeled using the interface material model implemented in ATENA. This material model was assigned to auxiliary contact volumes drawn at the girder-to-girder interface. In that material model, the friction coefficient was set to zero, this way, no tension was permitted, and full compression was assumed. Similarly, this interface material was used to model the interface between the precast girders and the enclosed grouted-shear keys (girder-to-grout interface), with adjusted coefficient of friction of 1.0 as per AASHTO

LRFD-9 (AASHTO 2020). A further simplified model was constructed assuming fixed contacts at the girder-to-grout interface. This simplified model was reported efficient in case there is no slippage between the girder-to-shear key interface (Semendary et al. 2017). In this study, such model was capable of capturing the behavior of the modeled bridge.

4.3.7. Load Application and Solution Method

The loading process of the bridge model comprised four different loading cases. In the first loading case, the prestress was applied to the longitudinal prestressing tendons. The prestress was simulated by applying initial strain, calculated based on the elastic modulus of the prestressed material, to the end nodes of the strands. The second loading case simulated the casting of the precast elements in the precast plant. This was achieved by activating the self-weight of the concrete material. In the third loading case, TPT stress was applied at the top flanges of the girders only. The final loading case included the application of the external vertical load. For each load case, the applied load was divided into several sequential steps. The standard Newton–Raphson iterative solution method implemented in ATENA-Studio was employed in the analysis. In this method, a set of nonlinear equations are solved for the vector of internal forces until four convergence criteria were satisfied. The first criteria checks the norm of relative deformation during the last iteration, the second one checks the norm of the out-of-balance forces, the third one checks out-of-balance energy and the fourth conditions checks out-of-balanced forces in terms of maximum components (Červenka et al. 2020). A conditional break criterion was set to stop the analysis when the convergence errors are large at the end of a given step. The default convergence error tolerance for the first three criteria in ATENA-Studio was set to 1%. By setting the step stop multipliers at 10, the analysis is stopped if the convergence error at the end of a given step exceeds 10%.

4.4. Model Validation

The accuracy of the FEM was calibrated against the experimental results in a two-stage validation process. In the first stage, where shear keys were perfectly intact, mid-span deflections and strains measured at the mid-width of each individual girder were validated under a monotonically increased service load up to 80 kN (below the cracking load of the bridge model). In the second stage, where shear keys were partially cracked, the cracking and the ultimate load capacity of the bridge model were verified.

4.4.1. Service Load Validation

Figure 4.6 and Figure 4.7 show the load-deflection and the load-strain relationships, respectively, for the experimental and FEM results. According to these figures, when the exterior girder was loaded, and a TPT force of 70 kN was applied at all nine ducts, the numerical model very well agreed with the experimental results in terms of load-deflection and load-strain behavior (within 5% difference). Similar trend was observed for all used TPT levels (50, 90 kN) and arrangements (5 ducts equally spaced at 1,500 mm).

4.4.2. Ultimate Load Validation

Labib et al. (2021) reported unexpected scenario during the ultimate load test. During loading of the exterior girder G1 (loading and unloading cycles), a portion of the shear key connecting the loaded girder G1 and the adjacent girders was deboned, triggering the TPT to come into play. When this occurred, the TPT was the sole load transfer mechanism and maintained the integrity of the bridge. Despite the presence of TPT prevented a potential catastrophic failure, the transverse load sharing mechanism was compromised. This eventually led to a sudden punching failure in the loaded girder G1. Accordingly, the constructed FEM was used to validate the cracking and ultimate load of the loaded girder G1. In the FEM, the analysis was terminated after reaching the

ultimate load and softening began to take over. Figure 4.8 shows the load-deflection response of the exterior girder G1. The FEM cracking was approximately 1.5% higher than the corresponding experimental load. The ultimate capacity was 232.06 kN, which is 1.0% higher than the experimental ultimate load (229.8 kN).

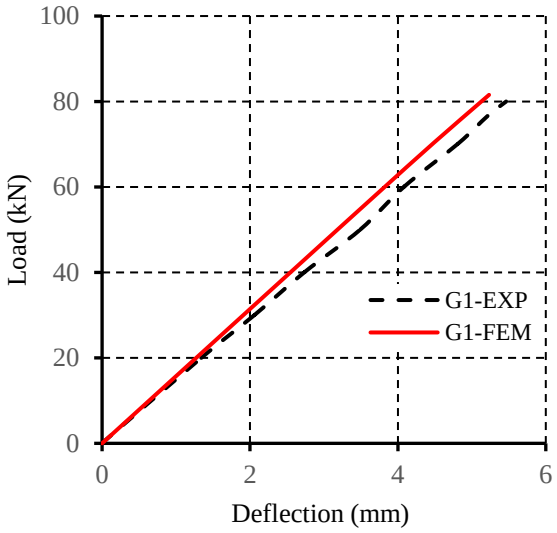

a) Load-deflection response of girder G1

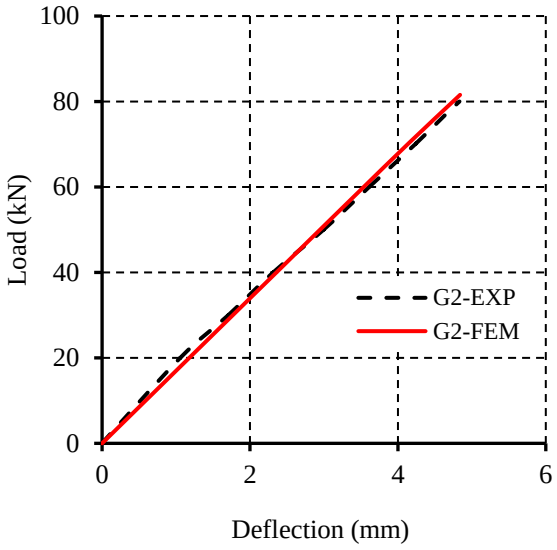

b) Load-deflection response of girder G2

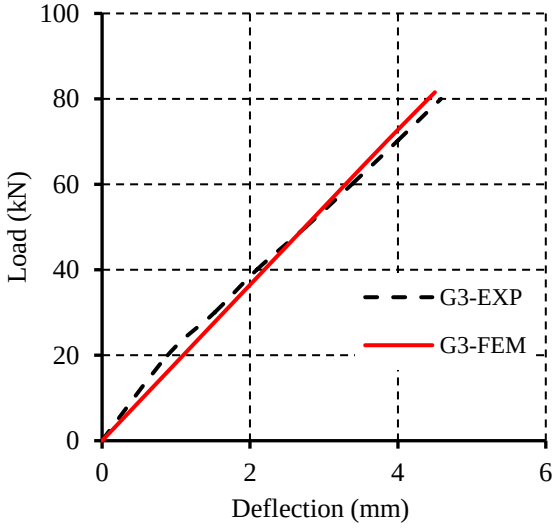

c) Load-deflection response of girder G3

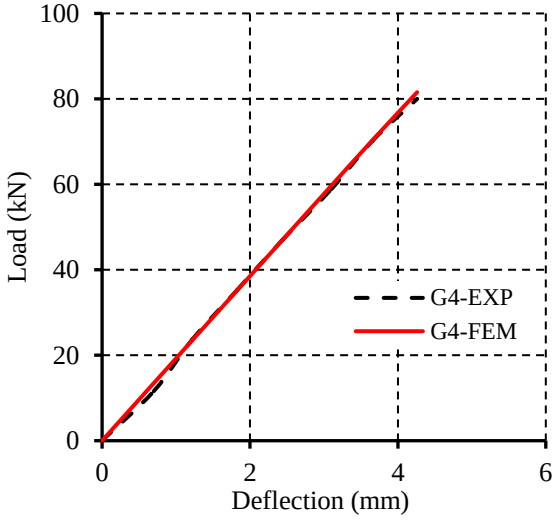

d) Load-deflection response of girder G4

Figure 4.6 - Validated load-deflection response of individual adjacent girders.

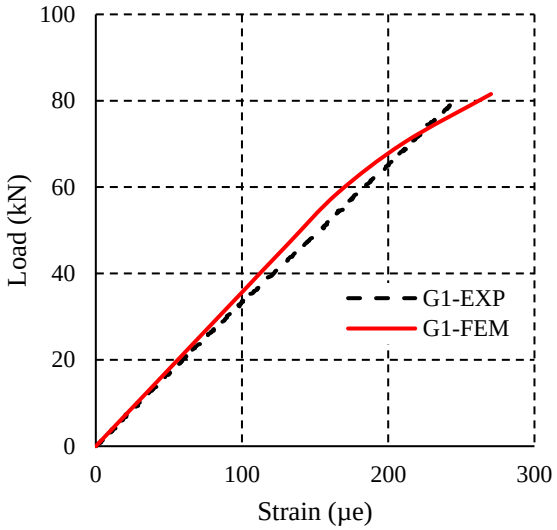

b) Load-strain response of girder G1

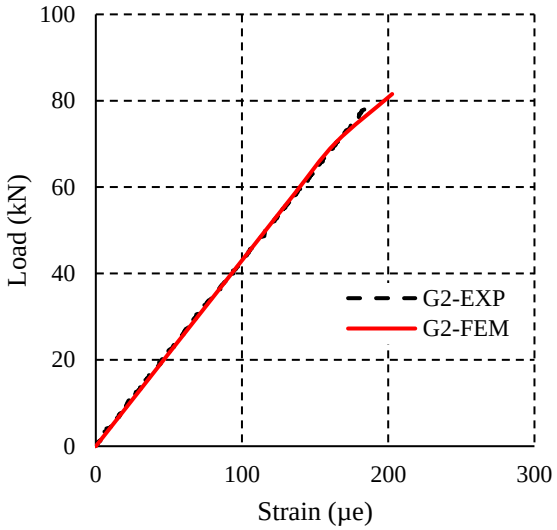

c) Load-strain response of girder G2

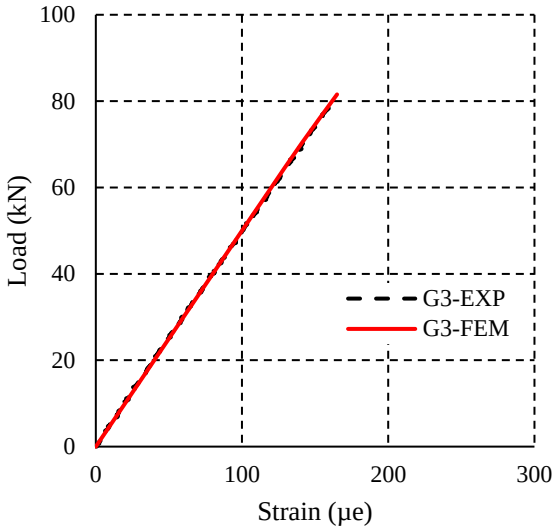

c) Load-strain response of girder G3

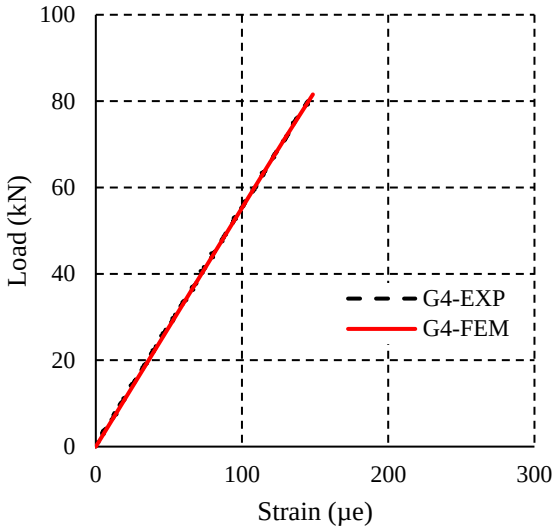

d) Load-strain response of girder G4

Figure 4.7 - Validated load-strain response of individual adjacent girders.

4.5. Parametric Study and Discussion

In this parametric study, the validated FEM was used to study the influence of key parameters on the transverse load distribution behavior of the tested bridge model in terms of mid-span

deflections and tensile flexural strains. The considered parameters included the effect of adding a concrete topping of different thicknesses (75, 100 and 150 mm), the effect of wheel location (the wheel load was moved transversely every 200 mm), and the effect of the bridge width (2,000, 2,400 and 2,800 mm). This parametric study was conducted considering a TPT level of 70 kN applied at all nine ducts equally spaced at 750 mm, which were selected based on the findings of the experimental study that such combination was capable of achieving the required prestress along the shear keys (Labib et al. 2021).

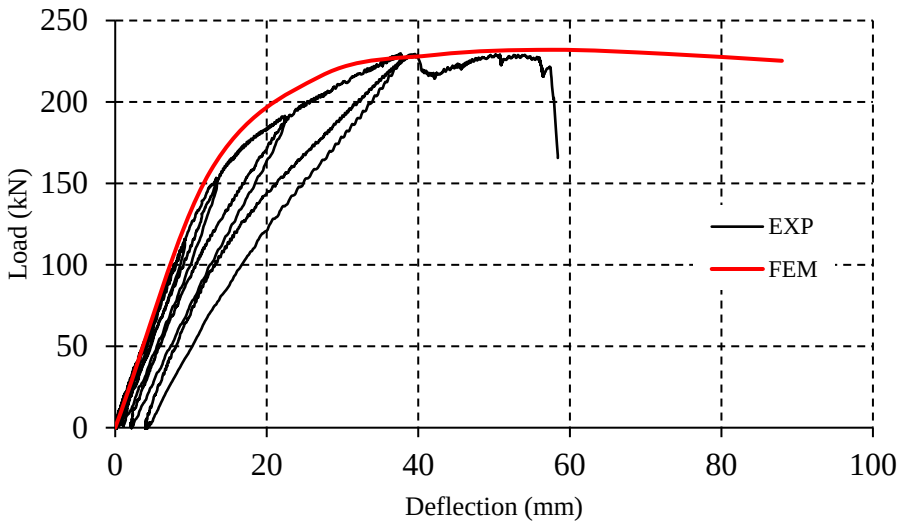

Figure 4.8 - Validated ultimate load for the loaded girder G1.

4.5.1. Effect of Adding Concrete Topping

The experimental program was conducted on box girders only without concrete topping. Such topping protects shear keys from cracking and promotes the uniform load distribution among adjacent girders. In this series of models, the effect of adding concrete topping was numerically investigated. Concrete topping of three different thicknesses (75, 100 and 150 mm) was considered. Figure 4.9 and Figure 4.10 show the mid-span deflection profiles and LLMDFs for

different thicknesses of concrete topping. As expected, the presence of concrete topping enhanced the overall stiffness of the bridge model through limiting deflections and adding to the transverse load sharing mechanism. For instance, when the exterior girder was loaded (80 kN), an overall reduction of mid-span deflections of 8% was recorded when using a concrete topping of 75 mm. A further reduction of 17%, and 25% was observed when using a concrete topping of 100 and 150 mm, respectively. Similar trend was observed when the interior girder was loaded. On the other hand, LLMDFs appeared to be insubstantially affected upon introducing concrete topping.

4.5.2. Effect of Load Location

In this series of models, the wheel load was placed transversely at different locations across the bridge width to determine the wheel location associated with the maximum load response (deflections and flexural tensile strains) for both the interior, and exterior girders, respectively. In this respect, the bridge model was loaded with five static load cases as shown in Figure 4.11. In these load cases, the wheel load was first placed at the edge of the bridge (Load Case I), and, then, transversely moved every 200 mm. Figure 4.12 and Figure 4.13 show the mid-span deflections and LLMDFs for different wheel load locations. The exterior girder experienced the highest deflections and LLMDFs when the wheel load was transversely placed at the edge of the bridge width (Load Case I). In this case, mid-span deflections of 5.24, 4.78, 4.41 and 4.16 mm were recorded at the mid-width of girders G1, G2, G3, and G4, respectively. These deflections are similar higher than the case of having the load applied to the centerline of the external girder, i.e., Load Case II (5.12, 4.74, 4.40 and 4.17 mm). Similar trend was observed for the LLMDFs, where the exterior girder developed a maximum LLMDF of 36.4 % under Load Case I, 6% higher than Load Case II (34.2%). Similar to the exterior girder, the interior girder developed a maximum deflection of 4.78 mm under Load Case I. This value is slightly higher than the case of having the

load applied to the centerline of the interior girder, i.e., Load Case IV (2.0% higher). This observation is in agreement with the experimental results reported by Labib et al. (2021), where the deflections of the interior and exterior girders were maximum when the load was placed towards the edge of the bridge width. Nonetheless, the interior girder developed a maximum LLMDF of 28.1% when the load was placed directly on the centerline (Load Case IV). This value is higher than the case of having the load directly applied to the shear keys, i.e., Load Case V (7.0% higher).

4.5.3. Effect of Bridge Width

Three different widths of 2,000, 2,400 and 2,800 mm corresponding to five, six, and seven box girders, respectively, were considered in addition to the original bridge width of 1,600 mm. For each bridge width, the wheel load was first positioned at the centerline of the exterior girder G1 and moved transversely every 400 mm such that the load was applied to the centerline of each girder. Figure 4.14 and Figure 4.15 show the mid-span deflections and LLMDFs when the exterior girder G1 and the interior girder G2 were loaded. As expected, increasing the bridge width resulted in increasing the overall bridge stiffness and eventually limited the overall mid-span deflections. For instance, when the exterior girder was loaded, the overall mid-span deflections were reduced by 15.0, 22.0 and 27.0% when the bridge width was increased from 1,600 mm to 2,000, 2,400 and 2,800 mm, respectively. Similar trend was observed when interior girders were loaded. On the other hand, the maximum LLMDF for both exterior and interior girders was reduced when the bridge width was increased. For instance, for a bridge width of 1,600 mm, a maximum LLMDF of 34.2 % was recorded for the exterior girder. Such LLMDF dropped to 29.6, 27.1 and 25.6% when the bridge width was increased to 2,000, 2,400 and 2,800 mm, respectively. Similar

observations were recorded for the interior girders, where the maximum LLMDF of 28.1% was associated with the least bridge width of 1,600 mm.

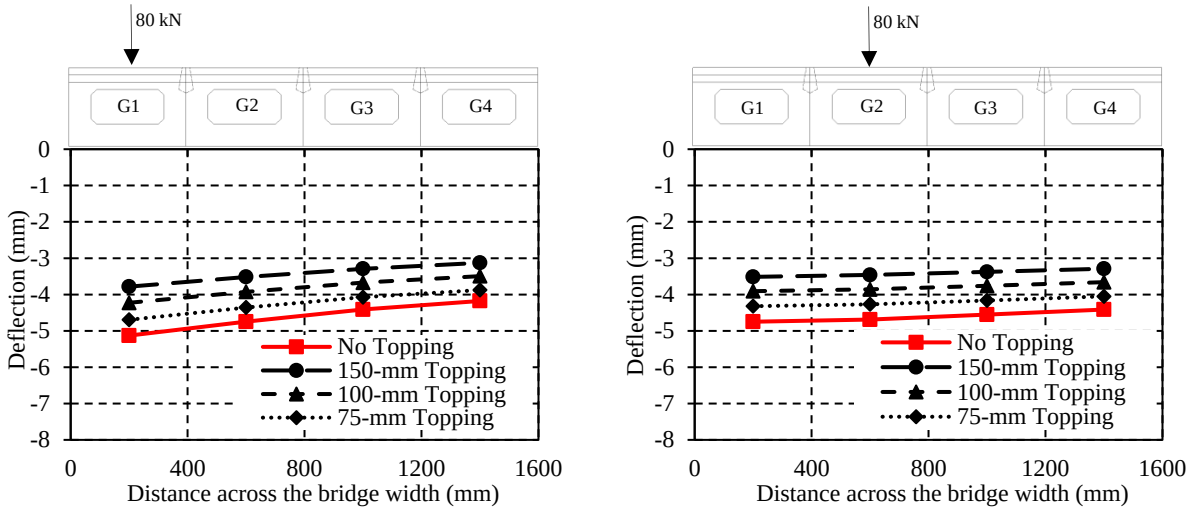

(a) External girder G1 loaded (b) Interior girder G2 loaded

Figure 4.9 - Mid-span deflection profile for different thicknesses of concrete topping.

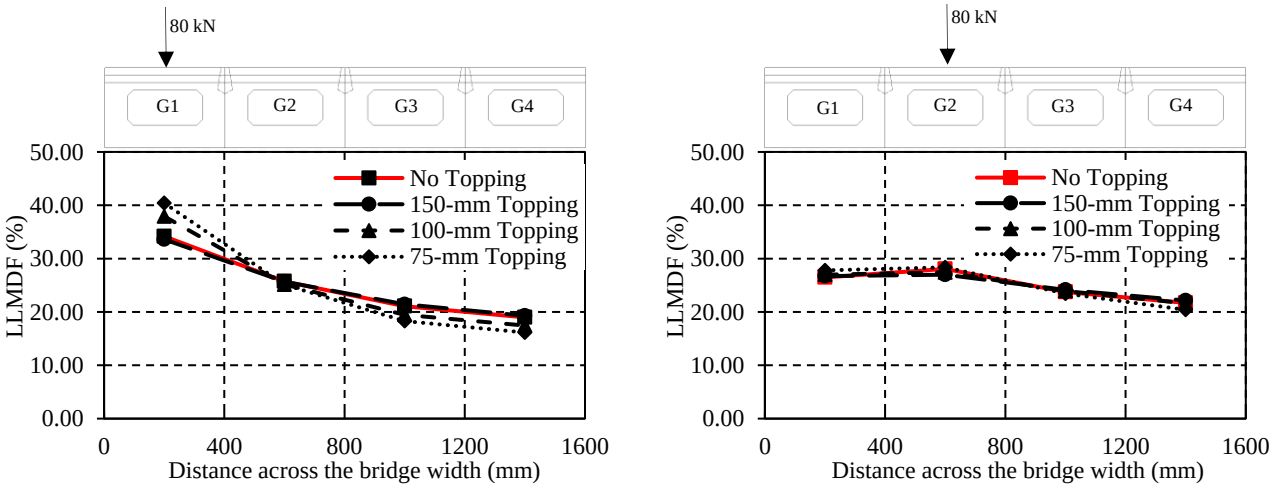

(a) External girder G1 loaded (b) Internal girder G2 loaded

Figure 4.10 - Mid-span LLMDFs for different thicknesses of concrete topping.

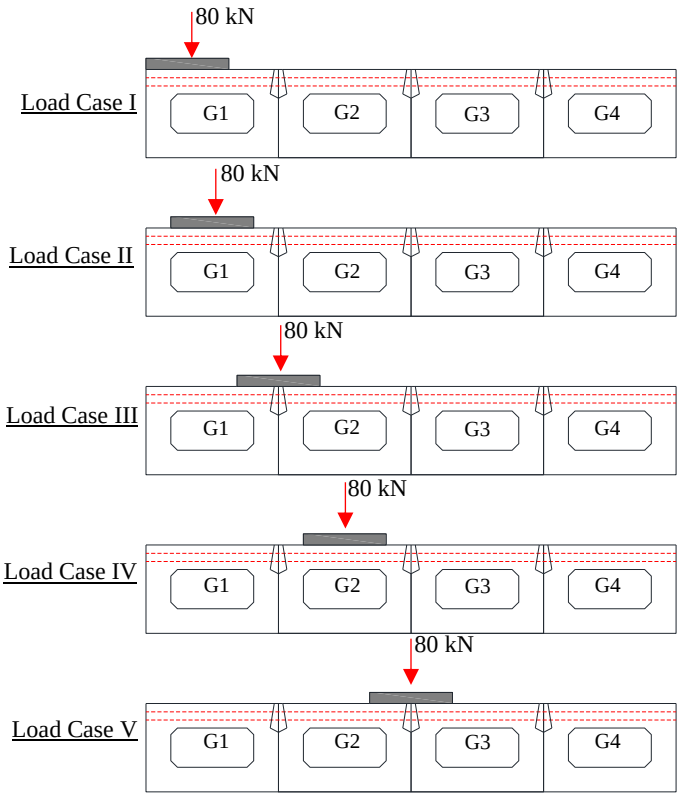

Figure 4.11 - Schematic for different wheel load locations.

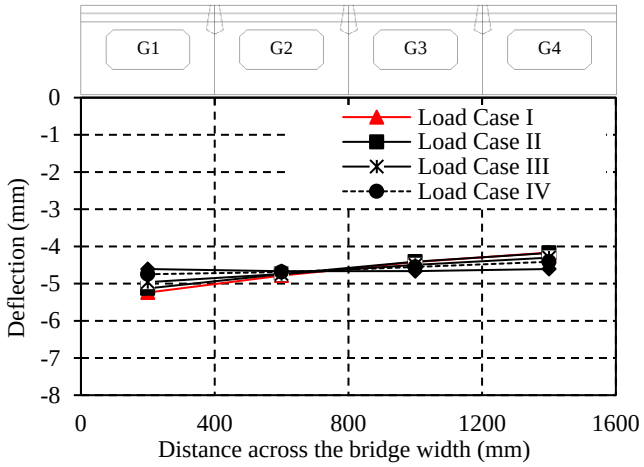

Figure 4.12 - Mid-span deflection profile for different wheel locations.

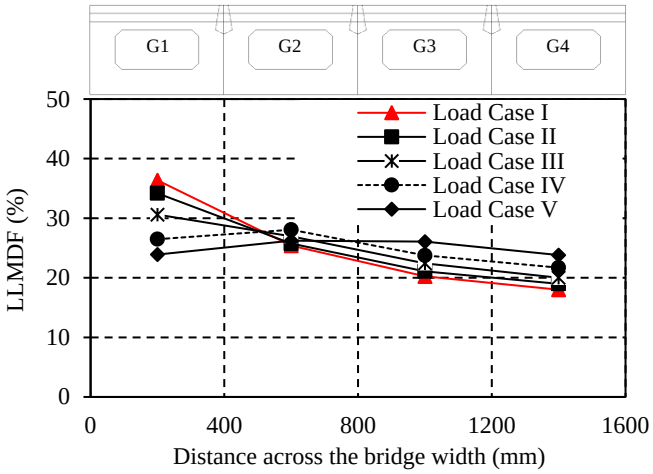

Figure 4.13 - Mid-span LLMDFs for different wheel locations.

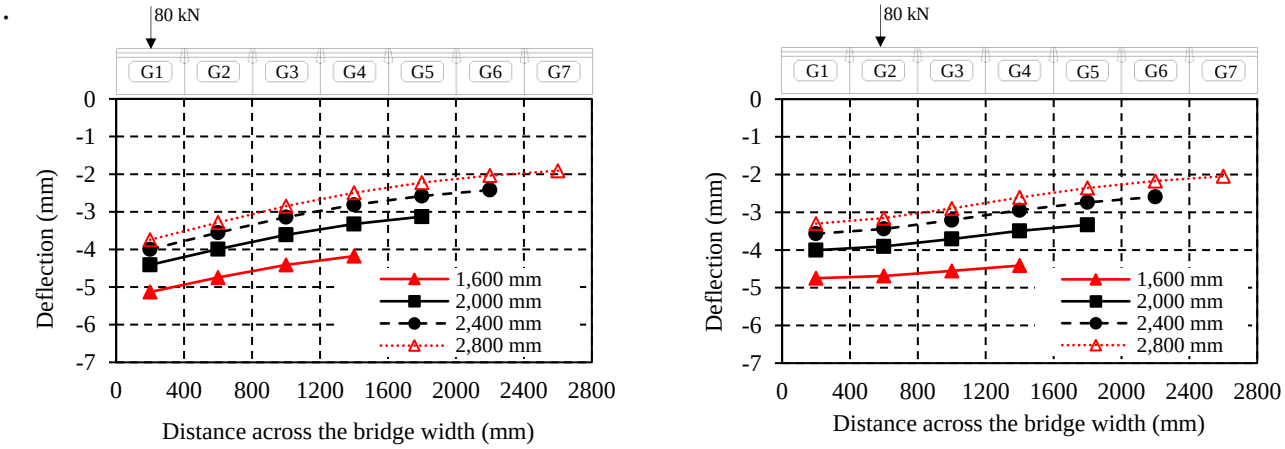

(a) Exterior girder G1 loaded (b) Interior girder G2 loaded

Figure 4.14 - Mid-span deflection profile for different bridge widths.

4.5.4. Evaluation of LLMDFs

The AASHTO LRFD-9 (AASHTO 2020) specifies an approximate method to calculate the live load moment distribution factor (LLMDFs) using empirical formulas. The considered box girder in this study falls in category (g) which governs precast concrete box girders with or without transverse post-tensioning (AASHTO 2020). For this specific category, the LLMDFs for an

interior girder was estimated using Eqs. (1) and (2) for one design lane, and two or more design lanes, respectively:

$$LLMDF_{\text{int}} = k\left(\frac{b}{33.3L}\right)^{0.5}\left(\frac{I}{J}\right)^{0.25} \quad \text{Equation 4.1}$$

$$LLMDF_{\text{int}} = k\left(\frac{b}{305}\right)^{0.6}\left(\frac{b}{12.0L}\right)^{0.2}\left(\frac{I}{J}\right)^{0.06} \quad \text{Equation 4.2}$$

and $$k = 2.5(N_b)^{-0.2} \geq 1.5 \quad \text{Equation 4.3}$$

where N_b = number of girders, b = width of a beam (in.), L = span of beam (ft), I = moment of inertia (in.^{4}); and J = St. Venant's torsional inertia for thin-walled closed sections (in.^{4}).

For an exterior girder, LLMDF is estimated as follows:

$$LLMDF_{ext} = e \times LLMDF_{\text{int}} \quad \text{Equation 4.4}$$

where the correction factor e is calculated using Eqs. (5) and (6) for one design lane, and two or more design lanes, respectively:

$$e = 1.125 + \frac{d_e}{30} \geq 1.0 \quad \text{Equation 4.5}$$

$$e = 1.04 + \frac{d_e}{25} \geq 1.0 \quad \text{Equation 4.6}$$

and d_e is the distance from the centerline of the exterior web of exterior girder to the interior edge of curb or traffic barrier (in.).

The above Equations are only applicable to a specific range of parameters. For example, Equation 4.1 and Equation 4.2 are only applicable to bridges consisting of at least five girders, with a

minimum girder width of 35 in. and a minimum bridge span of 20 ft. Since the tested bridge model is a one-third scale model of a real bridge with a limited number of girders (four girders), these formulas would not be applicable. Accordingly, for the sake of comparison, the actual dimensions of the one-third scale tested bridge model were used to evaluate such LLMDFs. By substitution, N_b = 5, b = 1,200 mm (47.25 in.), L = 18,000 mm (59 ft.), I = 43.20 × 109 mm^4 (103,788 in.4), J = 84.25 × 109 mm^9 (202,411 in.^{4}), the aforementioned formulas will yield LLMDFs of 33.1% and 34.4% for the interior and the exterior girders, respectively. These LLMDFs factors are conservatively higher the maximum LLMDFs of 23.8 and 29.6% obtained from the numerical study for both interior, and exterior girders, respectively (refer to Figure 4.15).

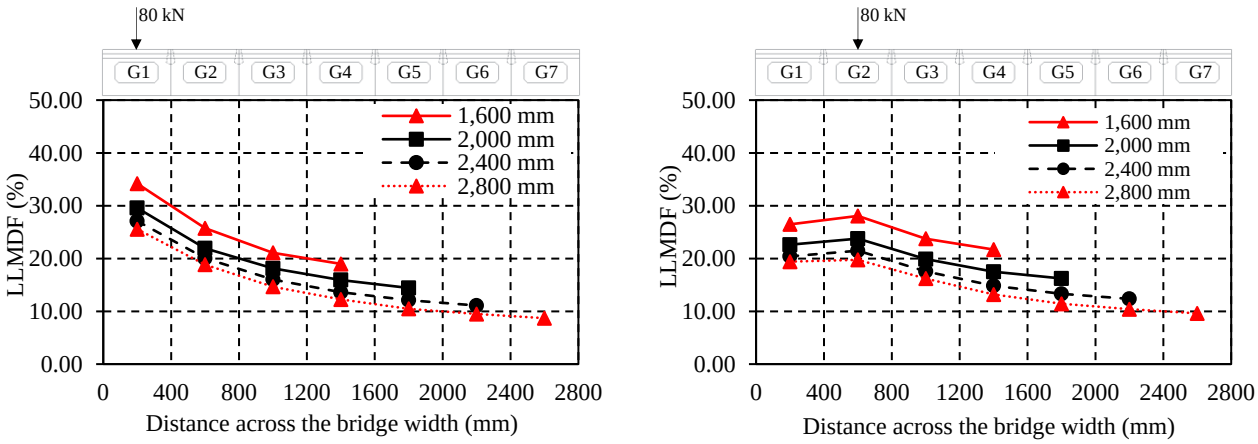

a) Exterior girder G1 loaded b) Interior girder G2 loaded

Figure 4.15 - Mid-span LLMDFs for different bridge widths.

4.6. Conclusions

A finite element model was constructed and validated against experimental results previously reported by the authors. An extensive parametric study was conducted to evaluate the influence of key parameters on transverse load distribution behavior of adjacent precast prestressed concrete

box girders. Based on the numerical results presented in this paper, the following conclusions can be drawn:

- The presence of concrete topping enhanced the overall stiffness of the bridge model by limiting mid-span deflections. Mid-span deflections were reduced by 8, 17, and 25% when concrete topping of 75, 100 and 150-mm thickness, respectively, was used. Nevertheless, the LLMDFs were found to be insignificantly altered when a concrete topping was incorporated.
- The LLMDFs were evaluated for multiple wheel locations to determine the location associated with the maximum response. The exterior girder exhibited the maximum LLMDF when the load was placed at the farthest possible point across the bridge width. On the other hand, the interior girder G2 exhibited the maximum LLMDF when the wheel load was centered with the girder centerline (Load Case IV).
- To satisfy the minimum number of girders required to utilize the LLMDFs proposed by the AASHTO-LRFFD, different bridge widths consisting of five, six and seven girders were investigated. For each bridge width, the wheel load was placed transversely at different locations to estimate the maximum LLMDFs. The LLMDFs were found to be reduced when the bridge width was increased. The maximum LLMDF for the exterior girder dropped by 25% when the bridge width was increased to seven girders (2,800 mm). Similar trend was observed for the interior girders.
- In lieu of size limitations dictated by the scaled bridge model, AASHTO LRFD-9 bridge design specifications were used to estimate the LLMDFs for both the exterior and the interior girders considering the actual dimensions of the one-third scale bridge model. The obtained LLMDFs were found to be conservative by 39%, and 16% for the interior, and

the exterior girders, respectively. This observation suggests that the existing LLMDFs proposed by AASHTO LRFD-9 could be used, as an initial step, to design the full-scale bridge structure of the tested bridge prototype.

Among future research needs, is the field investigation of LLMDFs of a full-scale bridge constructed utilizing the newly-developed transverse connection. In addition, the combined effect of temperature gradients and structural loading needs to be investigated.

5. CONCLUSIONS AND RECOMMENDATIONS

5.1. Summary

This study investigated the feasibility of applying TPT at the top flanges only of concrete box girder bridges instead of being accommodated in discrete rigid diaphragms. The study comprised two phases: experimental and numerical phase. In the experimental phase, a one-third scale precast prestressed concrete box girder bridge was erected and tested. The experimental program consisted of conducting four different tests, (1) Strain distribution test – uncracked shear key, (2) Load distribution test – uncracked shear key, (3) Load distribution test – cracked shear key, and (4) Ultimate load test. These tests were designed to evaluate the developed transverse strains as well as the load distribution behavior of such bridges under simulated service and ultimate loads. On the other hand, the numerical phase consisted of constructing and validating a FEM of the experimentally tested bridge using a commercial FEM package ATENA-GiD and ATENA-Studio. The validated FEM was used to conduct a parametric study investigating the maximum LLMDFs of the exterior and the interior girders under varying several parameters. These parameters were the presence of concrete topping, the wheel load location and the bridge width.

5.2. Conclusions

Based on the results of the experimental and numerical phase, the following conclusions can be drawn:

5.2.1. Conclusions from the Experimental Phase

- Regardless of the level of TPT force, the minimum required prestress of 1.7 MPa can only be achieved near the TPT locations even when TPT is applied at the top flanges of the girders, which is closer to the concrete surface.

- Distributing the TPT force at a shorter spacing along the length of the bridge is more efficient in producing the required concrete prestress along the entire length of shear keys than increasing the TPT force at discrete distant locations. At a relatively low TPT force of 70 kN spaced at one-eighth of the span, the measured compressive strains are higher than the minimum required value of 55 με.
- Under a monotonically increased vertical load of 80 kN, regardless of the position of the vertical load, the mid-span deflection was slightly reduced with increasing the TPT level from 50 to 70 kN, especially when TPT was applied at all nine ducts. However, further increasing TPT level to 90 kN did not affect the deflection of the girders.
- Regardless of the position of the vertical load, varying the TPT level and arrangement did not significantly affect the LLMDFs for all girders. At all TPT levels and arrangements, the loaded girder always had the highest LLMDF.
- Insignificant joint movement was observed when the bridge model was loaded. When the exterior girder was loaded (80 kN), the joints tended to close up with a maximum recorded joint closing of 0.07 mm. On the other hand, when the interior girder was loaded, the joints closest to the applied load tended to open with a maximum recorded joint opening of 0.10 mm.
- Under the applied vertical load of 80 kN, partially cracked shear keys performed comparably to the intact shear keys condition in terms of mid-span deflection profile, longitudinal concrete tensile strains, and joint movements.
- Differential deflections were slightly affected by the TPT force and arrangement. When Girder G2 was loaded under Case II arrangement, increasing the TPT force from 50 to 70 kN decreased the maximum differential deflection at Joint J1 by 17%. However, further

increasing the TPT force to 90 kN or changing the TPT arrangement to Case III did not significantly alter the mid-span differential deflections.

- The proposed TPT detail (TPT applied at the top flange only) managed to maintain the integrity of the bridge model following the failure of the shear key. Consequently, it significantly enhanced the deformability of the bridge model and prevented a potential catastrophic mode of failure.
- The proposed TPT system was proven to add redundancy to the assembled bridge model. When the shear key was fully fractured, no sudden failure nor rupture in the TPT strands was observed. Conversely, the separated girders (Girders G2, G3, and G4) continued to deform simultaneously with slight rotations about the loaded girder (exterior Girder G1).
- The mode of failure experienced by the bridge model was brittle punching shear. The ultimate load carrying capacity of 229.8 kN is 22% higher than the predicted punching shear capacity of 188.2 kN.

5.2.2. Conclusions from the Numerical Phase

- The presence of concrete topping enhanced the overall stiffness of the bridge model by limiting mid-span deflections. Mid-span deflections were reduced by 8, 17, and 25% when concrete topping of 75, 100 and 150-mm thickness, respectively, was used. Nevertheless, the LLMDFs were found to be insignificantly altered when a concrete topping was incorporated.
- The LLMDFs were evaluated for multiple wheel locations to determine the location associated with the maximum response. The exterior girder exhibited the maximum LLMDF when the load was placed at the farthest possible point across the bridge width.

On the other hand, the interior girder G2 exhibited the maximum LLMDF when the wheel load was centered with the girder centerline (Load Case IV).

- To satisfy the minimum number of girders required to utilize the LLMDFs proposed by the AASHTO-LRFFD, different bridge widths consisting of five, six and seven girders were investigated. For each bridge width, the wheel load was placed transversely at different locations to estimate the maximum LLMDFs. The LLMDFs were found to be reduced when the bridge width was increased. The maximum LLMDF for the exterior girder dropped by 25% when the bridge width was increased to seven girders (2,800 mm). Similar trend was observed for the interior girders.
- In lieu of size limitations dictated by the scaled bridge model, AASHTO LRFD-9 bridge design specifications were used to estimate the LLMDFs for both the exterior and the interior girders considering the actual dimensions of the one-third scale bridge model. The obtained LLMDFs were found to be conservative by 39 and 16% for the interior, and the exterior girders, respectively. This observation suggests that the existing LLMDFs proposed by AASHTO LRFD-9 could be used, as an initial step, to design the full-scale bridge structure of the tested bridge prototype.

5.3. Recommendation for Future Work

The findings of this study are encouraging to expand the scope of testing to consider full-scale bridge structures with different cases of loading and to characterize the long-term durability performance of the proposed TPT technique. In addition, the field investigation of LLMDFs of a full-scale bridge constructed utilizing the newly-developed transverse connection is needed. Furthermore, the combined effect of temperature gradients and structural loading needs to be investigated.

6. REFERENCES

AASHTO. (2004). “AASHTO LRFD Bridge Design Specifications 3rd Edition.” Washington DC, VR.

AASHTO. (2007). “AASHTO LRFD Bridge Design Specifications 4th Edition.” Washington DC, VR.

AASHTO. (2017). “AASHTO LRFD Bridge Design Specifications 8th Edition.” Washington DC, VR.

AASHTO. (2020). “AASHTO LRFD Bridge Design Specifications 9th Edition.” Washington DC, VR.

Abendroth, R., Klaiber, F., and Shafer, M. (1995). "Diaphragm Effectiveness in Prestressed-Concrete Girder Bridges." *Journal of Structural Engineering*, 121(9): 1362–1369.

Aktan, H., Attanayake, U., Ulku, E., Ahlborn, T., and Deshpande, Y. (2009). “Condition Assessment And Methods of Abatement of Prestressed Concrete Box-Beam Deterioration — Phase II.” MDOT RC-1527, Submitted to the Michigan Department of Transportation, Detroit.

Annamalai, G., and Brown, R.C. (1990). "Shear-Transfer Behavior of Post-Tensioned Grouted Shear-Key Connections in Precast Concrete-Framed Structures." *ACI Structural Journal*, 87(1): 53–59.

ASTM. (2015). “Standard Test Method for Compressive Strength of Grouts for Preplaced-Aggregate Concrete in the Laboratory.” ASTM C942 – 15, ASTM International.

Attanayake, U., and Aktan, H. (2015). "First-Generation ABC System, Evolving Design, and Half a Century of Performance: Michigan Side-by-Side Box-Beam Bridges." ASCE, *Journal of Performance of Constructed Facilities*, 29(3): 04014090.

Bigaj, A. (1999). “Structural Dependence of Rotation Capacity of Plastic Hinges.” PhD Thesis, Department of Civil Engineering, Delft, Netherlands.

Červenka, V., Jendele, L., and Červenka, J. (2020). *ATENA Program Documentation Part 1: Theory.* Červenka Consulting, Prague, Czech Republic.

Coll, A., Ribó, R., Pasenau, M., Escolano, E., Perez, J.S., Melendo, A., Monros, A., and Gárate, J. (2018). *GiD v.14 User Manual*. www.gidhome.com.

CSA. (2019a). “Canadian Highway Bridge Design Code and Commentary (CHBDC), CSA S6-19.” Canadian Standards Association (CSA), Toronto, ON.

CSA. (2019b). “Concrete Materials and Methods of Concrete Construction/Test Methods and Standard Practices for Concrete, CSA A23.1/A23.2-19.” Canadian Standards Association (CSA), Toronto, ON.

Cheung, M., Jategaonkar, R., and Jaeger, L. (1986). "Effects of intermediate diaphragms in distributing live loads in beam-and-slab bridges." *Canadian Journal of Civil Engineering*, 13(3): 278–292.

Deng, Y., Phares, B., and Steffens, O. (2016). “Experimental and Numerical Evaluation of a Folded Plate Girder System for Short-Span Bridges - A Case Study.” *Engineering Structures*, Elsevier Ltd., 113: 26–40.

El-Remaily, A., Tadros, M., Yamane, T., and Krause, G. (1996). “Transverse Design of Adjacent Precast Prestressed Concrete Box Girder Bridges.” *PCI Journal*, 41(4): 96–113.

Eom, J., and Nowak, A. (2001). “Live Load Distribution for Steel Girder Bridges.” ASCE, *Journal of Bridge Engineering*, 6(6): 489–497.

Fu, C., Pan, Z., and Ahmed, M. (2011). “Transverse Posttensioning Design of Adjacent Precast Solid Multibeam Bridges.” ASCE, *Journal of Performance of Constructed Facilities*, 25(3):

223–230.

Ghosn, M., Moses, F., and Gobieski, J. (1986). “Evaluation of Steel Bridges Using In-Service Testing.” *Transportation Research Record*, (1072): 71–78.

Graybeal, B. (2006). “Material Property Characterization of Ultra-High-Performance Concrete.” Rep. No. FHWA-HRT-06-103, Federal Highway Administration, Washington, D.C.

Graybeal, B. (2014). ‘‘Design and Construction of Field-Cast UHPC Connections.” Rep. No. FHWA-HRT-14-084, Federal Highway Administration, Washington, D. C.

Grace, N. (2000). “Response of Continuous CFRP Prestressed Concrete Bridges Under Static and Repeated Loadings.” *PCI Journal*, 45(6): 84–102.

Grace, N., Jensen, E., Enomoto, T., Matsagar, V., Soliman, E., and Hanson, J. (2010). "Transverse Diaphragms and Unbonded CFRP Post-Tensioning in Box-Beam Bridges." *PCI Journal*, 55(2): 109–122

Grace, N., Jensen, E., and Noamesi, D. (2011a). “Flexural Performance of Carbon Fiber-Reinforced Polymer Prestressed Concrete Side-by-Side Box Beam Bridge.” ASCE, *Journal of Composites for Construction*, 15(5): 663–671.

Grace, N., Patki, K., Soliman, E., and Hanson, J. (2011b). "Flexural Behavior of Side-by-Side Box-Beam bridges: A Comparative Study.” *PCI Journal*, 56(3): 94–112.

Grace, N., Jensen, E., and Bebawy, M. (2012). "Transverse Post-Tensioning Arrangement for Side-by-Side Box-Beam Bridges." *PCI Journal*, 57(2): 48–63.

Gulyas, R., Wirthlin, G., and Champa, J. (1995). "Evaluation of Keyway Grout Test Methods for Precast Concrete Bridges." *PCI journal*, 40(1): 44–57.

Hanna, K., Morcous, G., and Tadros, M. (2009). “Transverse Post-Tensioning Design and Detailing of Precast, Prestressed Concrete Adjacent-Box-Girder Bridges.” *PCI Journal*,

54(4): 160–174.

Hanna, K., Morcous, G., and Tadros, M. (2011). “Design, Detailing, and Testing of Non-Post-Tensioned Transverse Connections in Adjacent Box-Girder Bridges.” *PCI J.*, 56(4): 94–107.

Hansen, J., Hanna, K., and Tadros, M. (2012). “Simplified Transverse Post-Tensioning Construction and Maintenance of Adjacent Box Girders.” *PCI Journal*, 57(2): 64–79.

Huckelbridge, A., El-Esnawi, H., and Moses, F. (1995). “Shear Key Performance in Multibeam Box Girder Bridges.” ASCE, *Journal of Performance of Constructed Facilities*, 9(4): 271–285.

Huckelbridge, A., and El-Esnawi, H. (1997). " Evaluation of Improved Shear-key Designs for Multi-Beam box Girder Bridges ". Final Report No. FHWA/OH/97-009, Department of Civil Engineering, Case Western Reserve University, Cleveland, OH.

Hughs, E., and Idriss, R. (2006). “Live-Load Distribution Factors for Prestressed Concrete, Spread Box-Girder Bridge.” ASCE, *Journal of Bridge Engineering*, 11(5): 573–581.

Hussein, H., Sargand, S., Al-Jhayyish, A., and Khoury, I. (2017). “Contribution of Transverse Tie Bars to Load Transfer in Adjacent Prestressed Box-Girder Bridges with Partial Depth Shear Key.” ASCE, *Journal of Performance of Constructed Facilities*, 31(2): 04016100.

Hussein, H., Sargand, S., and Steinberg, E. (2018). "Shape Optimization of UHPC Shear Keys for Precast, Prestressed, Adjacent Box-Girder Bridges.” ASCE, *Journal of Bridge Engineering*, 23(4): 04018009.

Issa, M., Do Valle, C., Abdalla, H., Islam, S., and Issa, M. (2003). "Performance of Transverse Joint Grout Materials in Full-Depth Precast Concrete Bridge Deck Systems". *PCI Journal*, 48(4): 92–103.

Jendele, L., and Cervenka, J. (2006). "Finite Element Modelling of Reinforcement with Bond." *Computers and Structures*, 84(28): 1780–1791.

Kahl, S. (2005). "Box-Beam Concerns Found under the Bridge". Michigan Department of Transportation Construction and Technology Division. C&T Research Record, No. 102: 1–4.

Kim, S., and Nowak, A. (1997). "Load Distribution and Impact Factors for I-Girder Bridges." ASCE, *Journal of Bridge Engineering*, 2(3): 97–104.

Labib, S., El-Gendy, M., and El-Salakawy, E. (2021). "Adjacent Concrete Box Girders Transversely Post-Tensioned at Top Flanges Only: Experimental Investigation." ASCE, Journal of Bridge Engineering, 26(4): 04021017.

Lall, J., Alampalli, S., and DiCocco, E. (1998). "Performance of Full-Depth Shear Keys in Adjacent Prestressed Box Beam Bridges." *PCI Journal*, 43(2): 72–79.

Mahmoud, K., Anand, P., and El-Salakawy, E. (2018), "3-D Finite Element Modeling of Prestressed Hollow-Core Slabs Strengthened with Near Surface Mounted CFRP Strips." Computers and Concrete, 21(6): 607-622.

Markou, G., and Papadrakakis, M. (2013), "Computationally Efficient 3D Finite Element Modeling of RC Structures." Computers and Concrete, 12(4): 443-498.

Miller, R., Hlavacs, G., Long, T., and Greuel, A. (1999). "Full-Scale Testing of Shear Keys for Adjacent Box Girder Bridges." *PCI Journal*, 44(6): 80–90.

PCI. (2003). PCI Bridge Design Manual, 3rd Ed., Precast/Prestressed Concrete Institute, Chicago, IL.

PCI. (2014). PCI Bridge Design Manual, 4th Ed., Precast/Prestressed Concrete Institute, Chicago, IL.

Russell, H. (2011). "Adjacent Precast Concrete Bridges: State of The Practice." *PCI journal,*

56(1): 75–91.

Semendary, A., Steinberg, E., Walsh, K., and Barnard, E. (2017). “Live-Load Moment-Distribution Factors for an Adjacent Precast Prestressed Concrete Box Beam Bridge with Reinforced UHPC Shear Key Connections.” ASCE, *Journal of Bridge Engineering*, 22(11): 04017088.

Semendary, A., Walsh, K., Steinberg, E., and Khoury, I. (2018). “Effect of Thermal Load on the Behavior of an Adjacent Precast, Prestressed Concrete Box-Beam Bridge that Contains Ultra-High-Performance Concrete Shear Keys with Transverse Dowels.” *PCI Journal*, 63(3): 51–64.

Sengupta, S., and Breen, J. (1973). "The Effect of Diaphragms in Prestressed Concrete Girders and Slab Bridges". Research Report 158-1F, Center of Highway Research, University of Texas at Austin, TX.

Sithichaikasem, S., and Gamble, W. (1972). “Effects of Diaphragms in Bridges with Prestressed Concrete I- Section Girders”. Civil Engineering Studies, Structural Research Series No. 383, Department of Civil Engineering, University of Illinois, Urbana, IL.

Soliman, E. (2008). “Effect of Number of Diaphragms on the Behavior of Side-by-Side Box-Beam Bridges Using Unbonded Transverse Post-Tensioning CFRP Strands.” Master’s Thesis, Department of Civil Engineering, Lawrence Technological University, Southfield, MI.

Stallings, J., and Yoo, C. (1993). "Tests And Ratings of Short-Span Steel Bridges". *Journal of Structural Engineering*, 119(7): 2150–2168.

Sun, C., Tadros, M., Kopper, K., and Belill, T. (2018). “Innovative Precast Concrete Adjacent-Box-Beam System implemented in The St. Clair Road bridge in Michigan.” *PCI Journal*, 63(3), 41–50.

Ulku, E., Attanayake, U., and Aktan, H. (2010). "Rationally Designed Staged Posttensioning to Abate Reflective Cracking on Side-by-Side Box-Beam Bridge Decks." Transportation Research Record: *Journal of the Transportation Research Board*, 2172(1): 87–95.

Ventura-Gouveia, A., Barros, J., and Azevedo, A. (2011), "Crack Constitutive Model for the Prediction of Punching Failure Modes of Fiber Reinforced Concrete Laminar Structures." Computers and Concrete, 8(6): 735-755.

Yuan, J., and Graybeal, B. (2016). "Full-Scale Testing of Shear Key Details for Precast Concrete Box-Beam Bridges." ASCE, *Journal of Bridge Engineering*, 21(9): 04016043.

APPENDIX A – Design of the Bridge Assembly

Design was carried out according to **CSA S-6-19 (CSA 2019a)**

Materials Properties

Concrete

$f'_c = 55$ MPa $\qquad \alpha_1 = 0.85 - 0.0015 \times 55 = 0.7675 \qquad \beta_1 = 0.97 - 0.0025 \times 55 = 0.8325$

$f'_{ci} = 35$ MPa

$\gamma_c = 24$ kN/m^3

$$E_c = \left(3{,}000 \times \sqrt{55} + 6{,}900\right) \times \left(\frac{24{,}000/9.81}{2{,}300}\right)^{1.5} = 31{,}977 \text{ MPa}$$ **CSA S-6-19 – 8.4.1.7**

$f_r = 0.4 \times \sqrt{55} = 2.97$ MPa **CSA S-6-19 – 8.4.1.82**

Steel Reinforcement

1. *Non-Prestressing Steel Bars:*

$f_y = 400$ MPa

$E_s = 200$ GPa

$A_b = 100$ mm^2

2. *Prestressing Steel Strands:*

$f_{pu} = 1{,}860$ MPa

$f_{py} = 1{,}670$ MPa

$A_p = 99$ mm^2

Properties of Cross-Section

The cross section shown in Figure A.1 was used to calculate the cross-sectional properties.

$A = 78{,}800$ mm^2

$I = 600 \times 10^6$ mm^4

$y_t = y_b = 135$ mm

$e = 97.5$ mm

$A_s = 2 \times 100 = 200$ mm^2

$A'_s = 3 \times 100 = 300$ mm^2

$A_{ps} = 3 \times 99 = 297$ mm^2

$d = 233$ mm

$d' = 20$ mm

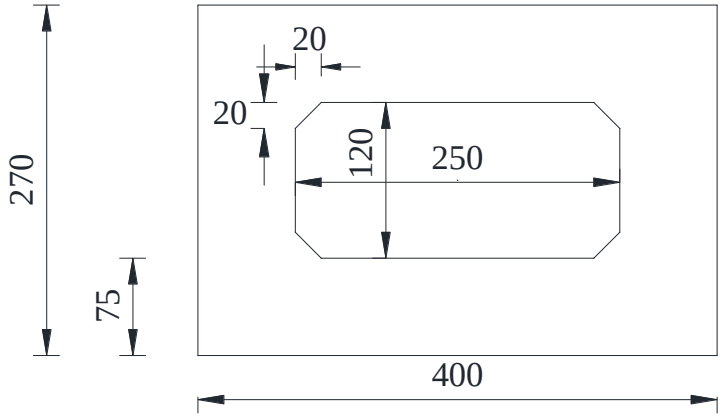

Fig. A. 1 – Girder cross section (dimensions in mm)

Loads

Self-Weight of Box-Girder

$$w_{sw} = A \times \gamma_c = \left(78800 \times 10^{-6}\right) \times 24 = 1.891 \text{ kN/m}$$

$$M_{sw,midspan} = \frac{w_{sw} l^2}{8} = \frac{1.891 \times (6)^2}{8} = 8.5 \text{ kN.m}$$

$$M_{sw,50d} = \frac{w_{sw} \times 50d \times (l - 50d)}{2} = \frac{1.891 \times \left(50 \times 13 \times 10^{-3}\right)(6.00 - 0.65)}{2} = 3.29 \text{ kN.m}$$

Prestressing Forces

$$f_j = 0.80\, f_{pu} = 0.80 \times 1860 = 1,488 \text{ MPa} \qquad P_j = (1,488 \times 297) \times 10^{-3} = 441.9 \text{ kN}$$

$$f_i = 0.74\, f_{pu} = 0.74 \times 1860 = 1376.40 \text{ MPa} \qquad P_i = (1,376.40 \times 297) \times 10^{-3} = 408.8 \text{ kN}$$

$$f_e = 0.67\, f_{pu} = 0.67 \times 1860 \simeq 1,246.20 \text{ MPa} \qquad P_e = (1,246.2 \times 297) \times 10^{-3} = 370.1 \text{ kN}$$

Check of Normal Stresses at Concrete

Allowable Stresses (at transfer) **CSA S-6-19 – 8.8.4.6**

$$f_{ci} = -0.6\, f'_{ci} = -0.6 \times 35 = -21 \text{MPa}$$

Stresses at Transfer

1. At Supports

$$f_t = -\frac{P_i}{A} + \frac{P_i e}{I} y_t - \frac{M_{sw,50d}}{I} y_t = -\frac{441.9 \times 1000}{78{,}800} + \frac{(441.9 \times 1000) \times 97.5}{600 \times 10^6} \times 135 - \frac{(3.25 \times 10^6)}{600 \times 10^6} \times 135$$
$$= -5.61 + 9.69 - 0.73 = 3.35 \text{ MPa}$$

$$f_b = -\frac{P_i}{A} - \frac{P_i e}{I} y_b + \frac{M_{sw,50d}}{I} y_b = -5.61 - 9.69 + 0.73 = -14.57 \text{ MPa} > -21 \text{ MPa}$$

2. At Mid-Span

$$f_t = -\frac{P_i}{A} + \frac{P_i e}{I} y_t - \frac{M_{sw,midspan}}{I} y_t = -4.52 + 7.48 - \frac{(8.4 \times 10^6)}{600 \times 10^6} \times 135$$
$$= -5.61 + 9.69 - 1.89 = 2.19 \text{ MPa}$$

$$f_b = -\frac{P_i}{A} - \frac{P_i e}{I} y_t + \frac{M_{sw,midspan}}{I} y_t = -5.61 - 9.69 + 1.89 = -13.41 \text{ MPa} > -21 \text{ MPa}$$

Elongation

$$\Delta L = \frac{(441.9 \times 10^3) \times 6000}{190000 \times 297} = 46.98 \text{ mm}$$

Cracking Moment (M_{cr}) **CSA S-6-19 –8.8.4.4**

Cracking moment including the total self-weight:

$$M_{cr} = \left(\frac{P_e}{A} + \frac{P_e e}{I} y_b + f_r \right) \frac{I}{y_b}$$
$$= \left(\frac{370.1 \times 1000}{78{,}800} + \frac{(370.1 \times 1000) \times 97.5}{600 \times 10^6} \times 135 + 2.97 \right) \frac{600 \times 10^6}{135} = 70 \times 10^6 \text{ n.mm} = 70 \text{ kN.m}$$

Cracking moment in excess of total self-weight:

$\Delta M_{cr} = M_{cr} - M_{sw,midspan} = 70 - 8.5 = 61.5$ kN.m

- Cracking load for load distribution test for single beam, $= \frac{4\Delta M_{cr}}{l} = \frac{4 \times 61.5}{6} = 41$ kN

  Cracking load for the bridge model, $p_{cr} = 4 \times 41 = 164$ kN

- Cracking load for ultimate test for single beam, $= \frac{2\Delta M_{cr}}{2.625} = \frac{4 \times 61.5}{(6 - 0.75)} = 46.89$ kN

  Cracking load for the bridge model, $p_{cr} = 4 \times 46.89 = 187$ kN

Flexural Resistance (M_r) **CSA S-6-19 –8.8.4.2**

Check the type of section:

$$a \simeq \frac{\varphi_s A_s f_y - \varphi_s A_s^{'} f_y + \varphi_p A_p f_{pu}}{\alpha_1 \varphi_c f_c^{'} b}$$

$$\simeq \frac{1 \times 200 \times 400 - 1 \times 300 \times 400 + 1 \times 297 \times 1860}{0.7675 \times 1 \times 55 \times 400} = 30.34 \text{ mm} < h_f = 75 \text{ mm}$$

Rectangular section behaviour.

$k_p = 0.3$

$$\frac{c}{d_p} = \frac{\varphi_s A_s f_y - \varphi_s A_s^{'} f_y + \varphi_p A_p f_{pu}}{\alpha_1 \varphi_c f_c^{'} \beta_1 b d_p + \varphi_p A_p k_p f_{pu}}$$

$$= \frac{1 \times 200 \times 400 - 1 \times 300 \times 400 + 1 \times 297 \times 1860}{0.7675 \times 1 \times 55 \times 0.8325 \times 400 \times 232.5 + 1 \times 297 \times 0.30 \times 1860} = 0.149 < 0.5$$

$c = 0.149 \times 232.5 = 34.6$ mm

$$f_{pr} = f_{pu}\left(1 - k_p \frac{c}{d_p}\right) = 1{,}860\left(1 - 0.30 \times 0.149\right) = 1{,}777 \text{ MPa}$$

Check the yielding of non-prestressed reinforcement:

$$\varepsilon_s = \varepsilon_{cu}\left(\frac{d-c}{c}\right) = 0.0035\times\left(\frac{232.5-34.6}{34.6}\right) = 0.02 > \varepsilon_y = 0.002$$

$$\varepsilon_s^{'} = \varepsilon_{cu}\left(\frac{c-d^{'}}{c}\right) = 0.0035\times\left(\frac{34.6-20}{34.6}\right) \simeq 0.002 = \varepsilon_y$$

Assumptions are correct, top and bottom steel have yielded.

$$\begin{aligned} M_r &= \varphi_p A_p f_{pr}\left(d-\frac{\beta_1 c}{2}\right) + \varphi_s A_s f_y\left(d-\frac{\beta_1 c}{2}\right) - \varphi_s A_s^{'} f_y\left(d^{'}-\frac{\beta_1 c}{2}\right) \\ &= 1\times 297\times 1777\times\left(232.5-\frac{0.8325\times 34.6}{2}\right) \\ &\quad + 1\times 200\times 400\times\left(232.5-\frac{0.8325\times 34.6}{2}\right) \\ &\quad - 1\times 300\times 400\times\left(20-\frac{0.8325\times 34.6}{2}\right) \\ &= 131.8 \text{ kN.m} \end{aligned}$$

Ultimate vertical load (Pu)

$$M_{LL} = M_r - M_{sw} = 131.8 - 8.5 = 123.3 \text{ kN.m}$$

As shown in Figure A. 2, two-point loading frame having a longitudinal spacing of 0.75 m was assumed to calculate the ultimate load capacity of the bridge assembly.

$$M_{LL} = \frac{P_u}{2}\left(\frac{L}{2}-\frac{l}{2}\right) \Rightarrow P_u = \frac{4M_{LL}}{(L-l)} = \frac{4\times 123.3}{(6-0.75)} = 93.9 \text{ kN}$$

Load carrying capacity of single box-beam, $P_u = 93.9$ kN

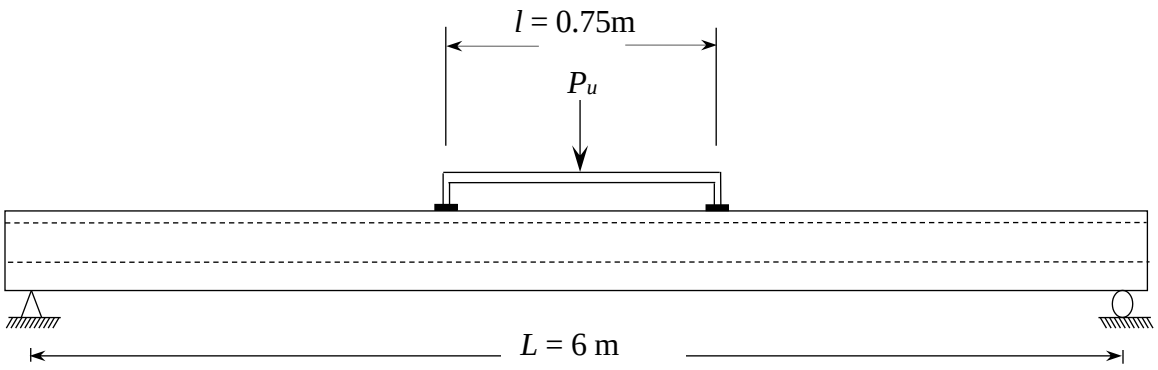

Fig. A. 2 – Two-point loading for ultimate load capacity calculation.

By assuming uniform distribution of the ultimate vertical load (Pu) in the transverse direction, the load carrying capacity of the bridge model would be:

$P_u = 93.9 \times 4 = 375.8$ kN

Shear Design

$d_v = 0.9d = 0.9 \times 232.5 = 209.3$ mm Governs

$d_v = 0.72h = 0.72 \times 270 = 194.4$ mm

Assume the factored shear = 100 kN

$V_c = \varphi_c \lambda \beta \sqrt{f_c'} b_w d_v = 0.7 \times 1.0 \times 0.18 \times \sqrt{55} \times 150 \times 209.3 = 29.3$ kN

Use 2 legged 10M stirrups

$$S_{\max} = \frac{A_v \times f_y}{0.06 b_w \sqrt{f_c'}} = \frac{(2 \times 100) \times 400}{0.06 \times 150 \times \sqrt{55}} = 1{,}199 \text{ mm}$$

$S_{\max} = 0.7 d_v = 0.7 \times 209.3 = 146.5$ mm Governs

$$V_s = \frac{\varphi_s A_v f_y d_v \cot\theta}{S_{\max}} = \frac{0.85 \times 200 \times 400 \times 209.3 \times \cot 35}{140} \times 10^{-3} = 145.2 \text{ kN}$$

$$V_r = V_c + V_s + V_p = 29.3 + 145.2 + 0 = 174.5 \text{ kN} > V_f = 100 \text{ kN}$$

$$V_{r,\max} = 0.25\varphi_c \lambda f_c' b_w d_v = 0.25 \times 1.0 \times 0.7 \times 55 \times 150 \times 209.3 \times 10^{-3} = 302.2 \text{ kN} > V_r = 174.5 \text{ kN}$$

Punching Shear Design **CSA S6-19 – 8.9.4.3**

As shown in Fig. A.3, two scenarios for punching shear failure were assumed. The critical shear perimeter was assumed to surround the footprint of each loading plate at a time (Scenario 1). Alternatively, the shear perimeter was assumed to be a combined perimeter surrounding the two loading plates (Scenario 2).

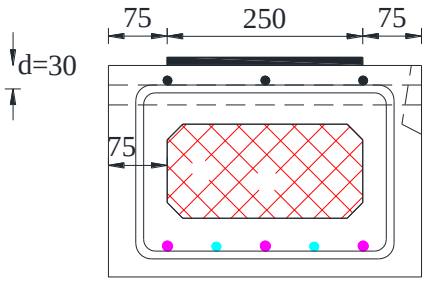

(a) Effective depth

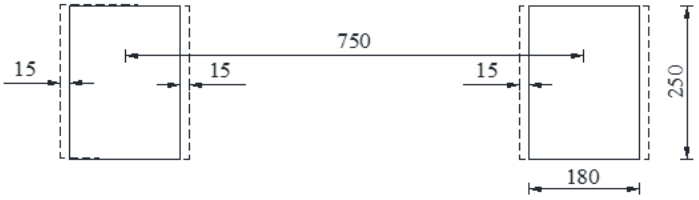

(b) Scenario 1

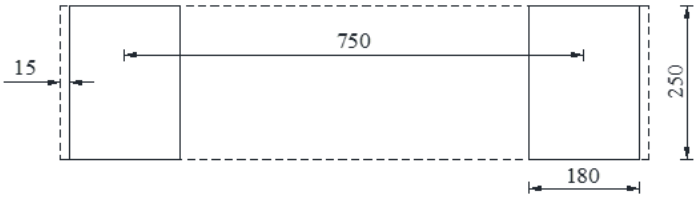

(c) Scenario 2

Fig. A. 3 – Punching shear perimeters

$b_o d)_1 = 2 \times 2(180 + 30 + 250) \times 25 = 46,000 \text{ mm}^2$

$b_o d)_2 = 2 \times (750 + 180 + 30 + 250) \times 25 = 60,500 \text{ mm}^2$ (governs)

$V_r = (\varphi_c f_{cr} + 0.25 f_{pc}) b_o d$

$$f_{pc \ \ longitudinal} = \frac{P_e}{A} - \frac{P_i e^2}{I} = \frac{310.7 \times 10^3}{78,000} - \frac{310.7 \times 10^3 \times 97.5 \times 97.5}{620 \times 10^6} = -0.78 \text{ MPa}$$

$$f_{pc \ \ Transverse} = \varepsilon E = 54 \times 10^{-6} \times 34,418 = 1.85 \text{ MPa}$$

$$f_{pc \ \ average} = \frac{1.85 - 0.78}{2} = 0.53 \text{ MPa}$$

$$f_{cr \text{ girder1}} = 0.4\sqrt{55.9} = 2.99 MPa$$

$V_r = (1 \times 2.99 + 0.25 \times 0.53) \times 60500 = 188.2 \text{ kN}$